

Peak-ratio Analysis Method for Enhancement of LOM Protection Using M Class PMUs

Feng Ding

A thesis submitted for the degree of Doctor of
Philosophy to Department of Electronic and Electrical
Engineering University of Strathclyde

July 2017

This thesis is the result of the author's original research. It has been composed by the author and has not been previously submitted for examination which has led to the award of a degree.

The copyright of this thesis belongs to the author under the terms of the United Kingdom Copyright Acts as qualified by University of Strathclyde Regulation 3.50. Due acknowledgement must always be made of the use of any material contained in, or derived from, this thesis.

Signed:

Date:

Abstract

Loss of Mains (LOM) occurs when part of the utility network containing distributed generation (DG) is disconnected from the remainder of the system. Detecting LOM will become more important in the future as higher amounts of DG will be connected to increase the use of renewable energy sources, to reduce emissions and to reduce power transmission losses. In some cases, DG can be capable of supplying loads within an island and the islanded system can remain stable. However, safety issues arise if LOM persists and, accordingly, islanded operation is not permitted in the majority of utility systems throughout the world. Wide area monitoring systems, using synchronised phasor measurements, which are beginning to play an increasing role in monitoring and control in transmission networks, may offer opportunities to improve the performance of LOM protection in distribution networks, but may require some form of communications.

A novel technique for LOM detection, using Phasor Measurement Unit (PMU) data, is described in this thesis. The technique, known as the Peak Ratio Analysis Method (PRAM), is shown to improve both the sensitivity and stability of LOM protection when compared to prevailing techniques. The technique is based on a Rate of Change of Frequency (ROCOF) measurement from M-class PMUs, but the key novelty of the method lies in the fact that it employs a new “peak-ratio” analysis of the measured ROCOF waveform during any frequency disturbance to determine whether the potentially-islanded element of the network remains connected to the main system or not (i.e. it detects when islanding, or loss of mains, has occurred). The proposed technique is described and several examples of its operation are compared with three competing LOM protection methods that have all been widely used by industry and/or reported in the literature: standard ROCOF, Phase Offset Relay (POR) and Phase Angle Difference (PAD) methods. It is shown that the PRAM technique exhibits comparable performance to the others, and in many cases improves upon their abilities; in particular for systems where the inertia of the main power system is reduced, which may be the case in future systems with increased penetrations of renewable generation and HVDC infeeds.

Acknowledgments

Firstly, I am grateful for and would like to thank my first supervisor Dr. Campbell Booth for accepting me as one of his PhD students and offering me an opportunity to undertake the project I'm interested in. He is more of a friend than a "supervisor" and I learnt a lot from him during the last few years working together.

I would also like to express my gratitude to my second supervisor Prof. Graeme Burt who supported my project with funding from the department.

A special thank you must go to Dr. Andrew Roscoe for his technical support with simulation using PMUs and input of my journal.

Thanks also to all my colleagues at the University of Strathclyde for their help in bringing this PhD project to completion and creating such a warm atmosphere like a family.

I would also like to thank all my friends for making these years so enjoyable and memorable.

Finally, thanks to my loving wife Haipeng Liu, daughter Rachel Yueqiao Ding and my parents Yushan Ding, Hongyan Chen for their love and belief in me. I would not have completed this PhD if it weren't for their support.

Feng Ding

July 2017

Contents

Chapter 1	1
Introduction.....	1
1.1 Introduction to the Research.....	1
1.2 Research Motivation.....	4
1.3 Principal Contributions.....	7
1.4 Thesis Overview	9
1.5 Publications	10
1.5.1 Conference publications.....	10
1.5.2 Journal publications	10
References	11
Chapter 2	13
Review of LOM protection.....	13
2.1 Power System Developments.....	13
2.1.1 Future power system	13
2.1.2 DG impact on power system protection.....	18
2.2 Introduction to LOM	25
2.3 Passive LOM Techniques and Methods.....	32
2.3.1 Rate of change of frequency (ROCOF)	32
2.3.2 Vector shift (VS).....	35
2.3.3 Reverse var method.....	37
2.3.4 Direct inter-tripping	39
2.3.5 Over/under voltage and over/under frequency.....	40
2.3.6 Rate of change of output power (ROCOP)	42
2.3.7 Rate of change of voltage (ROCOV).....	43
2.3.8 Rate of change of frequency over power	46
2.3.9 Voltage unbalance and evaluation of total harmonic distortion (THD) in the measured currents	48
2.3.10 Accumulated phase angle drift method.....	49

2.3.11	Phase offset relay (POR).....	51
2.3.12	Method based on Tufts-Kumaresan (TK) signal.....	53
2.3.13	Data-mining-based relay	54
2.3.14	Auto-ground method	56
2.3.15	Frequency difference method.....	57
2.3.16	Change of phase angle difference method (PAD).....	58
2.4	Summary of Review	59
	References	62
	Chapter 3	69
	Detailed Description of the Novel PRAM Method	69
3.1	Basic Function and Typical Applications of PMUs	70
3.1.1	Phasors	70
3.1.2	Basic PMU functions	71
3.1.3	Typical applications of PMU	75
3.2	Description of Developed LOM Method	79
3.2.1	M class PMUs used in simulation.....	79
3.2.2	Tripping logic and peak ratio algorithm.....	85
	References	90
	Chapter 4	94
	Simulation Methodology.....	94
4.1	Experimental Setup	94
4.1.1	Test distribution network	94
4.1.2	Test scenarios	97
4.1.3	PRAM relay setup	101
4.2	Generator Dynamic Response to LOM Events [4.6].....	106
	References	112
	Chapter 5	113
	PRAM - Sensitivity Tests.....	113
5.1	Testing Procedure	113
5.2	Discussion of Sensitivity Test Results	116
5.2.1	Active power imbalance with 90% DG output	116
5.2.2	Active power imbalance with 30% DG output	120
5.2.3	Reactive power imbalance with 90% DG output.....	123

5.2.4	Reactive power imbalance with 30% DG output.....	125
	References	128
Chapter 6	129
Stability Tests	129
6.1	Testing Procedure.....	129
6.2	Discussion of Stability Test Results	132
6.2.1	Single phase to earth fault	132
6.2.2	Phase to phase fault.....	140
6.2.3	Three phase to earth fault	148
6.2.4	Local small load change.....	155
6.2.5	Remote large load change	158
6.2.6	Capacitor switching.....	161
6.2.7	Transformer inrush.....	162
	References	164
Chapter 7	165
Conclusions and Future Work	165
Chapter 8	165
Chapter 9	165
	References	168

List of Figures

Figure 1: Estimated generation capacity in the UK by fuel types [1.1].....	14
Figure 2: Installed wind generation capacity of European countries in 2013 [2.4] ...	15
Figure 3: Proposed offshore grid scenario in Europe [2.5].....	16
Figure 4: System Inertia (H) Changes for Gone Green Scenario at 70% Wind Power Output [2.6].....	18
Figure 5: Example of blinding of protection when distribution network with DG connection experience a fault.....	22
Figure 6: Example 1 of discrimination issues of protection devices	23
Figure 7: Example 2 of discrimination issues of protection devices	23
Figure 8: Example of false tripping in two feeders distribution network.	24
Figure 9: Illustration of LOM event.....	26
Figure 10: Zero crossing estimation method.....	34
Figure 11: Principle of vector shift method during islanding event.....	36
Figure 12: Principle of reverse var method.....	37
Figure 13: Reactive power demand.....	39
Figure 14: Principle of direct inter-tripping scheme	40
Figure 15: Flow chart of ROCOP algorithm [2.34]	43
Figure 16: Flow chart of ROCOV based hybrid method [2.35]	45
Figure 17: Flow chart of rate of change of frequency over power [2.36].....	47
Figure 18: Block diagram of PAD [2.38]	50
Figure 19: Illustration of frequency estimation [2.38].....	50
Figure 20: Flow chart of POR algorithm	52
Figure 21: Schematic of islanding detection method based on TK signal [2.41]	53
Figure 22: Feature extraction chart [2.42].....	55
Figure 23: Decision tree generated during training considering extracted features... ..	56
Figure 24: Illustration of auto-ground system [2.43]	57
Figure 25: A sinusoidal waveform and its phasor representation [3.1]	70
Figure 26: The function blocks of a typical PMU [3.1].....	72
Figure 27: Overview of typical three-phase PMU algorithm.....	74
Figure 28: Typical Single-phase section of a PMU	74
Figure 29: Generally structure of phasor measurement systems [3.1].....	75
Figure 30: An example of transition from pre-event to post-event waveforms during a fault. The shaded windows contain mixed waveform data and could produce “fake” phasors. [3.1].....	82
Figure 31: Illustration of phasor estimation in samples during a transient [3.1]	82
Figure 32: Filter implementation scheme of M class PMUs used	83
Figure 33: Filter implementation scheme in single-phase section of M class PMUs used	83
Figure 34: Tripping logic of PRAM method	86

Figure 35: Illustration of peak ratio calculation for an unknown event with an example pick up threshold of 0.6Hz/s and peak recording time window of 170ms ..	87
Figure 36: Test network (Buses are indicated as B0, B1, B2 and etc.).....	96
Figure 37: Test network in SimPowerSystems	97
Figure 38: Package view of PRAM relay	102
Figure 39: ROCOF trigger algorithm of PRAM relay	103
Figure 40: Window generator of PRAM relay.....	103
Figure 41: Extraction of ROCOF waveform from windows triggered	103
Figure 42: Identification of zero crossings from ROCOF waveform in windows triggered.	104
Figure 43: Peak separator.....	104
Figure 44: Peak ratio calculation process.....	105
Figure 45: Trip signal generation	105
Figure 46: Schematic of an isochronous governor.....	106
Figure 47: Schematic of a governor with speed droop	107
Figure 48: Example of speed droop operation with 50% and 90% load at nominal frequency [4.7]	108
Figure 49: Schematic of generator voltage control loop.....	109
Figure 50: Frequency response for a range of different DG control options following an islanding event.....	110
Figure 51: Voltage magnitude response for a range of different DG control options following an islanding event	111
Figure 52: Illustration of pick up time after islanding initiation	117
Figure 53: Comparison of simulation results between two droop control scenarios	118
Figure 54: Single source network for transformer inrush test.....	131
Figure 55: ROCOF output of PRAM I during single phase fault initiation, clearing and reclosing	134
Figure 56: Scaled ROCOF output of PRAM I during single phase fault initiation, clearing and reclosing	135
Figure 57: Peak ratio output of PRAM I during single phase fault initiation, clearing and reclosing	135
Figure 58: Output of PRAM I during single phase fault clearing at location 3	136
Figure 59: ROCOF output of PRAM II during single phase fault initiation, clearing and reclosing	137
Figure 60: Scaled ROCOF output of PRAM II during single phase fault initiation, clearing and reclosing	138
Figure 61: Peak ratio output of PRAM II during single phase fault initiation, clearing and reclosing	138
Figure 62: Output of PRAM II during single phase fault clearing at location 3.....	139
Figure 63: ROCOF output of PRAM I during phase to phase fault initiation and clearing	142
Figure 64: Scaled ROCOF output of PRAM I during phase to phase fault initiation and clearing	143

Figure 65: Peak ratio output of PRAM I during phase to phase fault initiation and clearing	143
Figure 66: Output of PRAM I during phase to phase fault clearing	144
Figure 67: ROCOF output of PRAM II during phase to phase fault initiation and clearing	145
Figure 68: Scaled ROCOF output of PRAM II during phase to phase fault initiation and clearing	146
Figure 69: Peak ratio output of PRAM II during phase to phase fault initiation and clearing	146
Figure 70: Output of PRAM II during phase to phase fault clearing	147
Figure 71: ROCOF output of PRAM I during three phase fault initiation and clearing	150
Figure 72: Scaled ROCOF output of PRAM I during three phase fault initiation and clearing	150
Figure 73: Peak ratio output of PRAM I during three phase fault initiation and clearing	151
Figure 74: ROCOF output of PRAM II during three phase fault initiation and clearing	152
Figure 75: Scaled ROCOF output of PRAM II during three phase fault initiation and clearing	153
Figure 76: Peak ratio output of PRAM II during three phase fault initiation and clearing	153
Figure 77: ROCOF output of PRAM I during local load switching out and in	157
Figure 78: ROCOF output of PRAM II during local load switching out and in	157
Figure 79: ROCOF output of PRAM I during remote large load switching in with magnitude of 1.8 GW, 1.5 GW and 1.3 GW with grid inertia of 4s and 5s	160
Figure 80: ROCOF output of PRAM I and PRAM II during capacitor switching out with magnitude of 11 MVar and 8.17 MVar	162
Figure 81: ROCOF output of PRAM I and PRAM II for scenario 2 of transformer inrush	163

List of Tables

Table I: Settings recommended for DGs in G59.....	41
Table II: Comparison of reviewed passive LOM techniques and methods	60
Table III: Scenarios of Sensitivity Test.....	100
Table IV: Scenarios of Stability Test	101
Table V: Settings for all relays at all tests	115
Table VI: Test results for islanding with active power imbalances (90% DG output; X: fail to react; Times: tripping time; F: frequency; V: voltage).....	116
Table VII: Test results for islanding with active power imbalances (30% DG output)	120
Table VIII: Test results for islanding with reactive power imbalances (90% DG output)	123
Table IX: Test results for islanding with reactive power imbalances (30% DG output)	126
Table X: Test results for single phase faults at various locations (√: Successfully rode through; X: Failed to remain stable)	133
Table XI: Test results for phase to phase faults (fault clearing at Location 4 led to islanding).....	141
Table XII: Test results for three phase fault (fault clearing at Location 4 led to islanding).....	149
Table XIII: Test results for local load switching	155
Table XIV: Test results for remote large load switching.....	158
Table XV: Test results for capacitor switching out and transformer inrush	161

Glossary of Abbreviations

ADC	Analog to Digital (convertor)
AFD	Active Frequency Drift
AFDPF	Active Frequency Drift with Positive Feedback
ALPS	Adaptive Logic Phase Shift
APS	Automatic Phase-shift
AVR	Automatic Voltage Regulator
CB	Circuit Breaker
CCS	Carbon Capture and Storage
CHP	Combine Heat and Power
CT	Current Transformer
DFT	Discrete Fourier Transform
DG	Distributed Generator
DNO	Distribution Network Operator
ETR	Engineering Technical Report
FDR	Frequency Disturbance Recorder
FFT	Fast Fourier Transform
FIR	Finite Impulse Response
GPS	Global Positioning System
HVDC	High Voltage Direct Current Transmission
IED	Industrial Emissions Directive
KCL	Kirchhoff's Current Law
LCPD	Large Combustion Plant Directive
LOM	Loss of Mains
NDZ	Non-detection Zone
NGC	National Grid Company
Ofgem	Office of Gas and Electricity Market
PAD	Phase Angle Difference
PDC	Phasor Data Concentrators
PQ	Active Power and Reactive Power
PMU	Phasor Measurement Unit
POR	Phase Offset Relay

PRAM	Peak Ratio Analysis Method
PV	Power and Voltage (control)
RMS	Root Mean Square
ROCOF	Rate of Change of Frequency
ROCOFOP	Rate of Change of of Frequency Over Power
ROCOP	Rate of Change of Power
ROCOV	Rate of Change of Voltage
SMS	Slip-mode Frequency Shift Algorithm
THD	Total Harmonic Distortion
TK	Tufts-Kumaresan
TSO	Transmission System Operator
UK	United Kingdom
VS	Vector-Shift
VT	Voltage Transformer

Chapter 1

Introduction

1.1 Introduction to the Research

Power systems are expanding and developing with rising demand for electricity, which is due to the growing population, continued development and electrification and proliferation of new types of loads such as domestic heating (often previously gas-fired) and electric vehicles [1.1]. Future “smart grid” networks will invariably incorporate numerous sources of distributed energy to achieve objectives including improving efficiency, reduced transmission losses and facilitating the introduction of more renewable energy for generation such as wind power and solar energy; either directly connected to the system and or more often connected via power electronic interfaces [1.2]. The proliferation of renewable energy, connected at distribution level, helps to meet climate change objectives, but gives rise to increased risks, among which the risk of undetected islanding is of primary concern.

Islanding, which is one of the most critical operational issues associated with distributed (or embedded) generation, is when part of the network is disconnected from the main power grid, and distributed generators (DG) remain connected to the

segmented network, supplying energy to loads within the islanded network. It not only raises safety concerns but also leads to power quality and protection coordination problems [1.3]. For example, out of synchronism re-closing leading to damage of circuit breakers and generators, inadvertently operation in unearthed but energised network causing safety hazard to personnel and equipment, voltage or frequency deviations or collapses within the islanded network. As there will be a growing penetration of DGs in future power systems, traditional radial network structures will be replaced by more complicated topologies with bidirectional power flows. There will be more possible separation points within the network and each of them may trap some DGs and load which is not a case for traditional network. This may mean more frequent occurrences of islanding event and this could present greater challenges with respect to LOM protection.

Although a large proportion of DGs in terms of renewable energy are converter interfaced, this research mainly focuses on direct connected synchronous generators, as converter interfaced DGs are relatively more unstable (due to converter controllers often requiring a 50 Hz reference signal and often being unable to provide reactive power and voltage support) during islanding and therefore islanding is much easier to detect in a system where the island contains converter-interfaced sources [1.4]. Synchronous generators are relatively more likely to withstand islanding events. Frequency within the island may settle at a different operating point or drift away slowly from 50 Hz depending on its governor control strategy which makes frequency based LOM method difficult to detect, especially with fast reaction requirement. Furthermore, it can be particularly difficult to detect an island when there is a close match between DG output prior to islanding and the local load demand within the island [1.5]. A novel LOM protection algorithm on traditional

synchronous machines, which as explained earlier represents the most challenging scenario for the detection of islands, is proposed in this thesis.

1.2 Research Motivation

It is expected that massive amount of DGs will be introduced to power systems in future, as the European Union has a target of achieving as much as 20% of all generated power from renewable sources by 2020 and a massive reduction of 80-95% of greenhouse gases emitted by 2050 [1.6][1.7]. These DGs will significantly raise the risk of sustained islanding occurring. LOM protection is therefore very important to future power systems. There is of course the possibility that future systems may operate in islanded mode as well as interconnected mode (e.g. as “microgrids”) but a reliable means of detecting an islanded condition will still be required (e.g. to change control and protection settings and modes of operation when it is detected that the system has moved from interconnected to islanded operation).

Several islanding detection methods have been investigated by other researchers. Ideally, LOM protection should: not affect supplying power quality; be fast-acting; eliminate non-detection zone (NDZ – certain conditions when protection system fail to operate); avoid false tripping for non-LOM disturbances (e.g. short circuits in the vicinity of the LOP protection, large load changes); be inexpensive. [1.5]

ROCOF and VS, which are widely used at present, are both generally very sensitive (depending on their settings) to genuine islanding events and can be fast-acting (which is important if auto-reclose and fast network reconfiguration functions are used in the event of faults resulting in LOM conditions). However, the major issue with these techniques is with respect to false tripping, which may be caused due to major disturbances on the system such as fault events and load switching. [1.8]

Another major challenge for LOM protection in the future is due to decreasing system strength, in terms of both fault level and, importantly from a ROCOF LOM

perspective, the inertia in the system. This is due to conventional rotating machines used for generation of power being replaced by an increasing amount of renewable energy connected to the system using power electronics converters, which has the effect of reducing, or even eliminating, inertial response, and therefore results in the overall system frequency becoming more dynamic in nature. [1.2]

Already the maximum ROCOF that can be experienced in the mainland UK power system is increasing, and National Grid and the DNOs in the UK are already investigating the potential impact of increasing the settings on ROCOF relays from 0.125 Hz/s up to 0.5 or even 1 Hz/s in anticipation of more dynamic system behaviour in the future [1.9]. Settings of 1 Hz/s with a 0.5 s time delay have already been recommended for generators larger than 5 MW in [1.9]. Increasing the settings will of course make ROCOF relays more stable in terms of performance during non-LOM transients (e.g. faults, major load changes, loss of generation on the transmission system), but possibly at the expense of increasing the risk of non-detection. [1.10]

Therefore, a new method of LOM, ideally without the need for communications, which is both sensitive and stable under a wide range of grid “strength” (i.e. the short circuit level/ratio and inertia levels) [1.2] scenarios is extremely desirable. Developing and demonstrating such a function, using data from PMUs, which are becoming increasingly popular with system operators, is therefore the main objective of the work reported in this thesis.

A number of other research activities have been (or are still being) conducted in this area. However, there are a number of issues associated with these (details are provided in the literature review section of this thesis). Several barriers are identified to this vision:

- Active islanding detection methods are developed by injecting signals to the system with the advantage of nearly “zero” NDZ. However, power quality is unavoidably impaired by the injected signals themselves, the equipment can be expensive and possibly could be complex and relatively unreliable. Furthermore, the generic applicability of such system is questionable and there could be a degree of tuning or calibration required for different system and context applications.
- Monitoring the status of circuit breaker seems to be straightforward but it is seldom used due to the high cost and difficulties associated with deployment in a complex, and possibly changing, network – use of communications is required and the complexity grows with the number of potential “islanding” breakers and the numbers of individual DG units in various islands (and possibly sub-islands).
- A number of other techniques, each of which has relative advantages and disadvantages; these are further explained in a subsequent chapter which presents a critical review of several techniques.

Therefore, a reliable passive islanding detection algorithm with only local measurements is desired.

1.3 Principal Contributions

This thesis provides the following contributions to knowledge:

- A novel islanding detection algorithm with high sensitivity, which is fast-acting, sensitive and stable to non-LOM system events and transients has been developed, demonstrated and compared with alternative and established techniques. It is based upon the analysis of “peak ratios” of ROCOF curves immediately after the event measured from PMUs, which has not been reported anywhere before and is a completely new technique. It does not require communications, relying only on local measurement data. The operation of the proposed algorithm is compared against three competing LOM protection methods that have all been widely used by industry and/or reported in the literature: standard ROCOF, Phase Offset Relay (POR) and Phase Angle Difference (PAD) methods. The improvements offered by the new system are quantified.
- Demonstration of the performance of the system under a variety of different system “strength” scenarios to investigate its operation in future scenarios where power systems may become relatively weaker, primarily due to decarbonisation of energy sources and increasing use of power converters to interface sources (and other infeeds – e.g. HVDC links from other countries). This is achieved by varying the inertia of the grid connection in simulations.
- Demonstration of how the proposed method compare to other LOM methods under the effect of DG with different turbine governor and excitation control schemes following an islanding event. Different droops

of frequency and voltage are applied in sensitivity tests and DG performances under these droop settings are analysed in depth to reveal the influences.

1.4 Thesis Overview

The remainder of the thesis is structured as follows: Chapter 2 presents an overview of modern power transmission and distribution networks. It explains the basics operation and structure of the power system, associated protection systems and the development of the future system, focussing on the impact of DGs on power system behaviour and related protection challenges. Chapter 3 presents the LOM protection function, and introduces and compares a range of passive LOM protection methods, and explains the drawbacks associated with active methods. Chapter 4 introduces and illustrates the novel passive LOM protection algorithm, which is the main outcome of the research, in detail. It also includes the description of PMU functions and applications, and describes the M class PMUs that have been used in the tests and case studies reported in this thesis. Chapter 5 illustrates the simulation methodology including the test network, descriptions of the test scenarios, the structure of PRAM relay and the generator controller setup. Chapter 6 and 7 present and explain the results of sensitivity and stability tests conducted and compares the behaviours of all methods under study (i.e. the novel method against established existing methods). Conclusions and future work are described in Chapter 8.

1.5 Publications

The publications relating to the work undertaken and reported in this thesis are listed below.

1.5.1 Conference publications

Ding, Feng; Booth, C. D., "Applications of PMUs in Power Distribution Networks with Distributed Generation," *Universities' Power Engineering Conference (UPEC), Proceedings of 2011 46th International* , vol., no., pp.1,5, 5-8 Sept. 2011

Ding, Feng; Booth, C.D., "Protection and stability assessment in future distribution networks using PMUs," *Developments in Power Systems Protection, 2012. DPSP 2012. 11th International Conference on* , vol., no., pp.1,6, 23-26 April 2012

Ding, Feng; Booth, C.D., " The Application of Synchrophasors to Detect Islanded Conditions in Future SmartGrids," *Protection, Automation & Control World, 2012. PAC World 2012. 3rd International Conference on* , vol., no., pp.1,6, 25-28 June 2012

1.5.2 Journal publications

F. Ding, C. D. Booth and A. J. Roscoe, "Peak-Ratio Analysis Method for Enhancement of LOM Protection Using M-Class PMUs," in *IEEE Transactions on Smart Grid*, vol. 7, no. 1, pp. 291-299, Jan. 2016.

References

- [1.1] National Grid Transmission, "Wind Energy and The Electricity Network," [Online]. Available: <http://www2.nationalgrid.com/UK/Industry-information/Future-of-Energy/Future-Energy-Scenarios/> (Accessed: July 2014)
- [1.2] National Grid, "Electricity Ten Year Statement 2013" [Online]. Available: <http://www2.nationalgrid.com/UK/Industry-information/Future-of-Energy/Electricity-ten-year-statement/Current-statement/> (Accessed: July 2014)
- [1.3] Dysko, A; Booth, C.; Anaya-Lara, O.; Burt, Graeme M., "Reducing unnecessary disconnection of renewable generation from the power system," Renewable Power Generation, IET , vol.1, no.1, pp.41,48, March 2007
- [1.4] "Engineering Technical Report NO. 139: Recommendations for settings of loss of mains protection relays", Energy Networks Association, 2009.
- [1.5] J. Warin and W. H. Allen, "Loss of mains protection," in Proc. 1990 ERA Conf. Circuit Protection for industrial and Commercial Installation, London, U.K., pp. 4.3.1–4.3.12.
- [1.6] European Commission, "Renewable energy targets by 2020", [Online]. Available: http://ec.europa.eu/energy/renewables/targets_en.htm (Accessed: July 2014)
- [1.7] "EU Energy Policy to 2050: Achieving 80-95% emissions reductions," European Wind Energy Association, March 2011.
- [1.8] Ten, C.F.; Crossley, P.A, "Evaluation of Rocof Relay Performances on Networks with Distributed Generation, "Developments in Power System

Protection, 2008. DPSP 2008. IET 9th International Conference on , vol., no., pp.523,528, 17-20 March 2008

[1.9] "Engineering Recommendation G59/3 Amendment 1 - Recommendations for the connection of generating plant to the distribution network operators," Operations Directorate of Energy Networks Association, London, Engineering Recommendation 2014.

[1.10] National Grid, "Operating the Electricity Transmission Network in 2020", [Online]. Available: http://www.nationalgrid.com/NR/rdonlyres/DF928C19-9210-4629-AB78-BBAA7AD8B89D/47178/Operatingin2020_finalversion0806_final.pdf

(Accessed: July 2014)

Chapter 2

Review of LOM protection

2.1 Power System Developments

2.1.1 Future power system

Traditional generations in power system are large scale power stations fuelled by coal, gas or nuclear. These types of fuel are finite and have an emission problem of environmental pollution. New generation technologies with renewable energies, such as hydro, wind, solar and tidal, are developing fast and have been deployed all over the world. European Union targets 20 % of total energy consumption from renewable sources by 2020 and 80-95 % reduction in greenhouse gases from energy production by 2050 [1.6]. UK legislation sets a target of 15% of its energy consumption from renewable sources by 2020 and reducing at least 80% of greenhouse gas emissions in 2050 based on the data of 1990 [1.7]. An interim target of 34% reduction of emission in 2020 is also set. Figure 1 shows an estimated generation capacities categorised by fuel types under the Gone Green scenario proposed by NG. It is shown that coal fired power plants will be regularly shut down from a starting point of 20 GW decreasing to 16 GW by 2020 and to 2 GW by 2035. This is due to closures through Large

Combustion Plant Directive (LCPD) and Industrial Emissions Directive (IED) legislation [1.1]. Gas/CHP increases from 31 GW to 38 GW from 2013 to the years between 2025 and 2030. But it decreases back to 31 GW in 2035 due to shutting down of aging plant with introduction of CCS after 2030. And renewables, especially wind energy, will be massively deployed all across the UK (reaches 51 GW in 2035). Nuclear generation are expected to remain its status as the powerful ability of supplying the system and the potential intimidate to the environment both exist. Wind power has been recognised to be one of the most effective options in terms of meeting electricity demand and reducing greenhouse gases [2.4]. Figure 2 shows the installed wind generation capacity of European countries in 2013. It can be seen that a massive capacity of 121 GW of wind generation capacity has been installed in Europe, which has a growth of 25 GW in two years. Germany and Spain are two leading countries in Europe with wind generation capacity of 33 GW and 23GW, both increased by 4 GW and 1 GW. It is shown that the speed of deploying wind generation is significant.

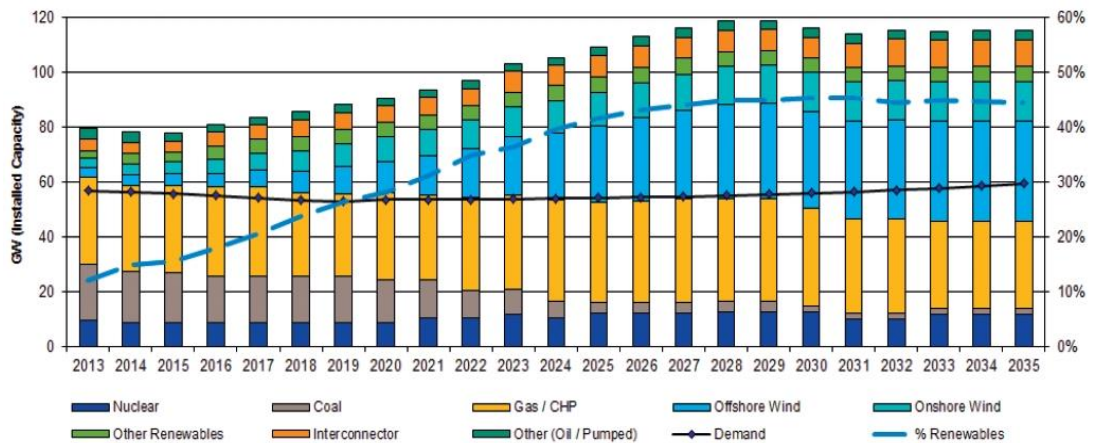


Figure 1: Estimated generation capacity in the UK by fuel types [1.1]

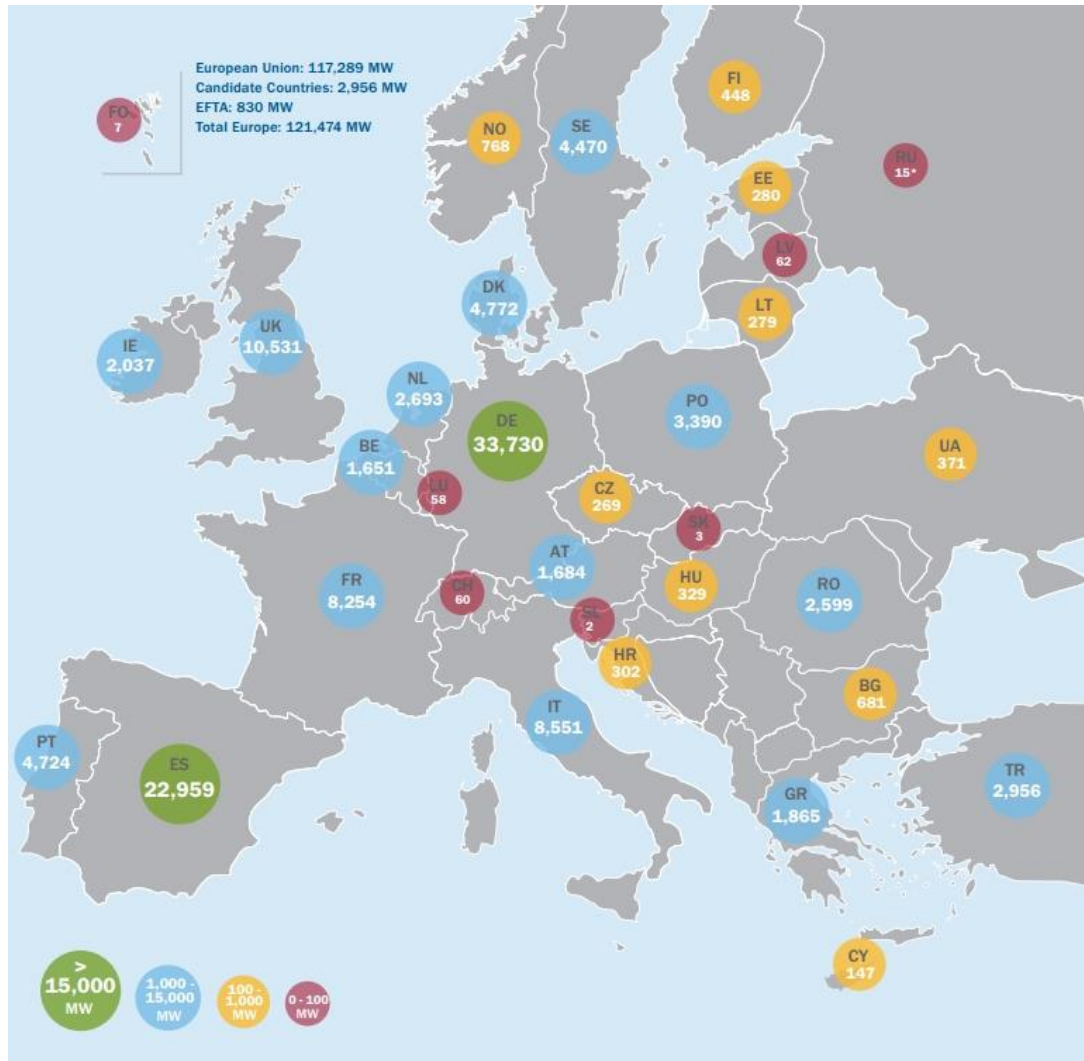


Figure 2: Installed wind generation capacity of European countries in 2013 [2.4]

It can also be seen in Figure 1 that the increase of offshore wind generation is much larger than onshore in the UK over the period to 2035, which reaches 37 GW out of 51 GW. This is due to the limited onshore sites to build wind farms but more possibilities in sea areas (offshore) for island country. Offshore grid is then designed to bring offshore wind generation to the grid and connect between countries for electricity trading. Figure 3 shows a proposed offshore grid scenario in Europe.

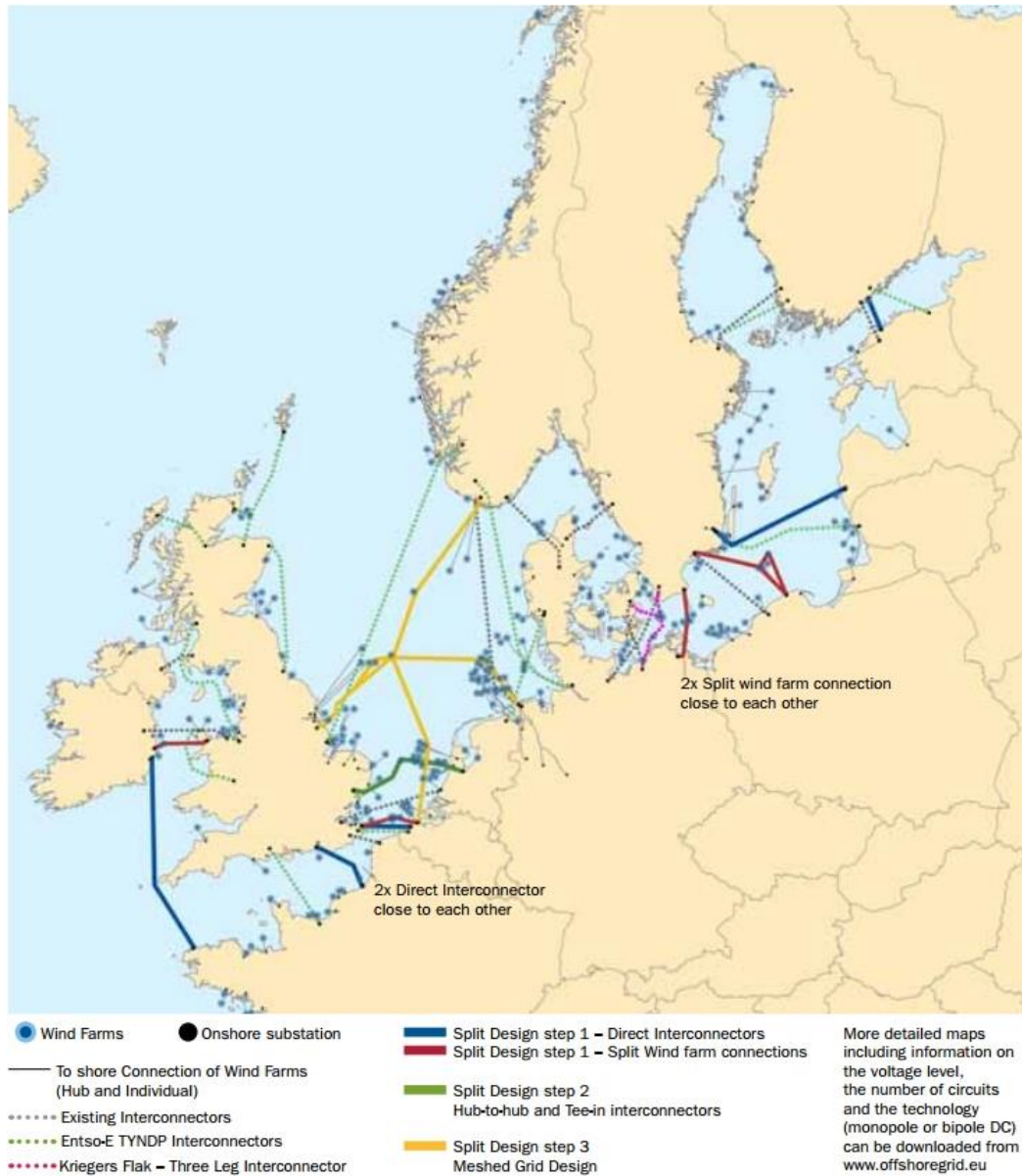


Figure 3: Proposed offshore grid scenario in Europe [2.5]

System Operability Framework (SOF) 2014 [2.6], which was published by NG, identifies how forementioned future (to 2035) energy scenario will impact on GB electricity transmission system operation. One of the most critical findings in the document is that “*higher ROCOF settings or alternative loss of mains protection approaches must be explored for new connections following the expected reduction in system inertia*” [2.6]. System inertia is “*the sum of kinetic energy stored within the rotating mass of machines (generators and motors) directly connected to the system*”

[2.6]. It is one of the key measures of system strength and contributes to system stability in frequency aspect as it provides damping to system disturbances and oscillations. Low system inertia will lead to higher ROCOF level, larger frequency deviation and rapid change of frequency. Therefore, it is very important to estimate system inertia and maintain sufficient inertia level for the possible generation and demand changes. As most sources of renewable generation are intermittent energy, power electronic devices are used to interface these types of generation to the power network. In addition, future power system will include more HVDC links due to the efficiency of power transfer, which also use power electronics. They are electrically de-coupled from system and almost contribute no inertia. Solutions for wind generation are explored and one of them is “synthetic inertia” [2.6]. It is a power electronic control scheme which quickly adjusts the active power output to comply with sudden system imbalance between generation and load, providing frequency response and acting as contributing to system inertia. However, technical issues still exist and future development of this technique is required.

As most LOM protection schemes for DGs are ROCOF, it becomes challenging when system inertia is reduced. A ROCOF level of a sudden generation loss may be largely enough to trigger LOM relay of certain DGs. Consequently, these DGs will be automatically disconnected and it may lead to the danger of cascade DG loss. Figure 4 illustrates how system inertia is predicted to change for Gone Green Scenario (most challenging case) [2.3] at 70% wind power output before 2035. It is shown in the figure that the reduction of system inertia before 2035 can be as large as 70%. According to [2.6], maintaining current ROCOF setting of 0.125 Hz/s can withstand generation loss of 922 MW for Gone Green Scenario, but can only withstand 263 MW in 2035. Even in the easiest case which is No Progression

Scenario [2.3], this setting can only withstand 397 MW of generation loss. The chance for ROCOF level exceeding 0.125 Hz/s will be 90% for Gone Green and 82% for No Progression in 2035 comparing to 19% at present. As well as generation/load change, fault initiation/clearing, reclosing of CB, transformer inrush and normal operation of switching capacitors may also falsely trigger ROCOF or other frequency based relays. The effects of these events are analysed and explained in later chapters.

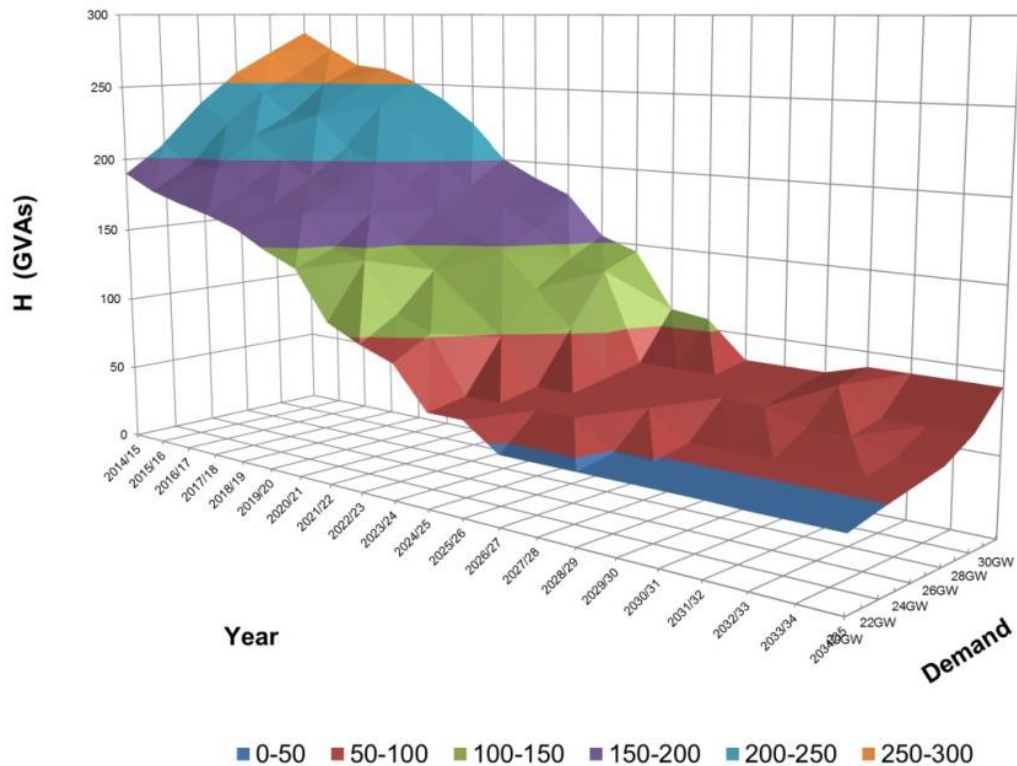


Figure 4: System Inertia (H) Changes for Gone Green Scenario at 70% Wind Power Output [2.6]

2.1.2 DG impact on power system protection

Traditional radial distribution network transports power from substation to load which makes it play a passive role in whole power system. It is reported that this structure is less reliable but less complex to adapt new demand of power system.

Protection scheme against fault is relatively simple as well, which directly isolates the faulted downstream part as there is only one direction of fault current in radial distribution network.

A large amount of distributed generation is introduced to the modern power system such as wind power generators, photovoltaic panels and small scale gas generators [2.7][2.8]. They can be installed in both transmission and distribution system. This means more links and nodes are introduced to the system and its structure is much more complicated and reverse power flow starts to appear in the network with DGs. As they are directly connected on the customer side, fault levels can be altered by many small or a few large DGs. The effectiveness of influence of DGs is different in terms of their types, sizes and placement. As renewable generation will be massively deployed and even replace conventional fossil fuelled plants in future, the overall system inertia will be significantly reduced. The rotating mass of these conventional plants are directly coupled to the system which are known as synchronous generation. Wind turbines are connected to the grid by power electronics, which de-couple their rotating mass from the grid so that they almost make no contribution to the system inertia. Photovoltaic panels have no rotating elements as well as HVDC links [1.1]. The low inertia of the system causes some system events a larger impact, such as generation or load change. These changes makes traditional protection schemes inadequate and more complex protection function design is required.

DG is designed to provide active power along the feeder and can be divided into certain types according to its technologies which are photovoltaics, wind turbines, fuel cells, small and micro sized turbine modules, sterling-engine based generators, and internal combustion engine generators. In the UK, DG can also be categorized as

micro (1W~5kW), small (5kW ~5 MW), medium (5 MW ~50 MW), and large (50 MW ~300 MW). [2.9]

The advantages of introducing DG to distribution network are: [2.10]

- Support of voltage
- Reduction of power losses as a lot of DGs are directly connected in distribution system
- Capacity release of transmission and distribution network
- Adaption of development of transmission and distribution infrastructure
- Improvement of network reliability
- For the implementation of renewable energy sources, emissions can be effectively reduced.

The potential problems for introducing DG to the network are: [2.10]

- False or nuisance tripping
- Blinding of protection
- Increased or decreased fault levels
- Unexpected islanding
- More harmonics are introduced
- The prohibition of automatic reclosing
- Unsynchronised reclosing

It is recognised that distributed generation has a significant impact on the protection distribution networks.

The key protection issues for the consideration of engineers are:

- Short circuit power
- Fault current level
- Device discrimination
- Reduction in reach of overcurrent and impedance relays
- Direction of power flow and voltage profile
- False tripping
- Mal-operation of auto reclosures

1) Blinding of protection

Blinding of protection occurs when the protection device fail to react to fault current. Figure 5 shows an example of blinding of protection in a distribution network with DG connection when a fault exists. It is shown that the total fault current is only partly observed by the protective device with DG contributing the other part. And DG normally supports voltage so that a smaller voltage depression can be “seen” from the relay. This causes the relay only react to fault closer to the measuring point which means a reduction of protection reach.

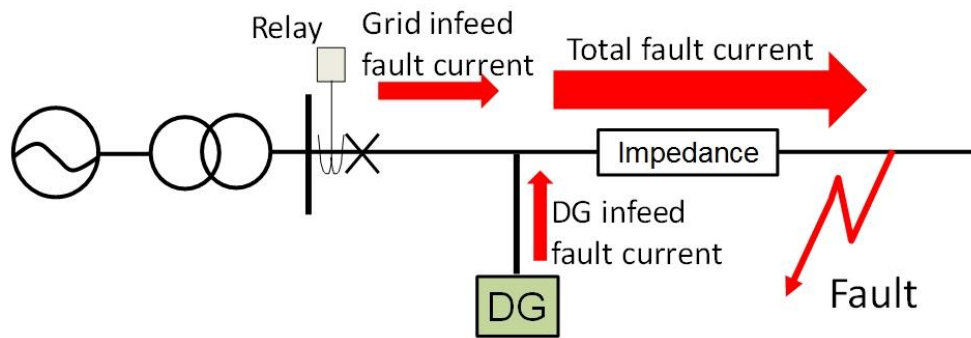


Figure 5: Example of blinding of protection when distribution network with DG connection experience a fault

2) Discrimination of protection devices

As mentioned in blinding of protection, fault current magnitude at each path can be altered by DG. This may cause problems for several coordinated protection devices on traditional network scheme. Figure 6 shows an example of discrimination problem of protection in a distribution network with DG connection when a fault exists. If DG does not exist, relay 2 should isolate the fault quickly and relay 1 should provide backup after a certain time delay. When DG is connected to the network, relay 2 should adjust its setting and can still detect the total fault current and react quickly. However, once relay 2 refuses to operate, relay 1 will have a problem of isolating the fault (either not able to detect or takes a long time to trip) as it can only detect part of the total fault current.

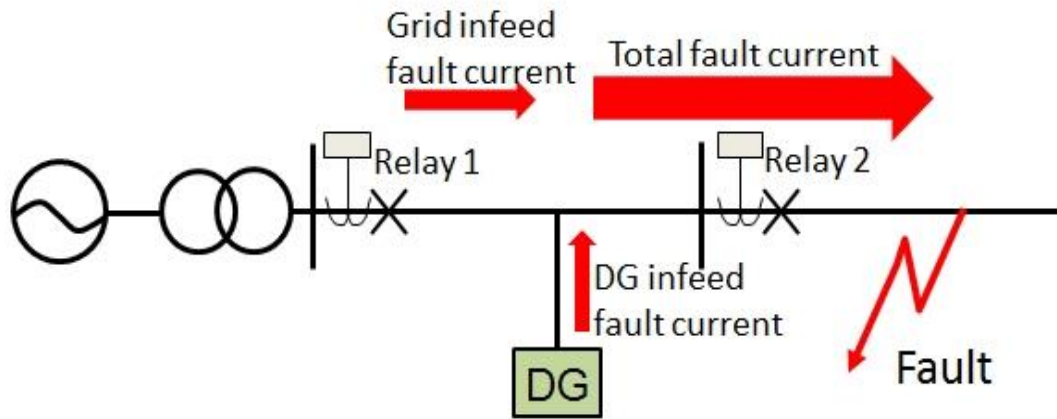


Figure 6: Example 1 of discrimination issues of protection devices

Another example of discrimination problem is shown in Figure 7. If DG does not exist, relay 3 should quickly isolate the fault and relay 2 should provide backup with a time delay. When DG is connected to the network at the position shown in Figure 7, relay 3 should adjust its setting to react to the fault. However, a large current contribution from DG may cause relay 2 to react to fault as quick as relay 3 and part of the system is unnecessarily isolated.

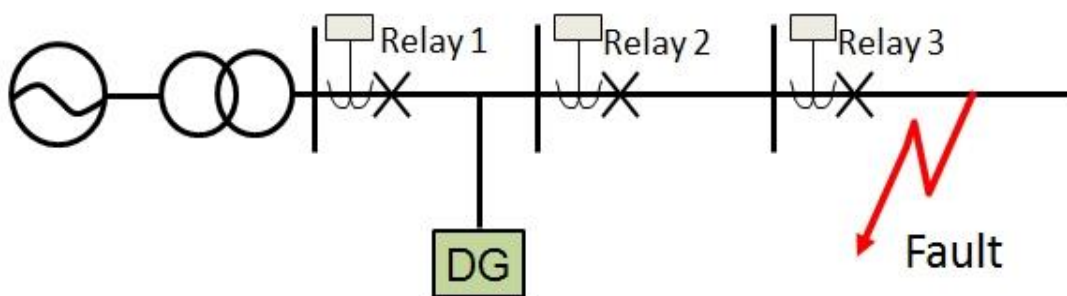


Figure 7: Example 2 of discrimination issues of protection devices

3) False tripping

DGs not only alter the magnitude of fault current, but also sometimes diverse the power flow at each path so that false tripping may happen. Figure 8 shows a two feeder distribution system with DG connected to one feeder. Once a fault occurs at feeder 2, relay 2 should quickly isolate the fault. But in this scenario, DG in feeder 1 may supply the fault current with the grid so that protective Relay 1 may trip and feeder 1 is unnecessarily isolated. This problem may be solved using directional overcurrent relay to block the detection of reverse fault current but some drawbacks have been recognised. This method may change the protection against bus faults and directional overcurrent relay is always more expensive and has a longer response time. And other devices may also be affected such as fuse and breaker.

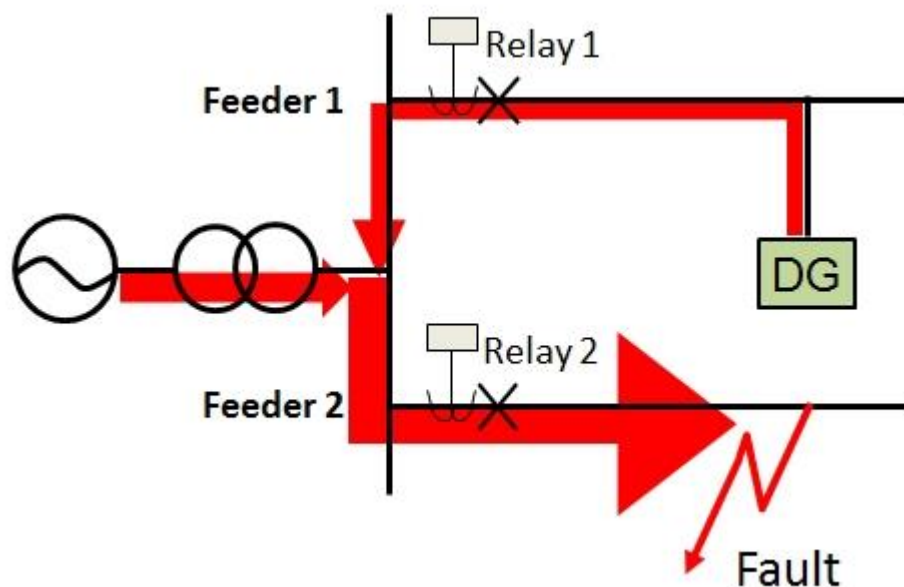


Figure 8: Example of false tripping in two feeders distribution network.

2.2 Introduction to LOM

LOM (islanding) occurs when part of the utility network containing DGs is disconnected from the remainder of the system, which is usually, but not always, caused by a system fault. Figure 9 illustrates a simple example of an LOM event. When CB 1 opens, the DG and both feeders form an islanded network. It is not permitted for DGs continuously energising the islanded network in the majority of utility systems throughout the world for following reasons: [2.10]

- System within the island may not be effectively earthed as, often, distributed generation is either not earthed or supplies the system through a step up transformer, the HV side of which is delta connected and/or not earthed [2.12]. This clearly increases the risk of undetected faults, rise of “earth” potential in premises and electric shocks.
- Unsynchronised reclosures may occur between islanded networks and the main grid of the power system. When LOM occurs, the frequency of DG within the islanded network will drift away from the main grid frequency. A subsequent reclosure with a significant angular and/or frequency difference across both systems being reconnected may lead to a large arcing current, possible generator damage and damage to switchgear and other equipment.
- Utility personnel may believe the system is not energised while it is actually live and potential safety issues to both personnel and equipment.

- Faults within an islanded network may not be detected as fault level can be drastically reduced compared to operation in grid-connected mode. This is dependent on the type and capacity of DGs in the island.

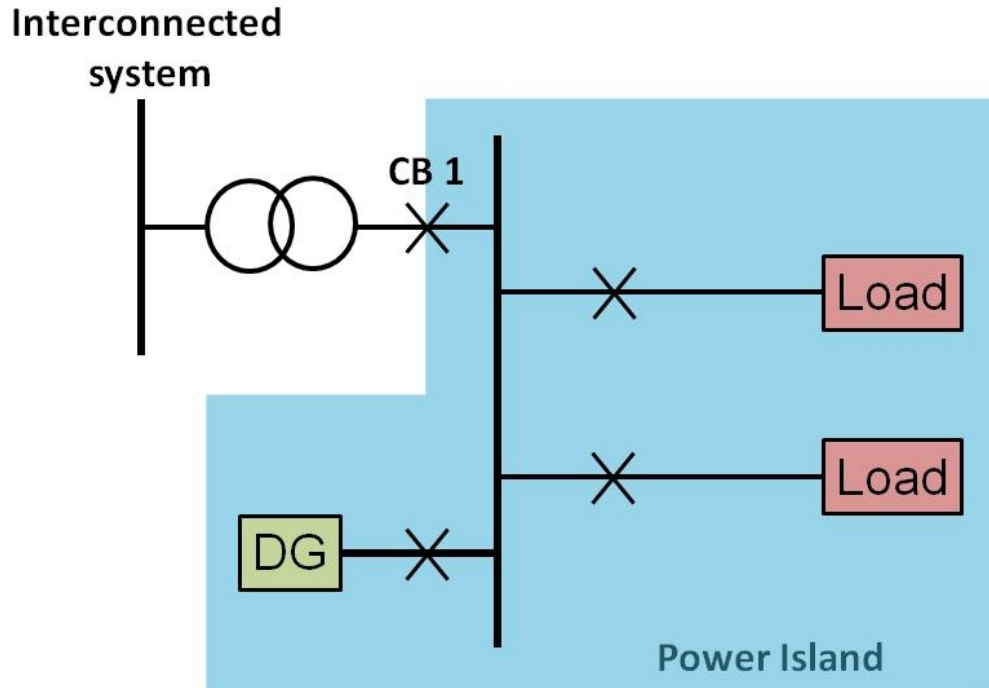


Figure 9: Illustration of LOM event

As significant amounts of DG are introduced to the power system in future, the number of potential faults may increase in the system and raise the risk of more frequent islanding events. Furthermore, many DGs use renewable energy sources, the vast majority of which will be interfaced to the system using power electronics, which contribute no or marginal inertia, reducing the overall inertia levels of the power system [1.1]. LOM protection is therefore very important to future power systems and methods based purely on ROCOF. It could be at risk from lower system inertia levels causing false operation during non-islanding transients (e.g. load changes, remote loss of generation or load). These events might have severe consequences if large amounts of DG are disconnected inadvertently due to incorrect operation of LOM protection.

There are two main aspects that should be taken into consideration in terms of evaluating a LOM protection system performance of its algorithm: [2.14]

- Sensitivity: the ability of the LOM protection to detect all islanding events correctly, regardless of the pre- or post-islanding conditions.
- Stability: the ability of the LOM protection to remain stable for non-islanding transient events such as remote loss of infeed/load, large changes in load, power quality disturbances such as increases in harmonics/interharmonics, short circuit faults that do not lead to islanding, etc.

LOM protection methods can be divided into two categories: [2.10]

- Passive methods: the decision-making within the LOM protection is based solely on local measurements of system data.
- Active methods: signals may be injected to the system to assist with the detection of islanding. (Reviewed at the end of this section.)

Passive LOM methods generally measure system parameters and process them and compare with certain threshold values. They are relatively low cost to implement and have no impact on the system performance, power quality or operation. The main challenge for passive detection methods is to detect islanding when the local load closely matches the generator output both in terms of active and reactive power prior to the islanding event occurring. Theoretically, when there is no power flow through the interconnecting CB (CB 1 in Figure 9), there should be no detectable change (in voltage/frequency/power etc.) in parameters measured locally at the DG if this breaker opens. The level of imbalance between islanded load and generator DG

output prior to islanding, below which LOM protection is not able to detect the islanded condition is defined as the “non-detection zone” (NDZ). Several passive methods have difficulties associated with NDZ. Furthermore, passive methods may sometimes mal-operate in response to non-islanding system disturbances and other events.

Active methods have been developed as an attempt to overcome the challenges associated with passive methods, most notably the NDZ problem. Active methods normally involve some form of perturbation injection to the system and use the observed response to differentiate between islanded and grid-connected states. Based on reviewed literature, the opening of a circuit breaker which leads to islanding event is also included as perturbation. As long as the algorithm focuses on identifying a system parameter change in response to a signal injection to the system, it is categorised as active method. Several active methods have been reported:

- Reactive power export error detection method [2.15]: this method using a reactive power export error detector to control DG excitation current, which is no longer supported once the DG is disconnected from the main grid. This method is reported to be highly sensitive but it takes several seconds to react.
- Impedance measurement method using an injected signal [2.16]: this method simply approximates the difference of part of the system impedance prior and after islanding event. This method is sensitive, fast acting and stated stable to system disturbances. However, it requires high frequency voltage signal injection equipment to generate ripple signal which is proportional to system impedance so that higher detection

accuracy can be achieved. Therefore, it directly influences the power quality.

- Slip-mode frequency shift algorithm (SMS) [2.17]: this method only applies for converter-interfaced generators. It implements the SMS algorithm through the design of input filter of inverter control to generate a positive feedback to destabilise the inverter during islanding mode. When islanding occurs, the frequency of isolated network is forced to drift away from nominal. The SMS algorithm is only driven by a perturbation generated by noise, measurement and quantisation errors. This method has the advantage of simple implementation with high sensitivity. However, the modification with positive feedback to inverter control not only decreases power quality, the risk of unstable transient responses at grid connected mode for other disturbance is increased. Furthermore, it is reported that the possibility of stable operation (NDZ) of an inverter is still possible in islanded conditions in some circumstances.
- Active frequency drift (AFD) [2.18][2.19]: the AFD method generally implements its algorithm within a microprocessor-based controller of an inverter to slightly modify the output current by expanding its zero-crossing (narrows each half-sinusoidal). This subsequently causes frequency measurement error and triggers the islanding detection algorithm when the DG disconnects from the main grid while it is impossible to modify system frequency at grid connected mode. The benefit of this method is that it is easy to implement, but degrades the output power quality. In addition, the potential for an NDZ still exists and

the capability of detection is degraded when multiple DG controllers attempt to drift the system frequency in opposite directions which makes this method difficult to be extensively deployed.

- Automatic phase-shift (APS) [2.20][2.21] : APS is also known as modified SMS, which is designed to address the NDZ problem for SMS and AFD by recording the accumulated voltage phase angle shift instead of the frequency shift. The perturbation generation process is similar to that used in the SMS method, but the accumulated voltage angle can still violate necessary thresholds even when the frequency remains stable at a slight off-nominal level. The shortcomings, except for power quality problem, it is difficult to cope with a nonlinear load with large inertia such as an induction motor (phase angle according to operating frequency and its difficult to control) [2.21].
- Pulse current injection based method [2.22]: this method generates pulses on output current from the inverter and estimates the magnitude of voltage responses. As the system impedance, measured from the DG terminals, is typically lower in grid connected mode, the voltage response to current pulse injection is expected to be relatively lower in grid-connected mode, but relatively higher in islanded mode. The advantage of this method is that it is fast-acting with small NDZ. However, a pulse generator is needed and it directly affects power output quality. Furthermore, the impedance threshold needs to be calibrated and measured for every network topology which makes it impractical to implement on a wide scale.

A detailed review of these techniques is not included in this thesis as the main disadvantage for active methods is the degradation of either local power quality or the performance of the power system. Power quality is normally affected during the modification of voltage or current waveform by injecting high frequency signal [2.16], applying chirps [2.17][2.20][2.21] or increasing the zero-crossing interval [2.18][2.19]. System performance is usually influenced by injecting disturbance signals [2.15][2.22] so that generator response can be captured by LOM protection. Some of the methods also require equipment to either inject additional signal or modify the inverter control. In addition, the main active methods reviewed do not yet fully eliminate the problem of NDZ. Finally, many techniques may require calibration or setting for each application, therefore making their widespread adoption impractical. The following section will review existing passive LOM protection techniques and methods proposed by other researchers in more detail.

2.3 Passive LOM Techniques and Methods

2.3.1 Rate of change of frequency (ROCOF)

A sudden imbalance between the input mechanical power (for a conventional synchronous machine driven by some form of turbine generator) and load will lead to a frequency change at the generator output. The equation for approximating the initial ROCOF in response to a generation-load imbalance is as shown below: [2.23]

$$dROCOF = \frac{\Delta P \cdot f}{2 \cdot G \cdot H} \text{ Hz/s} \quad (1)$$

Where:

ΔP is the change of active power output, f is system frequency, G is the nominal generator rating and H is the inertia constant of the generator.

Methods based on analysis of ROCOF represent the most commonly deployed LOM protection technique. A ROCOF relay is normally installed at the terminals of a DG unit and estimates or calculates the rate of change of frequency from measurements. If the ROCOF exceeds a predetermined value (sometimes for a specified time duration), which is deemed to be indicative of an islanded condition, then a trip signal is initiated to isolate the DG from the system by opening the circuit breaker at the point of connection between the DG and the main utility power system. ROCOF at a specific time k can be estimated as follows:

$$ROCOF = \frac{f_k - f_{k-NT}}{NT} \text{ Hz/s} \quad (2)$$

NT represents the length of measuring window which includes N cycles. A trip signal is initiated once a pre-set ROCOF threshold is violated; as mentioned previously, a time delay can be applied to enhance the stability of ROCOF-based protection (i.e. the ROCOF must remain constantly above the threshold value for a specified duration), but this may be at the expense of sensitivity and speed of operation.

Commercially-used ROCOF relays may employ different algorithms for estimating system frequency and calculating ROCOF [2.24]. Thus the response of different relays from different manufacturers, with the same applied setting and with the same system event can be different. Two main frequency determination techniques are described below:

- Zero crossing: these techniques estimate frequency by counting the number of samples which represents the time interval between zero crossings detected on measured voltage waveform as shown in Figure 10.
- Fourier transform: this technique is based on estimating the phase angle of the fundamental frequency component by monitoring the voltage waveform using a Fast Fourier Transform (FFT). A change in phase angle from a nominal initial value associated with 50 Hz (or the reference frequency) can be used to calculate frequency deviations and hence new values of frequency.

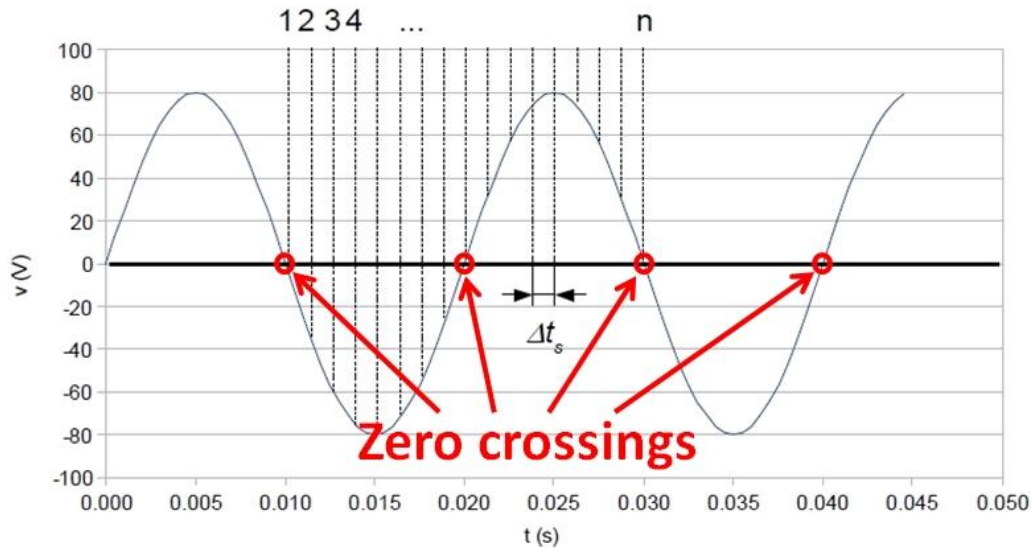


Figure 10: Zero crossing estimation method

The sensitivity and stability of ROCOF relays are highly affected by the configuration of the algorithm and the settings, which include parameters such as measuring window length, frequency measurement/estimation techniques, threshold settings and time delays. For the same sampling frequency, a longer measuring window typically possesses a higher estimation accuracy as it involves more samples. However, the response time will be delayed as a consequence of this. In the UK, the measuring windows used appear to range from 2 to 100 cycles based on a fundamental frequency of 50 Hz [2.23].

A lower threshold setting obviously increases the sensitivity of a ROCOF relay. However, it also increases the likelihood of mal-operation during other non-LOM disturbances and system events (i.e. the relay will exhibit relatively lower stability). The presented minimum setting recommended by Engineering Recommendation G59 is 0.125 Hz/s in mainland GB utility systems[2.31]. A longer time delay setting will result in higher stability of ROCOF-based protection, but may be at the expense of lowered sensitivity and longer tripping times for genuine islanding event.

It is often reported that ROCOF is sensitive and exhibits fast tripping during genuine islanding events, and the fact that no communication is needed is often stated as a benefit. However, it suffers from stability problems during faults and load changes – particularly when the overall system inertia is reduced as there will be more renewables connected in the future [2.23]. In the UK, ROCOF settings of 1 Hz/s with a 500 ms time delay have been proposed for future applications [2.25]. However, applying such settings will mean that the LOM protection will obviously be much less sensitive to true islanding events. While this could solve the stability problem, it has the potential to greatly decrease sensitivity and lead to much larger NDZs for detection of islanding conditions, which could be a potentially dangerous situation.

2.3.2 Vector shift (VS)

Vector shift (VS), or voltage vector shift (VVS), which is also widely deployed in practical applications, measures voltage phase angle changes over consecutive cycles (or half cycles) at the terminals of the DG. The value of phase shift (or “jump” as it is sometimes referred to) is then compared with a predetermined threshold, and if the threshold is exceeded the relay will trip – this is based on the premise that the impedance of the system when measured from the DG may change significantly when the system becomes island and therefore the voltage angle of the generator’s output will “shift” or “jump”. Zero crossing techniques are normally used to estimate the phase angle in VS relays. The principle of VS is illustrated in Figure 11. When islanding occurs, the impedance “seen” by the DG changes. The current in the circuit changes from I_1 to I_2 . As the electromotive force E_1 remains constant, the DG’s terminal voltage changes from V_1 to V_2 with an angle difference θ . Commercially-

used VS relays have a measurement window of one cycle and update once per zero crossing (i.e. once per half cycle) of the measured terminal voltage. The typical threshold settings applied to VS relays range from 2° to 20° [2.26].

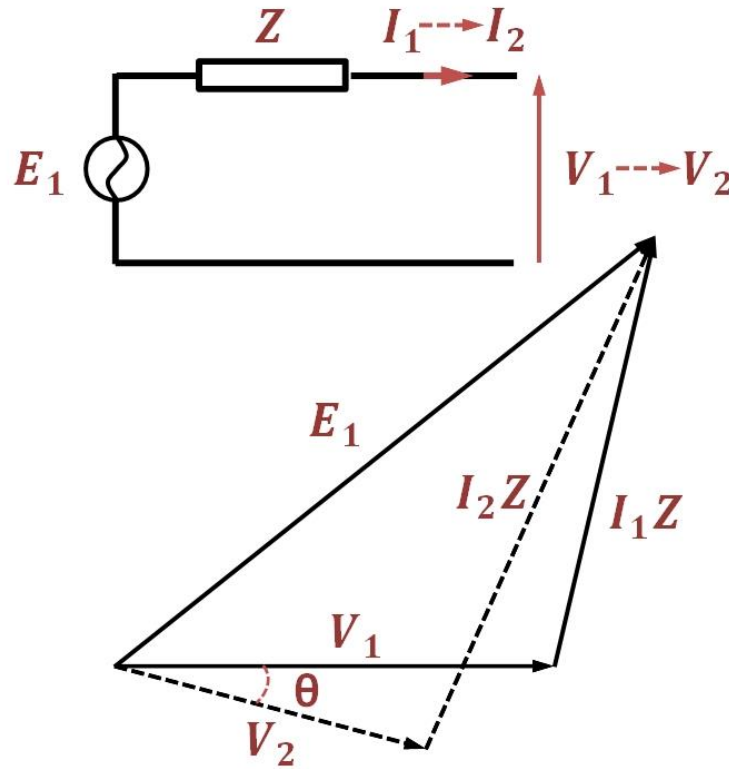


Figure 11: Principle of vector shift method during islanding event

It is reported that VS relays can operate very quickly when compared to other methods because of the short measurement window. The VS relay is relatively stable to changes in the rate of change of frequency so may be more immune to non-LOM transients. Another benefit of VS relays (as with ROCOF-based techniques) is that no communication facilities are required. However, VS is less sensitive to genuine islanding events than ROCOF and is reported as suffering from relatively larger NDZs than ROCOF techniques. Furthermore, VS relays are often reported as exhibiting unstable performance in response to network faults [2.26].

2.3.3 Reverse var¹ method

The reverse var technique monitors the reactive power generated by a DG and if this exceeds a predetermined threshold, a trip signal will be sent to isolate the DG. The principle of reverse var method is illustrated in Figure 12. As shown in the figure, in grid connected mode, reactive power consumption across the network is mainly supplied by the grid and DGs typically contributes solely active power, operating at a power factor of close to unity. When the network is islanded, the DG may be required to deliver reactive power to meet load demand and support the local voltage (although often DGs cannot provide this support, and will disconnect anyway).

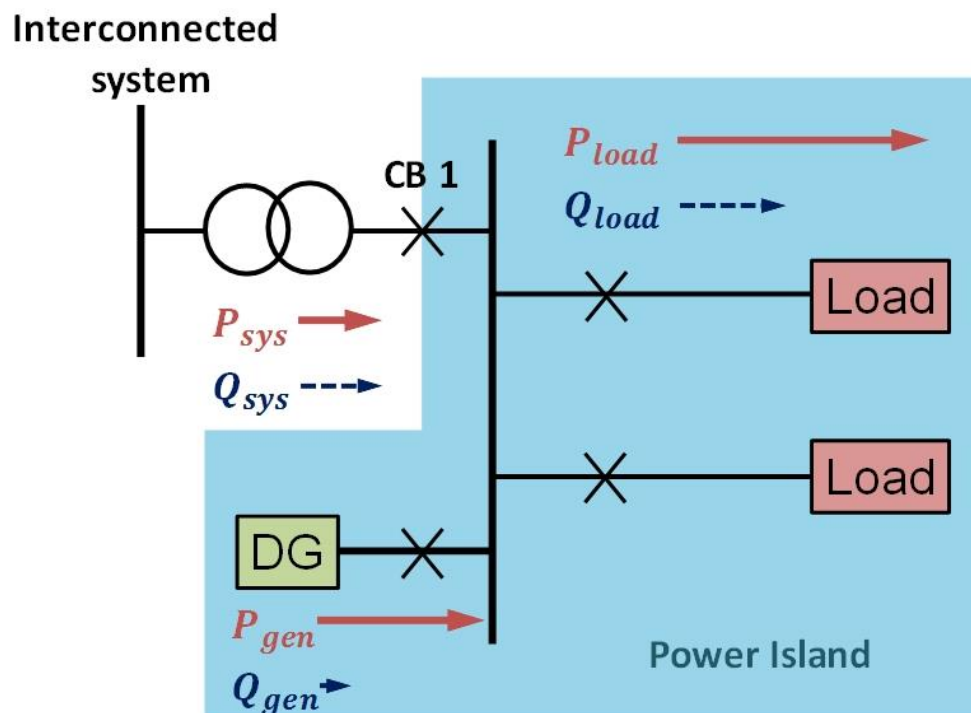


Figure 12: Principle of reverse var method

¹ Note that the term “var” (as opposed to “Var”, “VAR” or “VAr”) in lower case is used throughout, in accordance with the Council Directive on units of measurements 80/181/EEC [2.27].

The implementation and algorithm used in the reverse var method is simple, as it directly measures reactive power output of the DG. However, major drawbacks can be identified with this method. Firstly, it is highly dependent on the reactive power consumption level of the load which may be trapped in an island. If the reactive consumption of the load is low, reactive power output of the DG may be insufficient to trigger reverse var relay during an islanding event. For example, the capacitance of the cables is able to contribute to a large portion of the reactive power consumption. Furthermore, in some distribution networks, reactive power compensation devices are installed to support reactive power. When massive amounts of DG are introduced into the power system in the future, DGs will share reactive power output during islanding, causing difficulties to the reverse var relays. Finally, the reactive power demand in the UK appears to have significantly reduced in recent times as shown in Figure 13. It is clear that the reactive power demand is reduced by around 7 GVar between 2005 and 2016. The reduction of reactive demand is mainly attributed to higher energy efficiencies of loads, widespread adoption of LED and fluorescent lighting and the use of variable speed drives from large machines [2.13]. It is anticipated that the reactive power demand will continue to decrease in future. For all of the reasons mentioned above, it is proposed that reverse var method is not suitable and therefore it is not widely used.

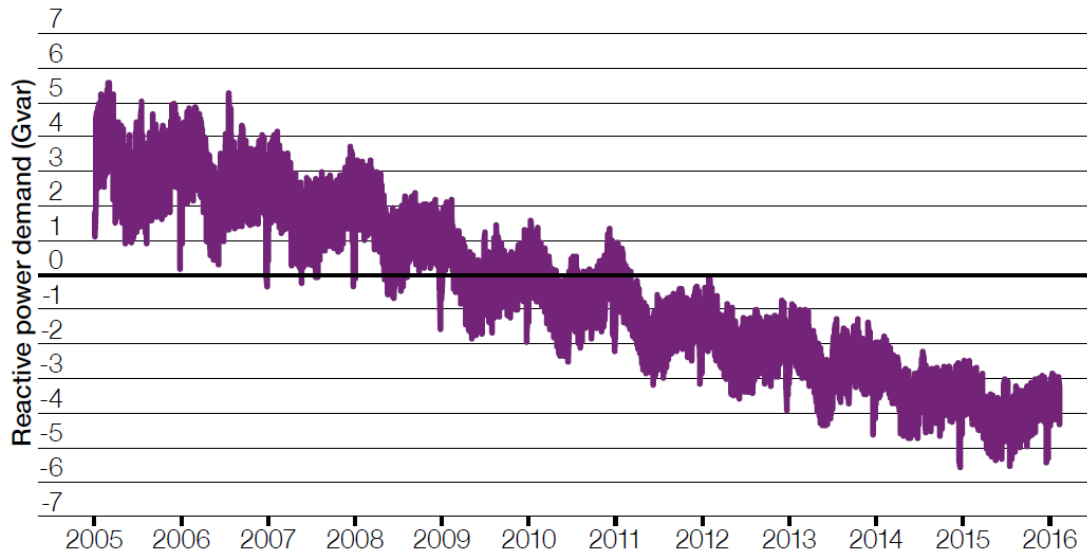


Figure 13: Reactive power demand

2.3.4 Direct inter-tripping

Some may propose inter-tripping techniques to be active, but as they do not inject any signals to the primary power system, these techniques are deemed to be passive in this dissertation. Direct inter-tripping schemes detect the opening of contacts at the point of disconnection that may lead to potential islanding and sends a signal to all DGs that may be “trapped” in an island. The principle of direct inter-tripping scheme is illustrated in Figure 14. As shown in the figure, any of CB 1, CB 2 and CB 3 opening will lead to DG involving in an islanding event. Thus the opened CB should send a signal to isolate the DG from the network. The media used for communication links include leased land line, radio, microwave, power line carrier and fibre [2.28].

Direct inter-tripping scheme seems to be the most straight forward method, since it does not depend on any measurements and the operation is almost instantaneous. However, drawbacks have been reported. First of all, the cost of the scheme is relatively high as communication links are introduced. Every CB which could potentially lead to islanding event should be linked to all DGs involved. With

massive amount of DGs being introduced to the system and network structures becoming more complicated, a significant number of links might be required which possibly making costs and maintainability prohibitive.

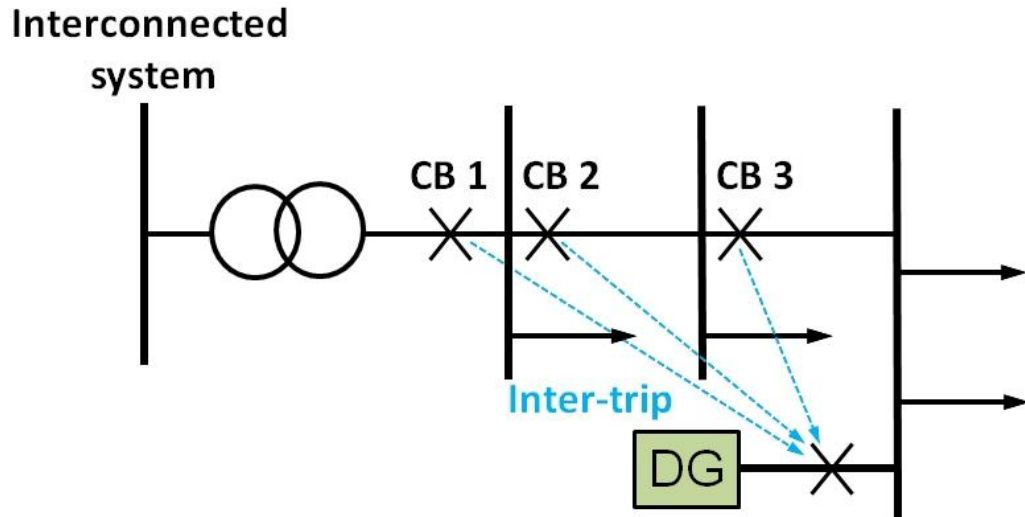


Figure 14: Principle of direct inter-tripping scheme

2.3.5 Over/under voltage and over/under frequency

Over/under voltage and over/under frequency protection are not dedicated LOM protection functions, but can perform LOM detection in certain circumstances. It is the most basic protection method and widely used across power systems and particularly to generation units, as voltage and frequency are the most important indicators of power system stability and general health. During an islanding event, the frequency of DG tends to drift away from nominal and the terminal voltage may increase or decrease depending on imbalance between DG output and load. Therefore, this protection scheme is often used as a general protection system for DG and includes the LOM function.

The main benefit of this protection scheme is low cost and simple implementation as voltage can be directly measured and frequency can be estimated locally. However, a large NDZ is often associated with these types of protection, as can be deduced from analysis of Table I which recommends the protection settings for DGs [2.29][2.30][2.31][2.32]. These settings will only result in tripping for islanding event where a very large imbalance between local generation and load exists, and it may take a long time to react. Therefore, over/under voltage and over/under frequency protection can only be applied as a backup to LOM protection in the majority of cases, unless it is deemed that generation within the island is incapable of supporting an island in any case, where under and over-frequency may suffice.

Table I: Settings recommended for DGs in G59

	G59/1 - 1991		G59/2 -2010 (Small LV connected DG)		G59/3 -2014 (Small LV connected DG)	
	Setting	Time delay	Setting	Time delay	Setting	Time delay
UV stage 1	-10% V_n	0.5 s	-13% V_n	2.5 s	-13% V_n	2.5 s
UV stage 2	-	-	-20% V_n	0.5 s	-20% V_n	0.5 s
OV stage 1	+10% V_n	0.5 s	+10% V_n	1.0 s	+14% V_n	1.0 s
OV stage 2	-	-	+15% V_n	0.5 s	+19% V_n	0.5 s
UF stage 1	47.0 Hz	0.5 s	47.5 Hz	20 s	47.5 Hz	20 s
UF stage 2	-	-	47.0 Hz	0.5 s	47.0 Hz	0.5 s
OF stage 1	50.5 Hz	0.5 s	51.5 Hz	90 s	51.5 Hz	90 s
OF stage 2	-	-	52 Hz	0.5 s	52 Hz	0.5 s

2.3.6 Rate of change of output power (ROCOP)

ROCOP generally monitors the fluctuation of DG output power. As an islanding event occurs, DGs obviously supply any load trapped in the island and a mismatch between pre-island output power and load will cause a change in the output of the DG when islanding occurs. In grid connected mode, a load change should not affect the DG output as significantly as it will when the system is islanded, due to the grid infeed acting to meet any changes in demand along with the DG(s). [2.33] and [2.34] describe and show the results of tests of the ROCOP algorithm. The flow chart of the ROCOP algorithm is shown in Figure 15. The instantaneous power is first derived from voltage and current measured at the terminal of DG and then the rate of change of power is calculated. The rate of change of power is then integrated over a moving window and if the absolute value of the calculation exceeds a pre-set threshold, then a tripping signal is issued by the relay. The adaptive clipping algorithm is used to limit the magnitude of rate of change of power signal during sub-transient response of the generator and its effect can be minimised.

It is shown in [2.34] that ROCOP could react to an islanding event within 120 ms, which is relatively very fast, and it remains stable to unbalanced local load changes and single-phase fault. However, the tests indicated that it successfully operated for a 10% increase of output in a laboratory generator test environment and a 50% decrease of output in a diesel-driven generator (3.75 MVA), both caused by islanding events. These results were not really conclusive in terms of proving adequate sensitivity and 50% change in output is rather significant – it is not clear whether the system would be sensitive to smaller changes in load post-islanding. Furthermore, the tests only indicated that ROCOP was stable to single-phase fault; no other fault types were tested. In terms of load changes, there was a reduction of effectiveness

with balanced load changes. With large increases in DGs in future, the power output of DGs may be subject to more frequency fluctuations under non-islanded conditions in future and this could make the use of ROCOP impractical.

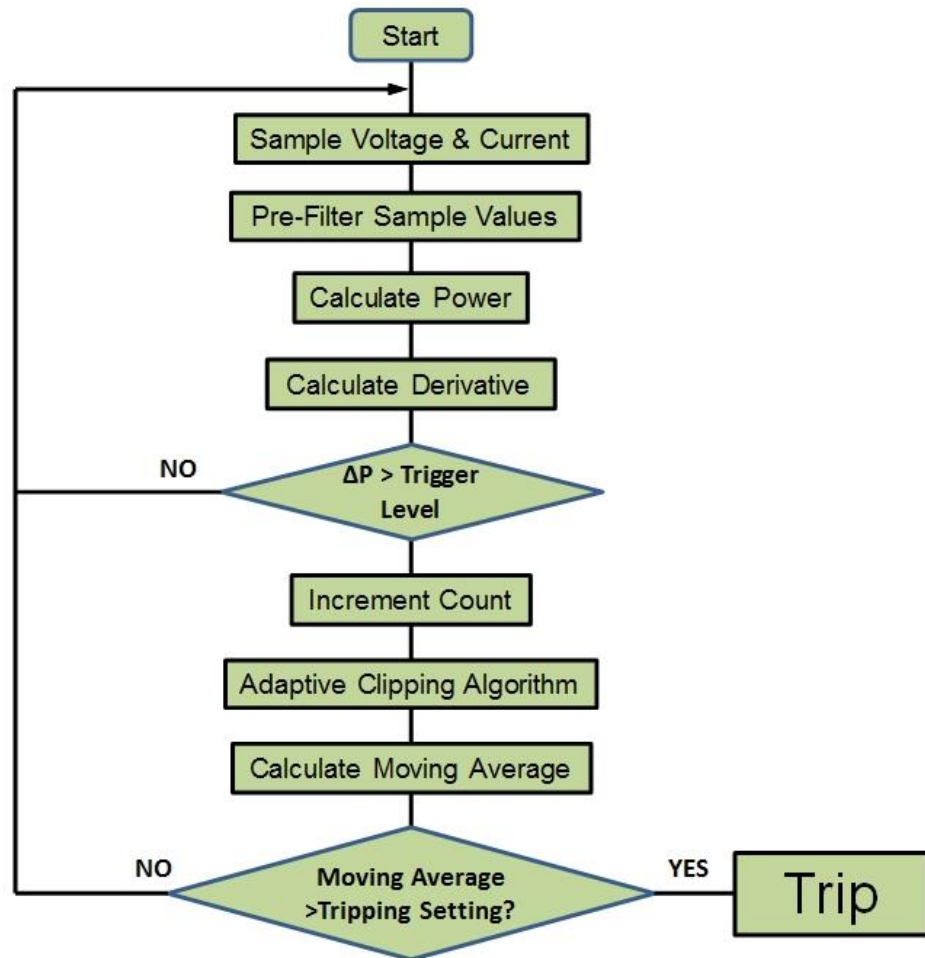


Figure 15: Flow chart of ROCOP algorithm [2.34]

2.3.7 Rate of change of voltage (ROCOV)

The principle of ROCOV is monitoring the fluctuation of voltage at the terminals of a DG. The derivative of voltage over a moving window is calculated and compared with a pre-set threshold. If the threshold is violated, a tripping signal is

issued and an islanding event is presumed to have occurred. This method is simply implemented and can be fast acting and sensitive if the threshold is set to a small enough value. However, false trips for other system events such as load changes and fault condition are reported. [2.35] proposed a hybrid detection technique which enhanced the stability of ROCOV. The flow chart of the algorithm is illustrated in Figure 16. The algorithm first measures voltage and calculates ROCOV for every cycle. If ROCOV is non-zero, another ROCOV over 5 cycles, $Av5$, is calculated and compared with two thresholds (V_{SMin} and V_{SMax}). If it is smaller than V_{SMin} , the algorithm concludes that no islanding event has occurred. If it is larger than V_{SMin} , the algorithm suspects islanding or some other event such as a load change may have occurred. $Av5$ is then compared with a larger threshold V_{SMax} and if this threshold is violated, an islanding event is detected and a tripping signal is issued. If $Av5$ lies between V_{SMin} and V_{SMax} , a function termed real power shift (RPS) is applied. The RPS changes the real power output and the terminal voltage of one of the DGs. A ROCOV over 20 cycles ($Av20$) is then calculated and compared with a threshold under RPS scenario, V_{SMaxU} . If it is violated, islanding event is indicated and tripping signal is sent.

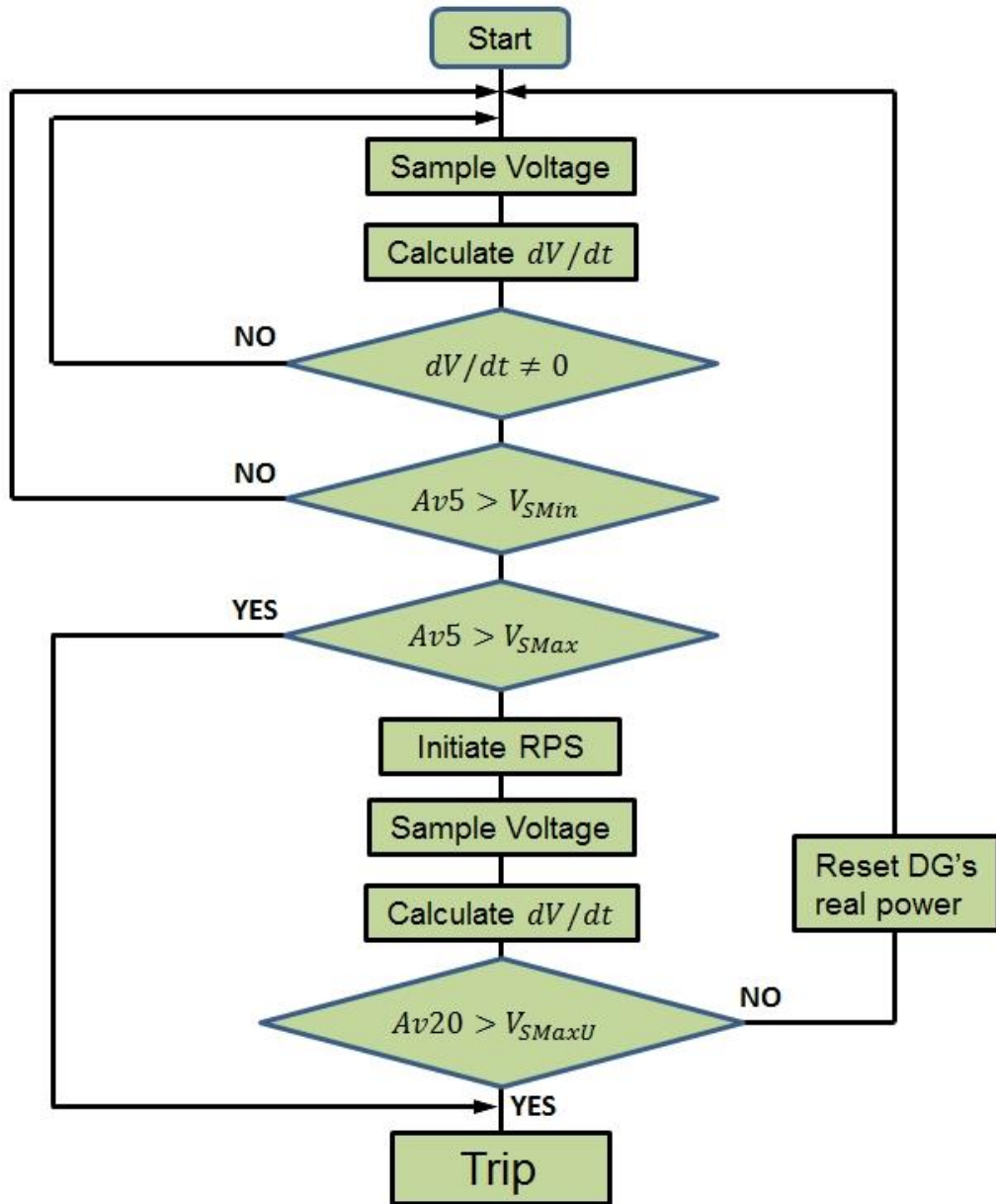


Figure 16: Flow chart of ROCOV based hybrid method [2.35]

This algorithm was tested in [2.35] and showed a very small NDZ which almost equal to zero. It is also shown how it could be stable for load changes, faults, induction motor starting exercises and generator switching events. However, this technique is only practical in certain distribution networks that contain synchronous generator-based DG where the active power output can be intentionally adjusted.

Furthermore, the method is relatively slow, relies on DG output being modified and this is deemed not to be a practical solution – the cost of integrating the scheme with a generator controller (and the ability of the generator output to be modified) is also not considered.

2.3.8 Rate of change of frequency over power

[2.36] proposed an islanding detection method termed “rate of change of frequency over power” (ROCOF/ROCOP). The flow chart of the algorithm is shown in Figure 17. The algorithm first measures voltage and current and detects if there is a zero crossing in the voltage signal. The rates of change of frequency and of change of real power output of the DG are then calculated once a zero crossing is detected. The detection index D is then derived which represents the rate of change of frequency over power (ROCOF/ROCOP). If D exceeds a pre-set threshold D_{th} , a counter starts to increment. If the increment number N violates another threshold N_{th} , a decision that an islanding event has occurred is issued and a tripping signal will be sent to the breaker.

It is explained in [2.36] that this method is very sensitive and fast acting and that it could be sensitive to pre-islanding power imbalances of down to 1% with approximately 100 ms detection time. It is stated that the method is stable for a sudden local load change of 100% DG output, total system harmonic distortion up to a level of approximately 6% and for 10% voltage sags. However, fault events, which often lead to waveform discontinuities, larger sags than 10% and phase angle changes which can masquerade as large ROCOF values (depending on the measurement algorithm used) and could lead to mal-operation are not investigated. Accordingly, the ability of the algorithm to survive under non-LOM transient

conditions is questionable. For example, a large load loss in somewhere of the system could lead to a frequency swing of the whole system, which would challenge this and other frequency based methods. Furthermore, large amount of DGs with renewable sources, which are likely to have changeable outputs with time, will challenge this algorithm.

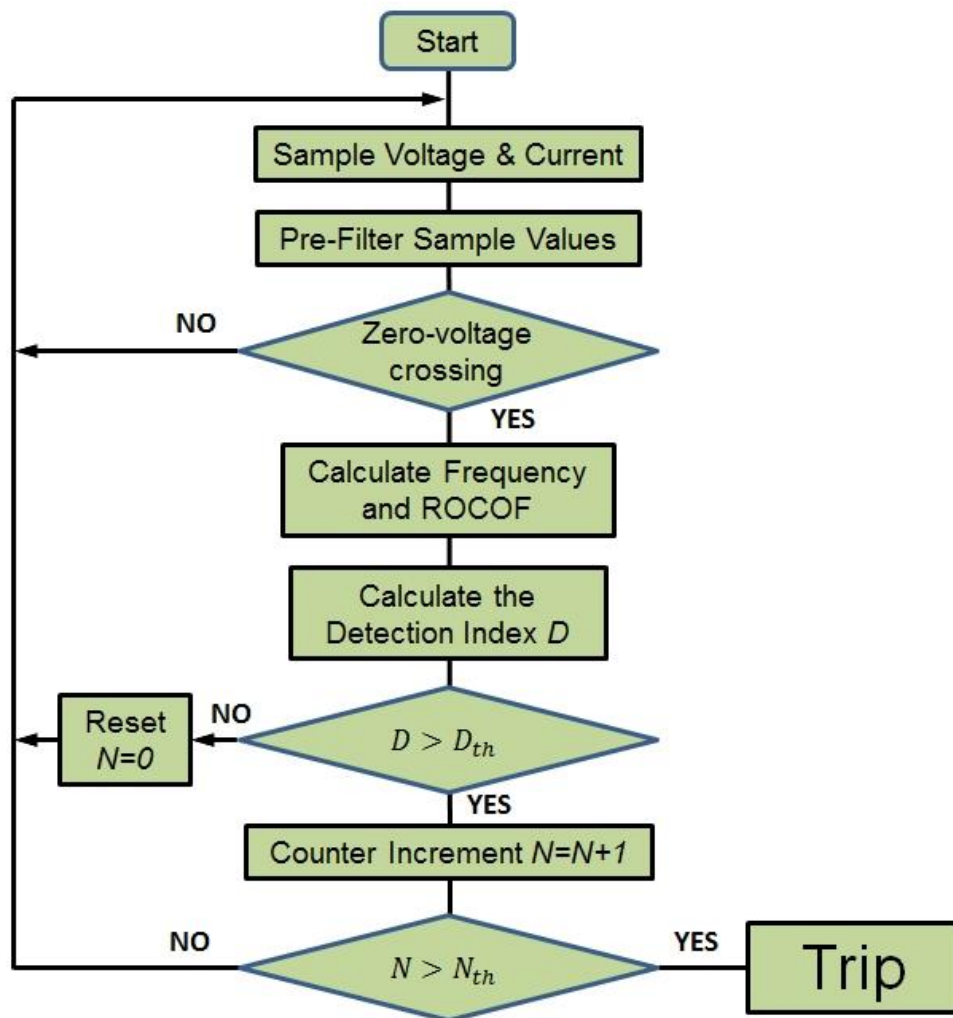


Figure 17: Flow chart of rate of change of frequency over power [2.36]

2.3.9 Voltage unbalance and evaluation of total harmonic distortion (THD) in the measured currents

[2.37] proposes an islanding detection algorithm which evaluates the combination of three parameters that are indicative of system status. The evaluation criteria are listed below:

- **Voltage unbalance variation:** the principle underpinning the evaluation of this parameter is that an islanding event will change the topology of the network and causes variation in voltage unbalance. The ratio of negative sequence to positive sequence voltages is calculated based on a one-cycle average window. A deviation of this ratio from the reference at steady state and normal loading conditions is also estimated. If the deviation of the ratio is within the range of -100% to +50%, the reference will be replaced by the estimated value at followed cycle. It also has a function to eliminate any abrupt changes of unbalance ratio within a relatively short time periods in order to avoid inaccurate measurements.
- **THD variation of the current:** the principle of evaluating this parameter is that an islanding event normally leads to variation on harmonics of the current. A ratio of rms value of the harmonic components (from 2th to 31th in [2.37]) and fundamental component is calculated based on a one-cycle average window. A deviation of this ratio from the reference at steady state and normal loading conditions is also estimated. If the deviation of the ratio is within the range of -100% to +75%, the reference will be replaced by the estimated value at followed cycle. It also has a function of eliminating the abrupt changes of THD ratio to ride through system transients.

- Three-phase voltage magnitude variation: This parameter is calculated as the three-phase average rms value of line to line voltage.

The first stage of this algorithm is check if the three-phase voltage unbalance is lower than 0.5 pu. If it is then a decision is made that indicates an islanding event. If it is not, the second stage of checking deviation of current THD (-100% to +75%) and deviation of voltage unbalance (-100% to +50%) is performed. If both parameters violate their pre-set thresholds, the algorithm determines an islanding event.

[2.37] states that this algorithm is very sensitive and fast acting and presents three tests, all of which result in tripping in 129 ms and it is shown how the system remains stable for scenarios of load changes. However, the levels of imbalance in the reported islanding tests are not quantified (only the breaker opening positions are indicated) and the level of maximum load changes (balanced or unbalanced) that the algorithm can remain stable for. Furthermore, fault events and other system events that can cause large harmonic levels were not reported in this paper. It is anticipated that this algorithm will suffer under three-phase fault conditions which would cause a large voltage depression. Furthermore, single-phase and phase to phase faults tend to cause voltage imbalance and increase the harmonic level which could also challenge the proposed algorithm.

2.3.10 Accumulated phase angle drift method

[2.38] proposed an islanding detection method which termed accumulated phase angle drift. The block diagram of the algorithm is shown in Figure 18. The principle of the phase angle drift method is comparison of estimated accumulated phase angle drift from a presumed reference value to a threshold. The circular buffer is used to

store frequency values as historical data which are measured within a time window with fixed length. It should be noted that the data in circular buffer keeps updating and the future grid frequency is continuously predicted by the grid frequency estimator. The accumulated phase angle drift is derived via a phase angle calculation block from the local system frequency and the frequency predicted. During an islanding event, the frequency of the island tends to drift away from the main system frequency as shown in Figure 19. At time n , estimated grid frequency f_n^{est} is calculated from the historical data over the time window T_W . T_D is the time band from the end of time window to n . f_n is the measured frequency at local. The phase angle deviation is estimated from the frequency difference and accumulated to compare with the threshold.

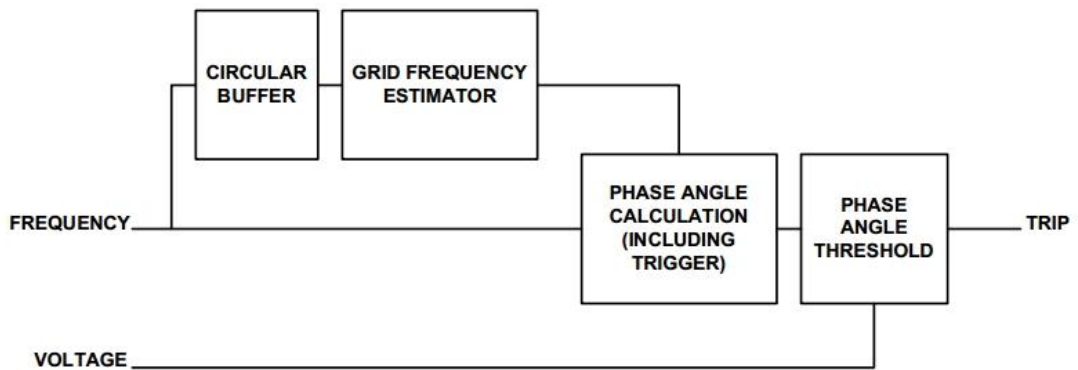


Figure 18: Block diagram of PAD [2.38]

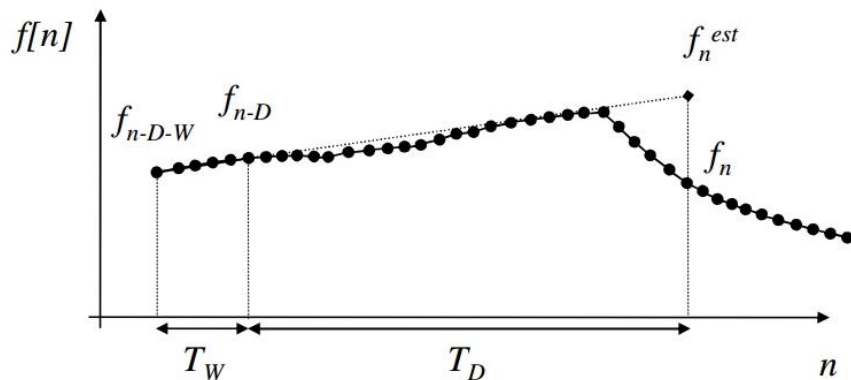


Figure 19: Illustration of frequency estimation [2.38]

[2.38] and [2.39] introduced several tests in terms of sensitivity and stability. It is shown that the algorithm is very sensitive and can detect islanding within 500 ms with a 2.5% pre-islanding imbalance using a threshold setting of 10° . It is also shown that it can ride through the majority of three phase faults. However, it is also stated in [2.39] that one of the two frequency fluctuation events caused the phase angle to accumulate to a maximum value of 40° . The algorithm survived during the event of small frequency fluctuations with largest variation from 49.965 Hz to 49.69 Hz, also accompanied by a large voltage dip. The event which caused the large phase angle accumulation was a bipole tripping on the UK-France interconnector on 28th September 2012 and the frequency reduced by 0.337 Hz over a period of 5.483 s. This means a larger threshold needs to be chosen to ride through large frequency disturbances, but this comes with a penalty of sacrificing sensitivity. Theoretically, a disturbance in the system such as a large generation loss will lead to a change of overall system frequency but the local prediction will be “blind” as historical data is used. This increases the risk of PAD relay tripping when it should not, and this risk may increase as overall system inertia reduces in the future.

2.3.11 Phase offset relay (POR)

[2.40] proposed an islanding detection algorithm which uses the measurement of frequency at the DG location. The flow chart of the detection procedure is shown in Figure 20. The frequency at the DG location is first estimated and ROCOF is calculated. If ROCOF is larger than a pre-set trigger threshold, $R_{trigger}$ (over a fixed trigger window), the frequency offset is calculated by integrating ROCOF over a time window. The phase offset Φ is calculated by integrating the frequency offset

and compared to an angle threshold, Φ_{th} . If the threshold is violated, an islanding event is determined and a trip signal will be issued.

One benefit of this technique is its ability to reject system noise. Although the calculation of frequency can involve noise and further calculation of ROCOF can amplify the effect of noise, the double-integral will substantially reduce the noise. As this method is compared with the algorithm proposed by the author of this thesis, the performance of POR will be further explained in the tests presented later in this dissertation.

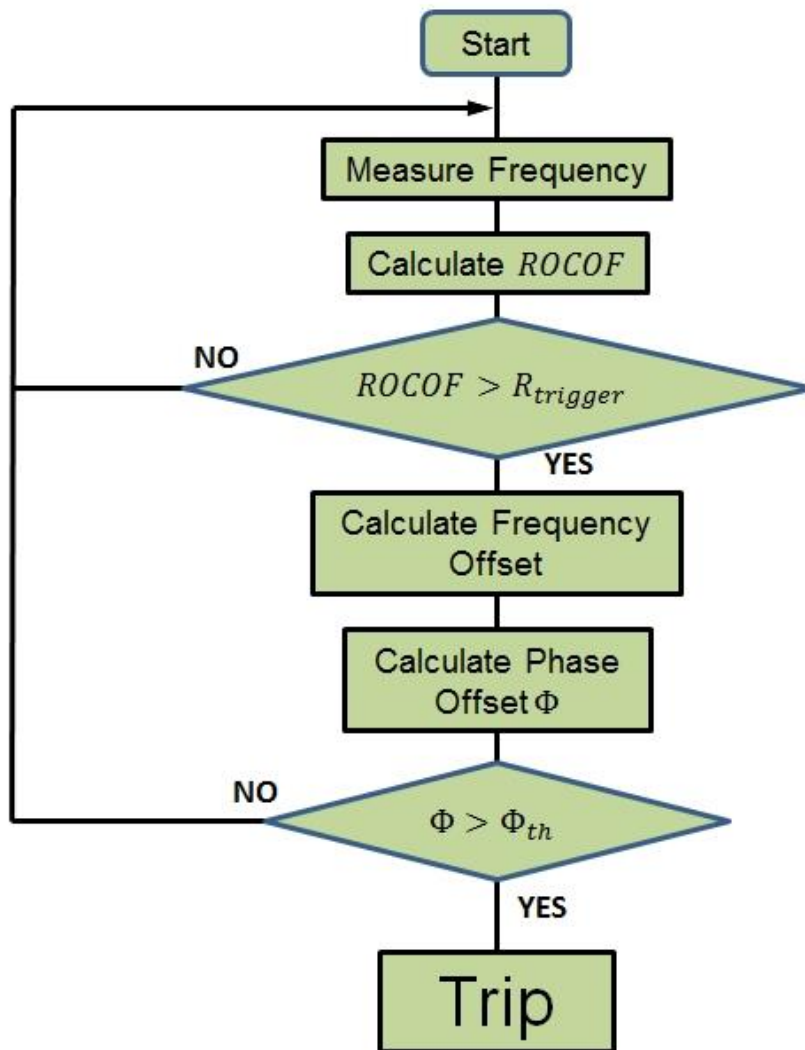


Figure 20: Flow chart of POR algorithm

2.3.12 Method based on Tufts-Kumaresan (TK) signal

[2.41] proposed an islanding detection method based on the Tufts-Kumaresan (TK) signal. The protection scheme is shown in Figure 21. The DG frequency is processed using parallel paths of analysis and the first path analyses for simple over/under frequency protection. This path ensures the sensitive performance of algorithm under islanding events with large power imbalances. The other path first monitors frequency deviation from nominal and if the absolute value exceeds 0.01 Hz, the TK process is triggered to further analyse the frequency signal and generates two coefficients (δ_1 and ω_1). These coefficients generally represent the damping factor and the oscillation frequency of the frequency deviation in response to system disturbances including islanding. If $\delta_1 > 0$ while $\omega_1 < \omega_L$ or $\omega_1 > \omega_U$, the algorithm remains stable. Otherwise it is an indication of an islanding event and a trip signal will be sent.

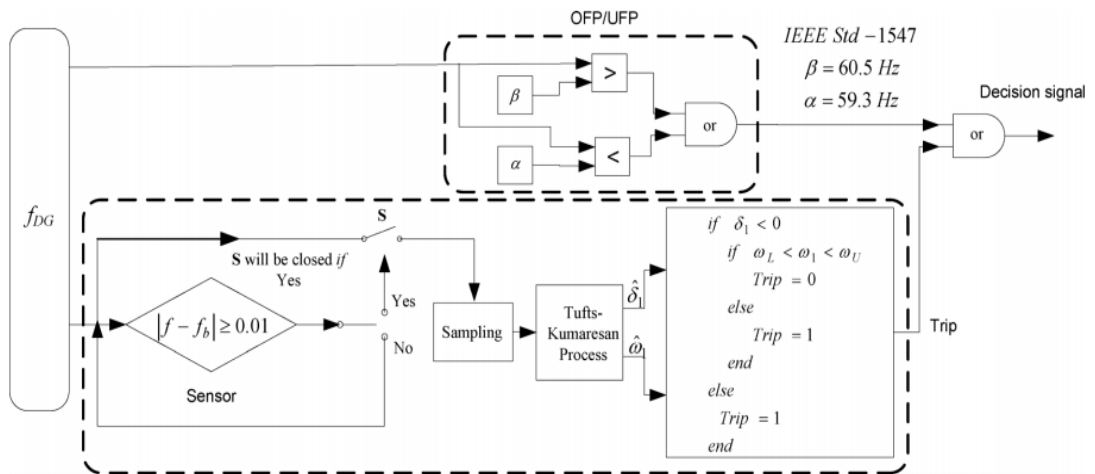


Figure 21: Schematic of islanding detection method based on TK signal [2.41]

This method had been compared to other two methods in [2.41]. One is the commonly-used ROCOF and the other is the aforementioned ROCOF over power (Section 3.2.8). It is explained that this method is fast acting and has a smaller NDZ

than the other techniques that is compared with while remaining very stable under other system disturbances including capacitor bank switching, load changes and different types of fault. However, it should be noted that the TK process will always pick up when the power system is running at off-nominal frequency with deviations of greater than 0.01 Hz from nominal. Furthermore, the thresholds ω_L and ω_U need to be trained during system simulations and a bespoke version of the method is required for every installation – this is not practical and if the system changes then the method would need to be re-trained. General thresholds are not applicable.

2.3.13 Data-mining-based relay

[2.42] proposed a data-mining-based anti-islanding protection relay. It extracts 27 features based on pre-processed voltage and current signals measured at the DG terminal as illustrated in Figure 22. A decision tree, which is shown in Figure 23, is then generated during training considering these features to determine if an islanding event is initiated.

The relay performance was compared with ROCOF and ROCOV. It is explained in [2.42] that the data-mining-based relay was fast-acting and achieved almost 100% performance levels in terms of sensitivity and stability. However, only load changes were considered for tests. The ability of rejecting harmonic/inter-harmonics and riding for system frequency events and faults were not mentioned at all.

customers with rotating machines which may also infeed to the fault, which could cause damage. If the system topology becomes more complicated over time, a CB opening does not effectively mean a presence of islanding, and the potential for a three-phase to ground fault to be supplied by the main grid exists. This system is therefore not practical and could be potentially dangerous.

Interconnected system

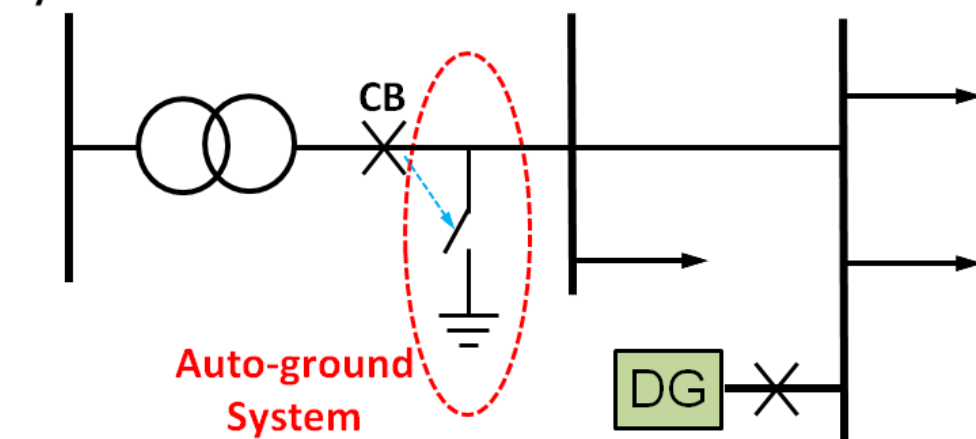


Figure 24: Illustration of auto-ground system [2.43]

2.3.15 Frequency difference method

[2.44] proposed a frequency difference method which directly measures frequencies at different sites with frequency disturbance recorders (FDR) installed. It compares the frequency at every single FDR site to the median frequency which is calculated from all FDR sites. If any of the differences exceeds a threshold of 20 mHz over a time duration of 3 s, an islanding event is indicated and all DGs in that FDR area will trip.

This method can be accurate for islanding events and stable for generation trip events, load shedding events, or system oscillation events. Experience of the

application of the system in America is presented in [2.44]. However, an acting time of 3 s is relatively slow and violates the required time (2 seconds by IEEE 1547 [2.45]). The most significant barrier to the scheme is high cost through the need for communications link. The system tends to mitigate the risk of islanding on a regional basis as (the area around an FDR site) as opposed to protecting a single DG unit. Installing one FDR per DG would be very costly and would require large amounts of data and calculations to obtain median frequency.

2.3.16 Change of phase angle difference method (PAD)

[2.44] proposed an islanding detection method based upon change of phase angle difference. PAD directly compares the voltage angle difference between two buses (one in the potential island and one in the main grid system) over a time window of 3 s. An islanding event will clearly lead to a large accumulation of phase angle difference between the two buses. The time delay of this scheme is 3 s and the threshold of the change of angle difference is set to 30° .

As this method is compared with the algorithm proposed by the author of this thesis, the performance of PAD will be further explained in the tests and analyses presented later.

2.4 Summary of Review

ROCOF is a long-established technique and still the most widely used as it represents the best local-measurement scheme and a broadly-acceptable compromise between performance (sensitivity and stability) and cost. Many other techniques have been proposed by researchers, but they all suffer from various drawbacks associated with sensitivity, stability, or cost (or combinations of all three). Furthermore, the reduction in system inertia that is anticipated in the future will further challenge frequency-based techniques and the potential for false operation (or no operation if settings are increased significantly) will increase. Accordingly, there remains a need to research and develop new techniques that can correctly identify LOM under all scenarios, including low system inertia, and that remain stable to non-LOM transients.

Table II: Comparison of reviewed passive LOM techniques and methods

Techniques and Methods	Sensitivity	Stability	Operating Time	Relative Cost	Comments
ROCOF	Sensitive (depends on setting)	Mal-operate for system disturbances (depends on setting and location/type of disturbance)	Fast	Low	
VS	Not sensitive	Mal-operate during fault	Fast	Low	
Reverse Var	Can be insensitive for low reactive power consumption	Can be unstable during load change	Fast	Low	
Direct Inter-tripping	Very sensitive	Very stable	Fast	High	Affected by network topology
Over/Under Voltage/Frequency	Insensitive	Very stable	Fast	Low	Less stable with lower system inertia
ROCOP	Can be insensitive (depends on generator type)	Can be unstable under balanced load an performance under faults other than single phase is not mentioned	Fast	Low	Can be affected by renewable DG
ROCOV	Sensitive	Stable	Fast	Low	Synchronous generator required and it needs to adjust DG output
Rate of Change of Frequency over Power	Sensitive	Performance not mentioned during faults	Fast	Low	Synchronous generator required

Voltage Unbalance and THD of Current	Sensitive	Performance not mentioned during faults and load change	Fast	Low	
Accumulated Phase Angle Drift	Sensitive	Can be unstable during large load change and frequency fluctuation	Fast	Low	
POR	To be compared to the algorithm proposed in this thesis			Low	
Method Based on TK Signal	Sensitive	Can be unstable when system is operated at off-nominal frequency	Fast	Low	No commonly suggested thresholds
Data-mining-based Relay	Sensitive	Performance not mentioned during faults and wide frequency events	Fast	Low	
Auto-ground	Very sensitive	Very stable	Instant	Low	Potentially introduce three-phase fault to the network and can be affected by topology
Frequency Difference	Sensitive	Stable	Slow	High	
PAD	To be compared to the algorithm proposed in this thesis			High	

References

- [2.1] European Commission, "Renewable energy targets by 2020" [Online]. Available: http://ec.europa.eu/energy/renewables/targets_en.htm (Accessed: July 2014)
- [2.2] European Wind Energy Association, "EU Energy Policy to 2050: Achieving 80-95% emissions reductions", March 2011.
- [2.3] *Electricity Ten Year Statement 2013* [Online]. Available: <http://www2.nationalgrid.com/UK/Industry-information/Future-of-Energy/Electricity-ten-year-statement/Current-statement/> (Accessed: July 2014)
- [2.4] The European Wind Energy Association, "Thirty Years Growing Together", Annual Report, 2013 [Online]. Available: http://www.ewea.org/fileadmin/files/library/publications/reports/EWEA_Annual_Report_2011.pdf (Accessed: July 2014)
- [2.5] Decker, J.D.; Kreutzkamp, P., "Offshore Electricity Grid Infrastructure in Europe", Offshore Grid Report, Oct 2011 [Online]. Available: http://www.ewea.org/fileadmin/ewea_documents/documents/publications/reports/OffshoreGrid_report.pdf. (Accessed: July 2014)
- [2.6] National Grid, "System Operability Framework (SOF) 2014" [Online]. Available: <http://www2.nationalgrid.com/UK/Industry-information/Future-of-Energy/System-Operability-Framework/> (Accessed: August 2015)
- [2.7] Hlatshwayo, M.; Chowdhury, S.; Chowdhury, S.P.; Awodele, K.O.; "Impacts of DG penetration in the reliability of Distribution Systems," *Power System Technology (POWERCON), 2010 International Conference on*, vol., no., pp.1-8, 24-28 Oct. 2010

- [2.8] Morren, J.; de Haan, S.W.H.; "Impact of distributed generation units with power electronic converters on distribution network protection," *Developments in Power System Protection, 2008. DPSP 2008. IET 9th International Conference on* , vol., no., pp.664-669, 17-20 March 2008
- [2.9] Guidance Notes - Synchronous Generating Units [Online]. Available: <http://www2.nationalgrid.com/UK/Services/Electricity-connections/Compliance/> (Accessed: July 2014)
- [2.10] Hussain, B.; Sharkh, S.M.; Hussain, S.; Abusara, M.A, "Integration of distributed generation into the grid: Protection challenges and solutions," *Developments in Power System Protection (DPSP 2010). Managing the Change, 10th IET International Conference on* , vol., no., pp.1,5, March 29 2010-April 1 2010
- [2.11] Dysko, A; Booth, C.; Anaya-Lara, O.; Burt, Graeme M., "Reducing unnecessary disconnection of renewable generation from the power system," *Renewable Power Generation, IET* , vol.1, no.1, pp.41,48, March 2007
- [2.12] Siemens, "Planning of Electric Power Distribution" [Online]. Available: http://w3.siemens.com/powerdistribution/global/EN/consultant-support/download-center/tabcardpages/Documents/Planning-Manuals/Planning_of_Electric_Power_Distribution_Technical_Principles.pdf
Accessed: July 2015
- [2.13] (2017, January). *Electricity Ten Year Statement 2016* [Online]. Available: <http://www2.nationalgrid.com/UK/Industry-information/Future-of-Energy/Electricity-ten-year-statement/Current-statement/>
- [2.14] Dysko, A; Booth, C.; Burt, AG.; Yip, H. T., "Testing methodology for LOM protection performance assessment," *Developments in Power System*

- Protection (DPSP 2010). Managing the Change, 10th IET International Conference on* , vol., no., pp.1,5, March 29 2010-April 1 2010
- [2.15] J. Warin and W. H. Allen, “Loss of mains protection,” in *Proc. 1990 ERA Conf. Circuit Protection for industrial and Commercial Installation*, London, U.K., pp. 4.3.1–4.3.12.
- [2.16] P. O’Kane and B. Fox, “Loss of mains detection for embedded generation by system impedance monitoring,” in *Proc. 6th Int. Conf. Developments in Power System Protection*, Mar. 1997, pp. 95–98.
- [2.17] Liu, F.; Kang, Y.; Zhang, Y.; Duan, S.; Lin, X., "Improved SMS islanding detection method for grid-connected converters," *Renewable Power Generation, IET* , vol.4, no.1, pp.36,42, January 2010
- [2.18] Lopes, L. A C; Yongzheng Zhang, "Islanding Detection Assessment of Multi-Inverter Systems With Active Frequency Drifting Methods," *Power Delivery, IEEE Transactions on* , vol.23, no.1, pp.480,486, Jan. 2008
- [2.19] M. E. Ropp, M. Begovic, and A. Rohatgi, “Analysis and performance assessment of the active frequency drift method of islanding prevention,” *IEEE Trans. Energy Convers.*, vol. 14, no. 3, pp. 810–816, Sep. 1999.
- [2.20] G. Hung, C. Chang, and C. Chen, “Automatic phase shift method for islanding detection of grid connected photovoltaic inverter,” *IEEE Trans. Energy Convers.*, vol. 18, no. 1, pp. 169–173, Mar. 2003.
- [2.21] J. Yin, L. Chang, and C. Diduch, “A new adaptive logic phase-shift algorithm for anti-islanding protections in inverter-based DG systems,” in *Proc. IEEE Power Electronics Specialists Conf.*, 2005, pp. 2482–2486.
- [2.22] Chung-Chuan Hou; Yu-Chun Chen, "Active anti-islanding detection based on pulse current injection for distributed generation systems," *Power Electronics, IET* , vol.6, no.8, pp.1658,1667, September 2013

- [2.23] Ten, C.F.; Crossley, P.A, "Evaluation of Rocof Relay Performances on Networks with Distributed Generation, " *Developments in Power System Protection, 2008. DPSP 2008. IET 9th International Conference on* , vol., no., pp.523,528, 17-20 March 2008
- [2.24] Beddoes, Andy; Thomas, Peter; Gosden, Mark, "Loss of mains protection relay performances when subjected to network disturbances / events," *Electricity Distribution, 2005. CIRED 2005. 18th International Conference and Exhibition on* , vol., no., pp.1,5, 6-9 June 2005
- [2.25] (2014, July). *Frequency Changes during Large Disturbances and their Impact on the Total System* [Online]. Available: <http://www.nationalgrid.com/NR/rdonlyres/D3F18F81-BFE8-4BA1-8B82-CCD6CD0A0A4F/62018/GC0035IndustryConsultationv10.pdf>
- [2.26] Freitas, W.; Wilsun Xu; Affonso, C.M.; Zhenyu Huang, "Comparative analysis between ROCOF and vector surge relays for distributed generation applications," *Power Delivery, IEEE Transactions on* , vol.20, no.2, pp.1315,1324, April 2005
- [2.27] (2014, July). *Council Directive on the approximation of the laws of the Member States relating to units of measurement and on the repeal of Directive 71/354/EEC* [Online]. Available: <http://eur-lex.europa.eu/LexUriServ/LexUriServ.do?uri=OJ:L:1980:039:0040:0050:EN:PDF>
- [2.28] (2014, July). *Assessment of Islanded Operation of Distribution Networks and Measures for Protection* [Online]. Available: <http://webarchive.nationalarchives.gov.uk/+/http://www.berr.gov.uk/files/file15099.pdf>

- [2.29] "Engineering Recommendation G59/1 - Recommendations for the connection of Embedded Generation Plant to the Public Electricity Suppliers," Energy Networks Association, London 1991.
- [2.30] "Engineering Recommendation G59/2 - Recommendations for the connection of generation plant to the distribution systems of licensed distribution network operators (Version 2)," Operations Directorate of Energy Networks Association, London, Engineering Recommendation 2010.
- [2.31] "Engineering Recommendation G59/2 - Recommendations for the connection of generation plant to the distribution systems of licensed distribution network operators (Version 3.4)," Operations Directorate of Energy Networks Association, London, Engineering Recommendation 2013.
- [2.32] "Engineering Recommendation G59/3 - Recommendations for the connection of generation plant to the distribution systems of licensed distribution network operators," Operations Directorate of Energy Networks Association, London, Engineering Recommendation 2014.
- [2.33] Redfern, M.A; Usta, O.; Fielding, G., "Protection against loss of utility grid supply for a dispersed storage and generation unit," *Power Delivery, IEEE Transactions on* , vol.8, no.3, pp.948,954, July 1993
- [2.34] Redfern, M.A; Barrett, J. I; Usta, O., "A new microprocessor based islanding protection algorithm for dispersed storage and generation units," *Power Delivery, IEEE Transactions on* , vol.10, no.3, pp.1249,1254, Jul 1995
- [2.35] Mahat, P.; Zhe Chen; Bak-Jensen, B., "A Hybrid Islanding Detection Technique Using Average Rate of Voltage Change and Real Power Shift," *Power Delivery, IEEE Transactions on* , vol.24, no.2, pp.764,771, April 2009

- [2.36] Fu-Sheng Pai; Shyh-Jier Huang, "A detection algorithm for islanding-prevention of dispersed consumer-owned storage and generating units," *Energy Conversion, IEEE Transactions on* , vol.16, no.4, pp.346,351, Dec 2001
- [2.37] Sung-Il Jang; Kwang-Ho Kim, "An islanding detection method for distributed generations using voltage unbalance and total harmonic distortion of current," *Power Delivery, IEEE Transactions on* , vol.19, no.2, pp.745,752, April 2004
- [2.38] Yip, H. T.; Millar, G.; Lloyd, G.J.; Dysko, A; Burt, G.M.; Tumilty, R., "Islanding detection using an accumulated phase angle drift measurement," *Developments in Power System Protection (DPSP 2010). Managing the Change, 10th IET International Conference on* , vol., no., pp.1,5, March 29 2010-April 1 2010
- [2.39] An, C.; Millar, G.; Lloyd, G.J.; Dysko, A; Burt, Graeme M.; Malone, F., "Experience with accumulated phase angle drift measurement for islanding detection," *Universities Power Engineering Conference (UPEC), 2012 47th International* , vol., no., pp.1,6, 4-7 Sept. 2012
- [2.40] (2014, July). A. J. Roscoe, "Measurement, control and protection of microgrids at low frame rates supporting security of supply," PhD thesis, Department of Electronic and Electrical Engineering, University of Strathclyde, Glasgow, 2009, (Online) Available: <http://strathprints.strath.ac.uk/39631/>
- [2.41] Bakhshi, M.; Noroozian, R.; Gharehpetian, G.B., "Anti-Islanding Scheme for Synchronous DG Units Based on Tufts–Kumaresan Signal Estimation Method," *Power Delivery, IEEE Transactions on* , vol.28, no.4, pp.2185,2193, Oct. 2013

- [2.42] Kar, S.; Samantaray, S.R., "Data-mining-based intelligent anti-islanding protection relay for distributed generations," *Generation, Transmission & Distribution, IET* , vol.8, no.4, pp.629,639, April 2014
- [2.43] Abbey, C.; Brissette, Y.; Venne, P., "An Autoground System for Anti-Islanding Protection of Distributed Generation," *Power Systems, IEEE Transactions on* , vol.29, no.2, pp.873,880, March 2014
- [2.44] Zhenzhi Lin; Tao Xia; Yanzhu Ye; Ye Zhang; Lang Chen; Yilu Liu; Tomsovic, K.; Bilke, T.; Fushuan Wen, "Application of wide area measurement systems to islanding detection of bulk power systems," *Power Systems, IEEE Transactions on* , vol.28, no.2, pp.2006,2015, May 2013
- [2.45] IEEE Standard for Interconnecting Distributed Resources with Electric Power Systems," *IEEE Std 1547-2003* , vol., no., pp.1,28, July 28 2003

Chapter 3

Detailed Description of the Novel

PRAM Method

This chapter introduces the basic functions and typical applications of PMUs to provide background information relating to the specific M class PMUs that are used in the developed LOM detection method. The M class devices are explained in detail in the second section of this chapter; this section also illustrates the tripping logic and peak ratio algorithm used within the developed PRAM method.

3.1 Basic Function and Typical Applications of PMUs

3.1.1 Phasors

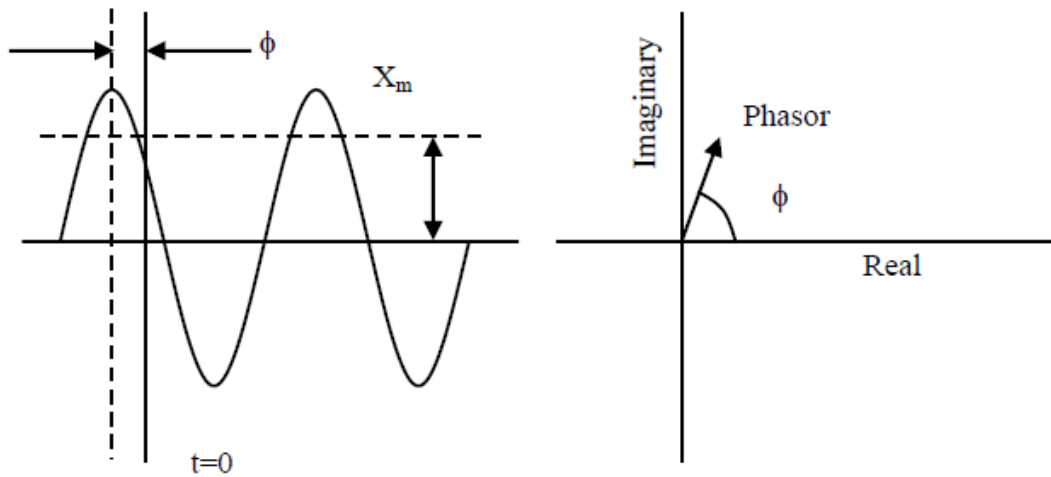


Figure 25: A sinusoidal waveform and its phasor representation [3.1]

As shown in Figure 25, a sinusoidal waveform can be represented using the equation:

$$x(t) = X_m \cos(\omega t + \varphi) \tag{3}$$

Where ω is the angular velocity that equates to the frequency of the signal, φ is the angle between a reference point of observation and the time of the positive peak. X_m is the peak amplitude of the waveform, and the root mean square (RMS), or effective value of the sinusoid, is $(X_m/\sqrt{2})$.

In reality, the waveform is invariably distorted by other signals and a Fourier analysis can be used to represent these distortions as other sinusoids with multiples

of the fundamental signal's frequencies, known as harmonics. However, a phasor representation equates to a pure sinusoidal waveform [3.1]. Therefore, it is very important to extract the component of the signal with the specific frequency to be analysed (usually the fundamental frequency). In a digital measurement system, this is usually realised by the "discrete Fourier transform" (DFT) or the "fast Fourier transform" (FFT) [3.2]. Errors can be introduced if the input frequency of the signal is different from the nominal (assumed) frequency. It is essential to eliminate high frequency components which could cause aliasing errors, so pre-processing to filter out these components and measure the fundamental frequency is normally carried out prior to DFT/FFT operations. [3.3]

Each phasor measurement is normally derived from a specific portion of time span which is also known as the "time window". Phasor measurement continuously samples the waveform in each time window and updates the value of the phasor that is output. [3.3]

3.1.2 Basic PMU functions

PMUs are being increasingly deployed in many parts of the world as they can provide highly accurate voltage and current phasor measurements (synchronised using the GPS system clocks) that can be used for many monitoring, control and protection applications [3.1][3.4]. There is no uniform structure adopted for commercially-available PMUs, as several companies provide such offerings. However, the functional blocks of a typical PMU are generic, and the common components are shown in Figure 26.

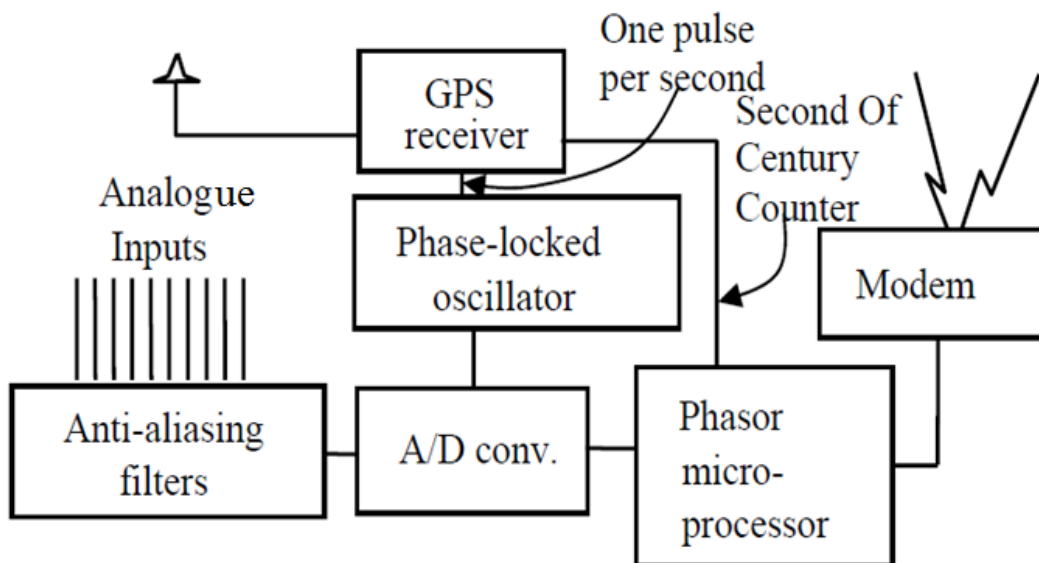


Figure 26: The function blocks of a typical PMU [3.1]

As shown in Figure 26, analogue input signals, which are derived from a scaled version of the primary system quantity measurement using voltage and current transformers (and then through interposing transformers that provide analogue inputs to the PMU's input filters in a typical range of $\pm 10\text{V}$ [3.1]), are initially passed through anti-aliasing filters to remove any high frequency components that could potentially result in A/D conversion errors. A PMU may collect data from different locations in the system on a simultaneous basis and normally requires data from all three phases to extract the positive-sequence component from the measurement data, which is normally of most interest to protection and control functions and contains information that can be used to assess the state of the power system (although negative and zero sequence components are also of interest for certain applications).

PMUs are synchronised by satellites through a GPS receiver. The accuracy of the timing system (i.e. the accuracy of clock signals between geographically-separate PMUs and the master clock) is typically $\pm 0.2 \mu\text{s}$ [3.5]. Time stamps are created by

the GPS receiver as a label for the measurement data and for subsequent comparison of measurements (e.g. from different locations). The other important function of the GPS receiver is that it can generate a one pulse-per-second signal to a phase-locked oscillator to synchronise and lock the phase of the sampling clock.

An A/D convertor samples the signals from the output of the anti-aliasing filter. To achieve higher levels of stability and accuracy, over-sampling is used in several commercially-available systems. The highest economically-achievable sampling rate is always used so that the accuracy of the phasor measurement/estimation can be improved [3.6]. Early PMUs used typical sampling rates in the region of 720 Hz, but this can be as high as 7 kHz or more for modern PMUs [3.1].

The microprocessor uses the digital signal from the A/D converter to calculate the quantities required, including the magnitude and phase angle of the voltage and/or current, the measured frequency and in some cases the rate of change of frequency. The quantities from different geographic measurement locations can be communicated and compared using the time stamps as unique and synchronised references, regardless of any latency or jitter associated with the communication system. [3.3]

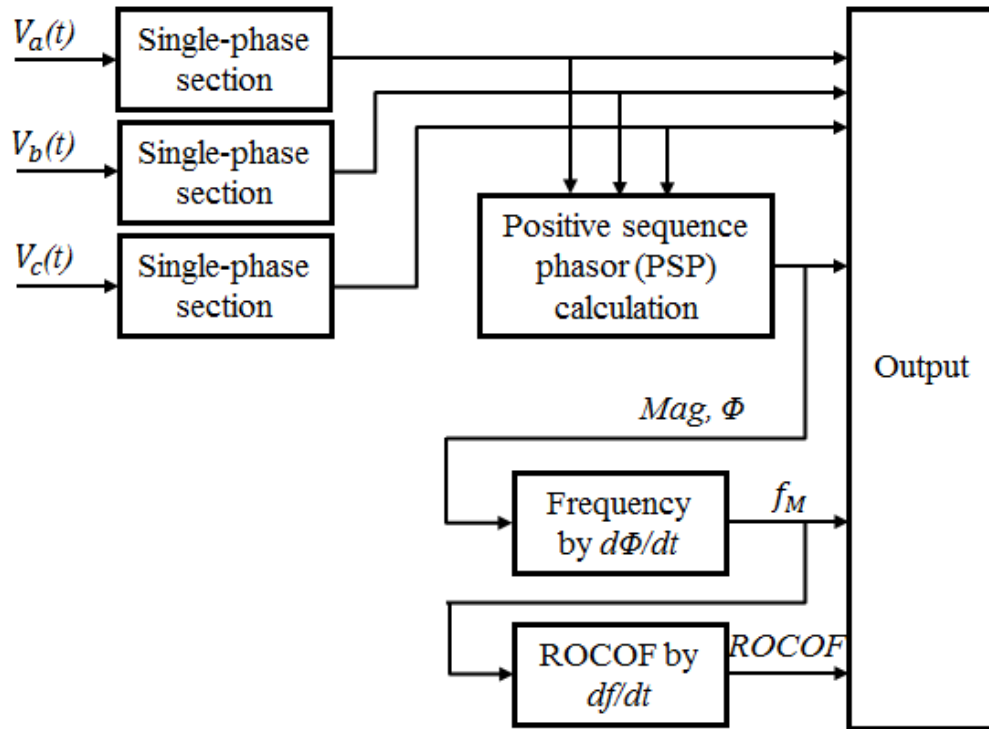


Figure 27: Overview of typical three-phase PMU algorithm

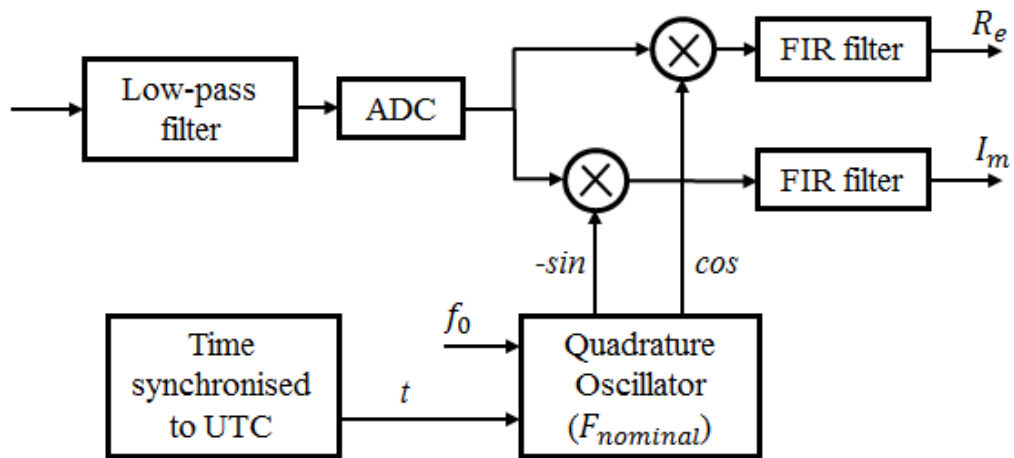


Figure 28: Typical Single-phase section of a PMU

A high-level overview of a three-phase PMU algorithm is shown in Figure 27 and Figure 28. Figure 27 shows how a PMU is capable of calculating and reporting frequency and ROCOF.

PMUs are usually installed in power system substations. For the majority of applications that use PMU data as input, it is not necessary to install a PMU in every substation since the whole system can be “observed” using a suitable placement strategy (although strictly-speaking this may be required for certain applications) [3.7]. Phasor Data Concentrators (PDCs) are used to gather the data from several PMUs as shown in Figure 29 and these can also be used to analyse the output from a number of PMUs and reject bad data. In [3.7], it is shown that PDCs can align the time-stamps and record the data to coordinate with other PDCs through a device termed the “Super Data Concentrator”. [3.3]

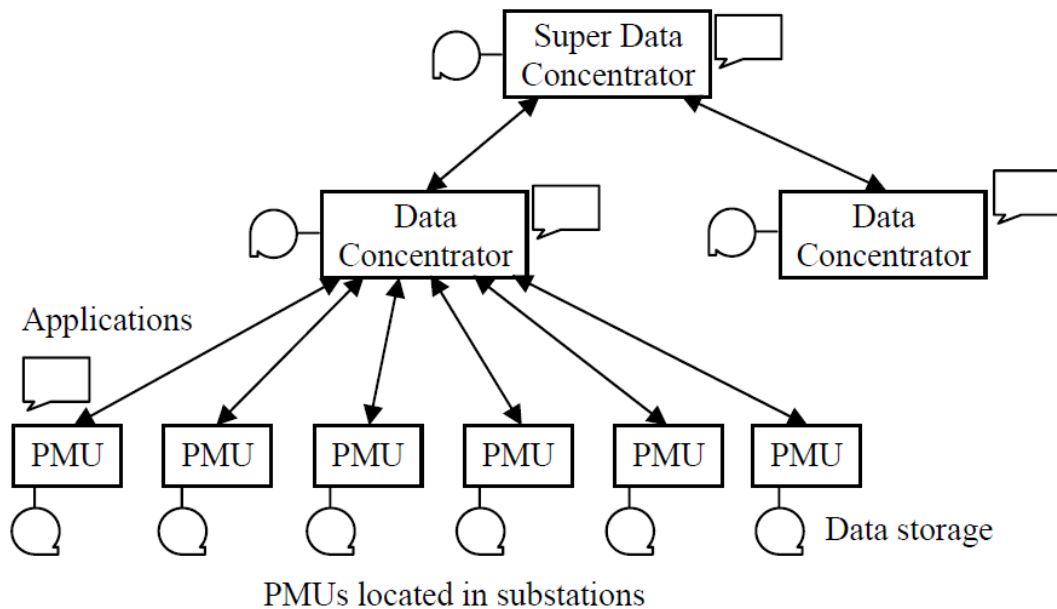


Figure 29: Generally structure of phasor measurement systems [3.1]

3.1.3 Typical applications of PMU

- 1) State estimation

Before the use of state estimation, the power system was monitored and operated using operating guides and rules produced according to the results of off-line load

flows and stability analyses. However, unexpected actual events were always present and uncertainty in measurements had to be accepted and compensated for, if possible, by system operators.

The complex (i.e. magnitude and relative phase angle with respect to some reference quantity) bus voltage measurements are typically used to compute and represent the state of the system in terms of real and reactive power flows, monitoring for stability limits and excess power flows, etc. To address the aforementioned uncertainty, early state estimation systems used both real and reactive power flows to estimate the magnitudes and angles of voltages at the buses in the system [3.1]. However, the efficiency of this method can be very low and it cannot truly represent the real time state of the power system due to the time involved in processing and estimation using the input data. Later methods of state estimation used Supervisory Control and Data Acquisition (SCADA) systems which can offer higher amounts of measurement data from Remote Terminal Units (RTUs) distributed throughout the power system [3.1]. The polling process takes a long enough time that the estimated system state is slightly different from the actual state at the beginning of the initial measurements (in a polling cycle – historically, data was typically gathered serially in SCADA systems) being gathered – although advances in measurement systems and reductions in latencies and delays are constantly improving the performance of such systems. At the present time, synchronised phasor measurements present an opportunity to accurately and directly measure the “state” of the power system, with possibly no real need for estimation if the amount, update frequency and resolution of measurements is high enough. Simultaneous measurements of positive sequence voltages at different buses are typically taken. Voltage angles can be directly compared between buses in the

system to calculate power flow with high accuracy. These systems also provide the possibility of gathering data with higher reporting rates to achieve very near-real-time state estimation. [3.4][3.8][3.9]

2) Protection and control

Protection or control systems which are required to react to power system disturbances normally consist of several of the following analysis methods: identification, prediction, classification, location, decision and action [3.4]. The ideal input to a protection or control system is a complete set of measurements over the entire section of the power system being supervised, which can generate real-time system state represented by several network parameters. However, the technical complexity and high cost of installation means that such systems are normally not available. In many cases, information obtained through a partial set of measurements from the system is usually applied. The parameters measured by PMUs at key locations within the system include: voltage and current magnitude, voltage and current angle, frequency and rate of change of frequency. These parameters are also comparable with high precision time reference which can subsequently calculate other critical parameters such as voltage angle differences and power flows between locations.

Differential protection can obviously benefit from synchronised phasor measurement as differential protection across large distances can be rendered difficult using traditional algorithms, particularly if the communication latencies are variable [3.1]. Without high precision time stamps, the communication delay has to be compensated (using different methods) in traditional differential protection schemes. For wide area system protection, it is difficult to design a scheme with fixed settings due to the constant changing of system conditions [3.4]. PMUs provide an

opportunity to apply an adaptive approach to protection system design and operation such as adaptive out-of-step protection [3.1] and adaptive under-frequency protection [3.10]. Load and generation control can also benefit from synchronous phasor measurements, as PMUs can estimate and trace local frequency at different locations. More precise control actions can be applied in desired areas to efficiently address generation/load imbalance – techniques such as load shedding and incremental control of generation and demand can be implemented with the assistance of PMUs [3.11].

3) Instability prediction

Power system instability may be defined as a condition where the power system is not able to remain in a normal operating status during or after a disturbance, although “small signal” instability may also be experienced [3.12]. Power flows are normally managed to remain below thermal or stability limits with a certain amount of margin. Before synchronous phasor measurements were available, this margin would be kept relatively large to cope with system uncertainties and contingencies. PMUs provide the opportunity of operating the system closer to stability limits with greater confidence by precisely estimating, or even measuring, the operating point of the system [3.13]. Real-time data generated from PMUs also allows system operator more time to take control action to prevent possible system instability. Main areas of PMU applications to power system stability applications are frequency stability, voltage stability, rotor angle stability, system inertia estimation [3.14] and inter-area oscillation detection [3.15].

3.2 Description of Developed LOM Method

3.2.1 M class PMUs used in simulation

According to phasor measurement standard IEEE C37.118.1 (measurements) [3.5], two classes of performance are defined:

- P class: *“intended for applications requiring fast response and mandates no explicit filtering. The letter P is used since protection applications require fast response.”*
- M class: *“intended for applications that could be adversely effected by aliased signals and do not require the fastest reporting speed. The letter M is used since analytic measurements often require greater precision but do not require minimal reporting delay.”*

The standard indicates that the two classes defined are not dedicated to certain application and the user can choose one of the classes suitable for a particular application. Together with IEEE C37.118.1 (the standard for synchrophasor data transfer and communication) [3.16], these standards define exacting requirements in terms of measurement performance during dynamic events and for cases where measurement signals include harmonic/interharmonic content. As illustrated in Figure 27, measurement of frequency is based on the derivative of the measured phase angle with respect to time, and ROCOF requires a further differentiation of frequency.

These two differentiation stages make the measurement of ROCOF highly susceptible to instrumentation and sampling noise, and to interfering harmonic or inter-harmonic signals [3.17][3.18]. It has been identified by the IEEE synchrophasor working group WG-H11 and several other researchers that the measurement of ROCOF is extremely difficult to accomplish during these conditions [3.18]. Furthermore, there is no standard governing the performance of traditional “ROCOF-based” relays and methods and performance varies widely between manufacturers. Only through careful filter design and use of sufficiently-long windows can ROCOF accuracy and noise/ripple be contained to within acceptable levels. Therefore, the use of a PMU algorithm to measure ROCOF is justified even without using its synchrophasor, since it gives at least a minimum level of guaranteed and standardised performance. Recently, an amended standard, C37.118.1a [3.19], has been published which increases the limit of ROCOF accuracy/noise/ripple during nominal conditions to between 0.1 and 0.4 Hz/s, reflecting the difficulty that some PMU devices have in making accurate ROCOF measurements.

Most actual M-class PMU devices can demonstrate lower accuracy/noise/ripple than 0.1 Hz/s during “normal” grid conditions (i.e. without excessive flicker/inter-harmonics, harmonics, or ROCOF events), but the possibility of excessive ROCOF measurement errors under transient conditions must always be considered. Accounting for knowledge of typical PMU behaviour, two M class PMUs with reporting rates (f_s) of 50 Hz have been used in simulation to provide an appropriately-accurate and timely ROCOF response to islanding events and other disturbances. Such PMUs have window lengths of approximately of 5-6 cycles.

Another challenge associated with the use of PMUs is concerned with calculating phasors during system transients when the measuring window contains segments of

waveforms that occupy the time periods both before and after the initiation of the transient event, as shown in Figure 31. Commonly, it is suggested that such data (and calculated phasors) should be discarded and not used by any application [3.20]. However, this work reported here is concerned with analysis of these phasors (referred to as “fake” phasors in [3.20]) during disturbances to extract information that can be used to execute more effective LOM protection. These “fake” phasors are calculated over a very short time period (dependent on the measuring window of the PMU) after the initiation of the system transient.

Since most PMUs use a DFT/FFT to estimate the phasor, the time window applied to this estimation can dramatically affect the measurement of both frequency and ROCOF during system transients. As shown in Figure 31, the voltage waveform may experience severe amplitude and angle transients during system events. DFT/FFTs tend to estimate phasors based on an assumption that there may be significant transients or discontinuities in the originally-sampled waveforms, which are normally measured over a moving window [3.21]. As already mentioned, the work reported here is based upon analyses of the ROCOF behaviour of such “fake” phasors to improve LOM protection.

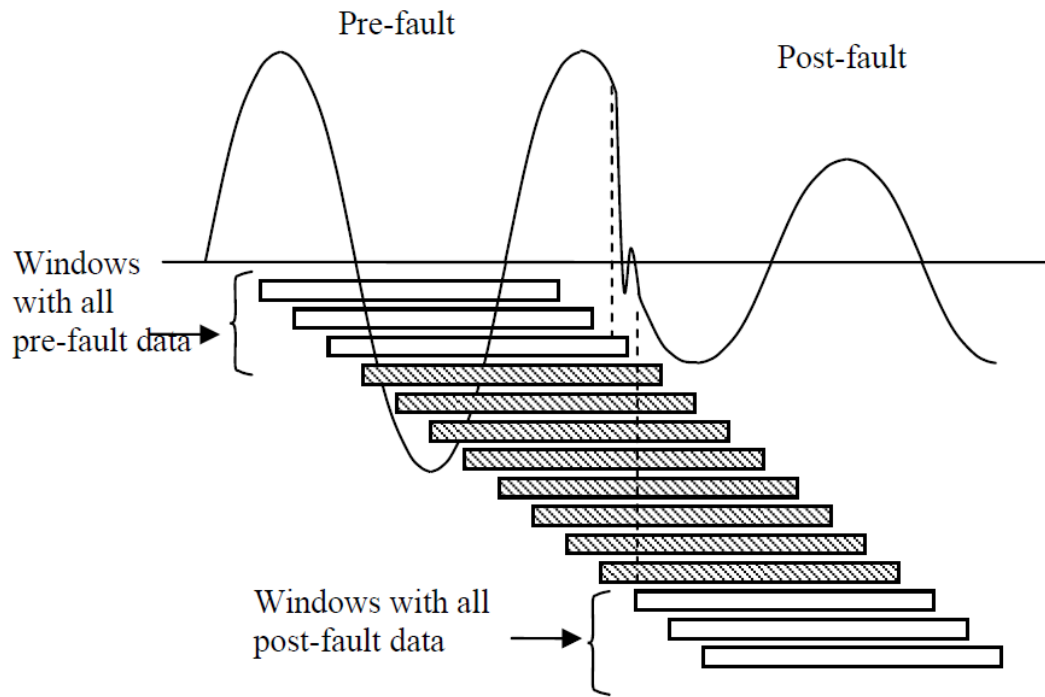


Figure 30: An example of transition from pre-event to post-event waveforms during a fault. The shaded windows contain mixed waveform data and could produce “fake” phasors. [3.1]

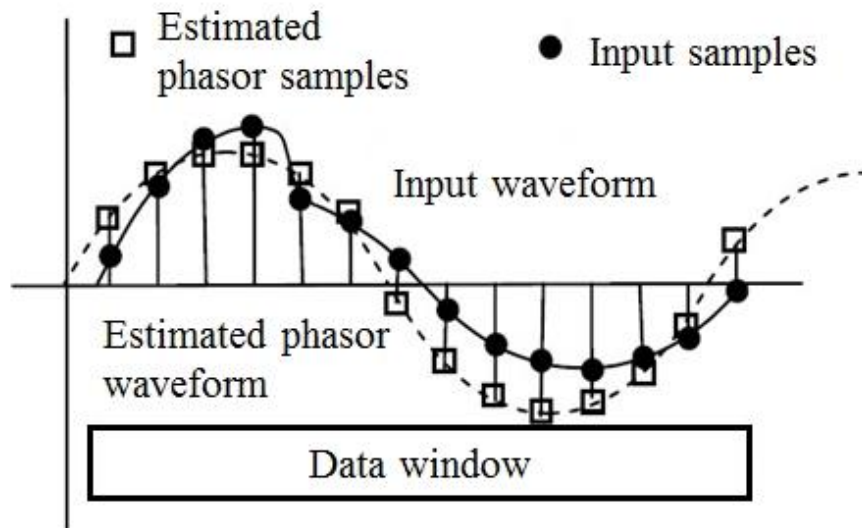


Figure 31: Illustration of phasor estimation in samples during a transient [3.1]

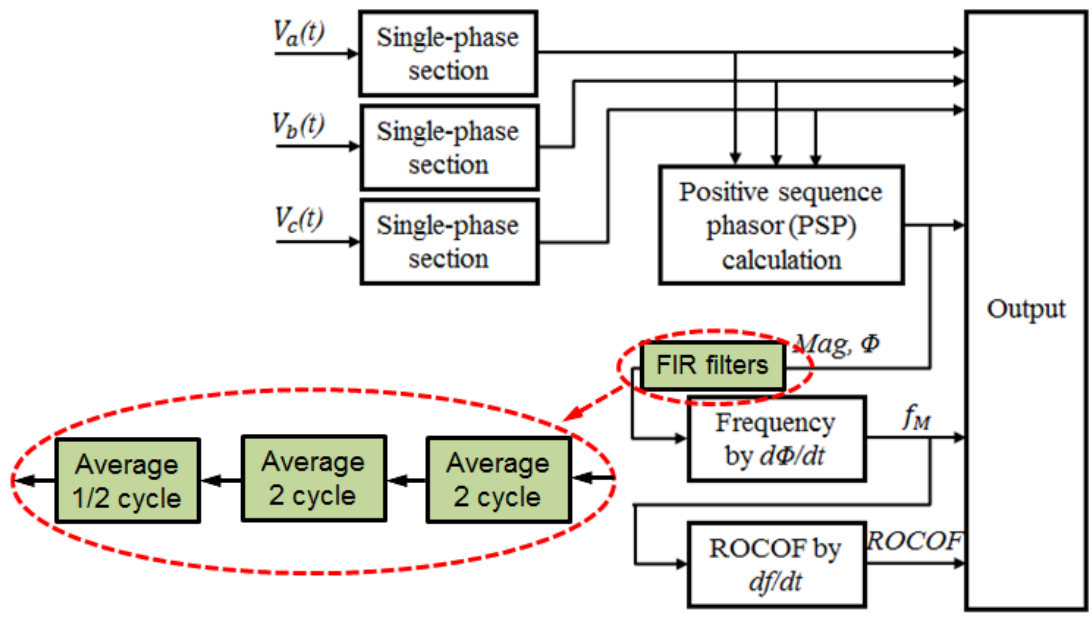


Figure 32: Filter implementation scheme of M class PMUs used

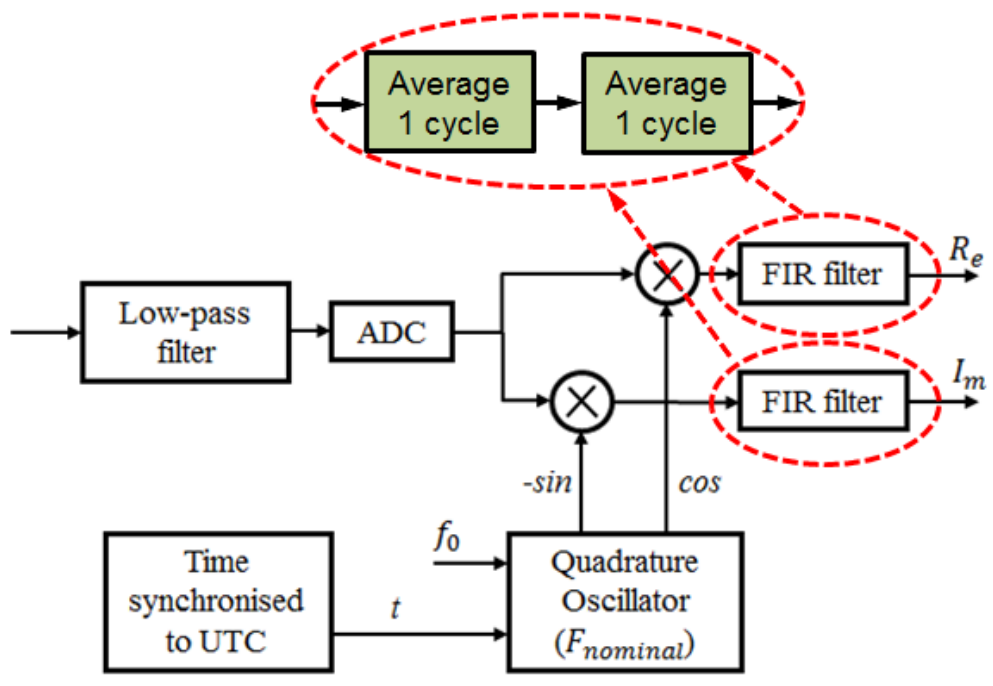


Figure 33: Filter implementation scheme in single-phase section of M class PMUs

used

As no commercially-available PMUs comply with the 2011 version of the C37.118.1 standard, two types of M class PMUs, both of which were originally designed to comply with the 2011 version of the C37.118.1 standard, have been implemented in simulation. These are a fixed-filter and an adaptive-filter version of the M class PMU algorithm reported in [3.22]. In both cases, the M-class filters are configured to comply as far as possible with the reporting rate (F_S) of 50 Hz requirements in C37.118.1. As shown in Figure 32 and Figure 33, the FIR filter consists of four main boxcar filter stages which are cascaded. The lengths of each of the boxcar sections are 1, 1, 2 and 2 cycles respectively [3.22]. Additionally, prior to the calculation of frequency, a further fifth boxcar stage of 0.5 cycles in duration is added to place frequency and ROCOF measurements at 1/2-cycle and 1/4-cycle after the timestamp given for phasor measurement. This also affects the ROCOF measurement.

- Fixed-filter PMU:

In this PMU, the boxcar filter lengths are fixed at times corresponding to multiples of the nominal frequency period, and the correlation waveform (quadrature oscillator, Figure 28) is fixed at nominal frequency.

- Adaptive filter PMU:

In this PMU, the boxcar filter lengths and correlation waveform are adaptive depending upon the measured fundamental frequency [3.22]. This type of PMU is “virtually ideal” in terms of its abilities to reject harmonics, cater for unbalance and in performing under off-nominal frequency conditions.

3.2.2 Tripping logic and peak ratio algorithm

The tripping logic applied within the PRAM method is illustrated in Figure 34. The ROCOF signal measured by the PMU at the DG terminals is first compared to a pick up threshold value of ROCOF – in this case an experimentally-derived value of 0.6 Hz/s has been used for all tests. This value has been selected to achieve acceptable levels of sensitivity for particular scenarios which will be explained in the chapter that reports the results of sensitivity tests. When the threshold is violated, the peak ratio function is enabled and processes the measured ROCOF value from the PMU for a predetermined time period. This time period is determined by the filter length through from the input of PMU to its ROCOF output and other factors which will be further explained later.

The first peak is captured as illustrated in Figure 35 and during the subsequent time period, the “peak recording time window” in Figure 35, a peak will be recorded whenever ROCOF experience a zero crossing, then the highest subsequent peak (in the positive or negative direction) following the zero crossing is recorded, with a final peak being recorded after the final zero crossing at the end of the peak recording time window.

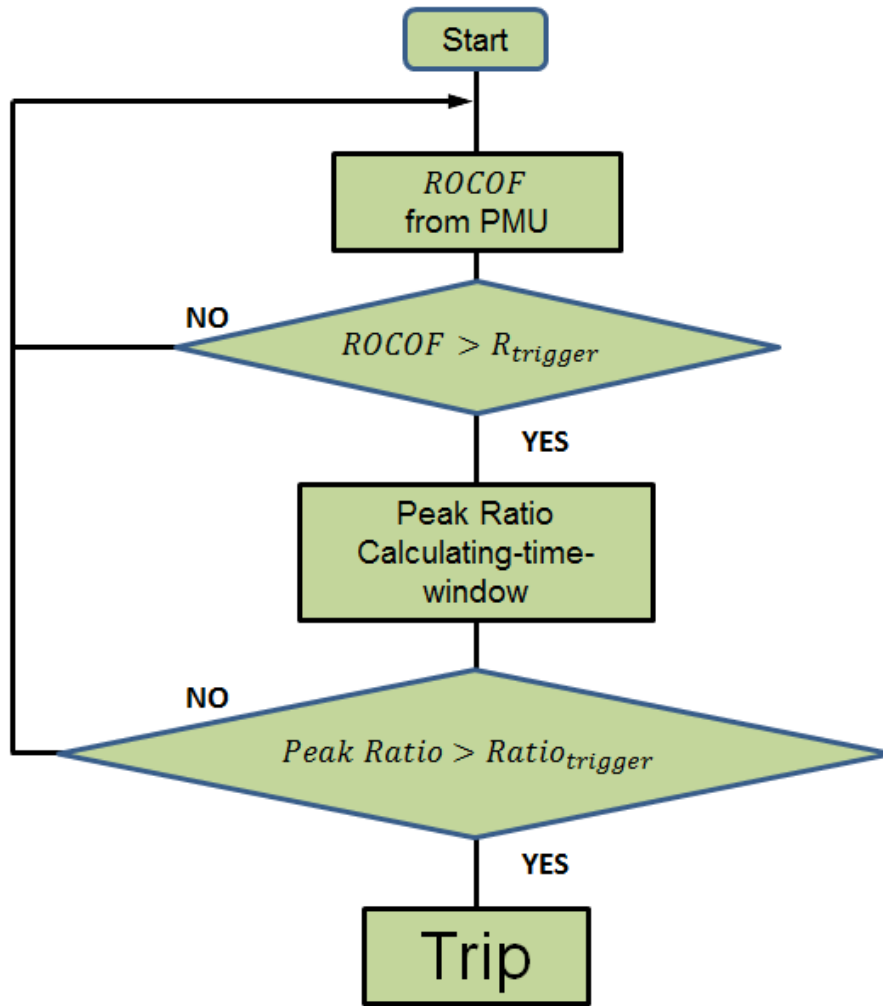


Figure 34: Tripping logic of PRAM method

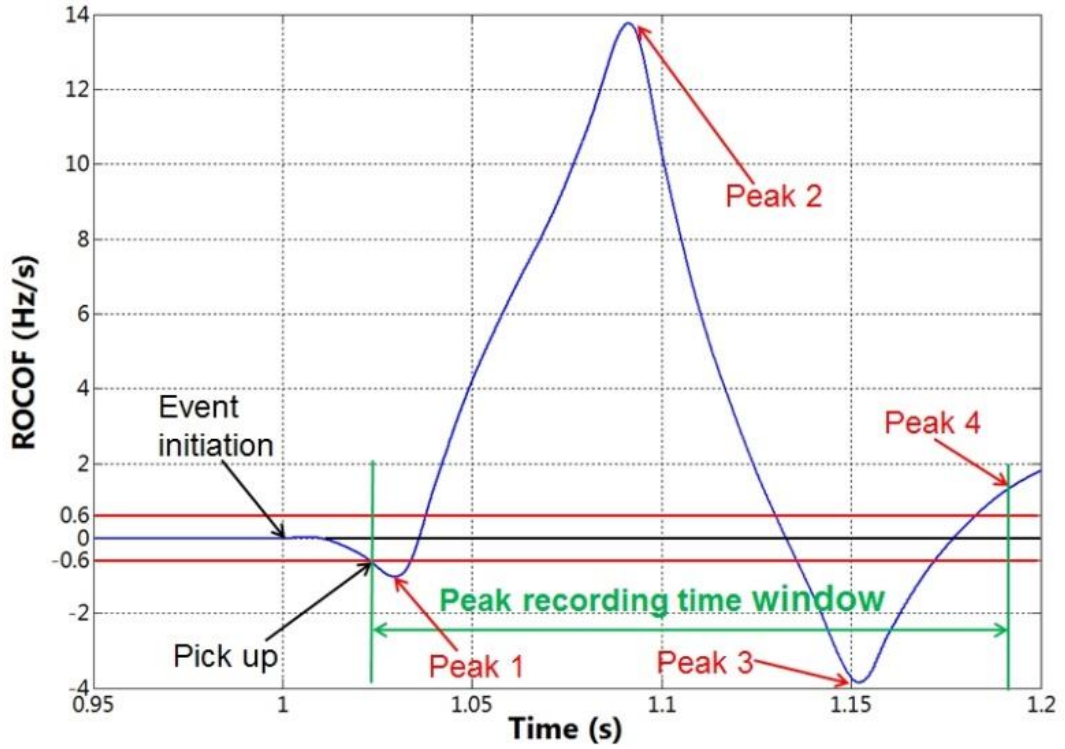


Figure 35: Illustration of peak ratio calculation for an unknown event with an example pick up threshold of 0.6Hz/s and peak recording time window of 170ms

The peak ratio of the ROCOF waveform is calculated as shown in Equation (4):

$$Peak\ Ratio = \frac{\sum Peaks_A}{\sum Peaks_B} \quad (4)$$

$Peaks_A$ and $Peaks_B$ are calculated after the expiration of the analysis time window (e.g. 170 ms after triggering as shown in Figure 35). As shown in Figure 35, the largest peak values in each of the polarities ($Peak_2$ and $Peak_3$) are recorded. Subsequently, $Peaks_A$ contains $Peak_2$ and all other peaks with the same polarity (in this case $Peak_4$). $Peaks_B$ contains $Peak_3$ and all other peaks with the same polarity (in this case $Peak_1$). If all ROCOF values that are calculated during the processing time period have the same sign, then $\sum Peaks_B$ is defined as 0, the peak ratio is infinite, and the algorithm will always trip in such cases. In Equation (4), the largest values of the various peaks reveal the information about the nature of the associated

frequency deviation. The 1st main peak of the measured ROCOF value gives an indication of how much the frequency will deviate from nominal and the subsequent peak in the opposite direction after the zero crossing illustrates how much it will tend to return to nominal. The ratio of these elements is indicative of the overall severity of the frequency deviation. Non-LOM (e.g. switching or fault) events usually manifest as a rapid voltage phase-angle change at the point of measurement. This, from a measured ROCOF perspective, usually results in initial positive and negative ROCOF peaks of similar amplitudes, assuming that the overall “aggregate” network frequency does not change substantially due to the event. The opposite-sign ROCOF peaks are due to the finite measurement time window. However, for a genuine load-change, islanding, or loss-of-generation event, the perceived ROCOF will be a combination of the “switching” aspect previously described, combined with a more uni-directional frequency change due to the altered generation/load balance, further compounded by the complex action of generator governor and AVR actions, etc. which can cause (hopefully damped) oscillatory frequency effects. Therefore, during these events which correspond to genuine LOM events, the ratio of 1st to 2nd (or 2nd to 3rd) ROCOF peaks moves away from equilibrium, towards a situation where the ROCOF peak on one side of zero can have a peak value significantly greater than the ROCOF peak of the opposite sign.

In the extreme, an islanding event in which no governor action whatsoever takes place will have a very high and potentially “infinite” Peak Ratio. In some cases, only one very large 1st peak may be observed, if the switching effects happen to cause a ROCOF disturbance in the same direction as the real frequency deviation. In other cases there may be a small 1st peak caused by an initial “fake” phasor due to

switching, which will then be dwarfed by the 2nd peak as local frequency rapidly diverges from the initial value.

If both ROCOF and peak ratio thresholds are violated, a tripping signal will be sent to isolate the DG (and potentially any other DGs that may be in the island). In all tests reported in this thesis, it was found through experimentation that peak ratio thresholds of 2.0 and 2.1 for the fixed-filter and adaptive PMU methods were the optimal to produce the best compromise between sensitivity and stability. Rules for setting and selection of thresholds for different applications will be established through future work. It should be noted that if analysis of the Peak Ratios does not result in tripping, the logic reverts to stand alone ROCOF to ensure sensitivity to true LOM events, with the main benefits of PRAM being in enhancement of stability of LOM protection, particularly in low inertia systems of the future.

References

- [3.1] A.G. Phadke; J.S. Thorp, 2008: *Synchronized Phasor Measurements*. Springer Science+Business Media, 247pp.
- [3.2] Bolinder, E.F., "The Fourier integral and its applications," *Proceedings of the IEEE* , vol.51, no.1, pp. 267, Jan. 1963
- [3.3] Ding, Feng; Booth, C. D., "Applications of PMUs in Power Distribution Networks with Distributed Generation," *Universities' Power Engineering Conference (UPEC), Proceedings of 2011 46th International* , vol., no., pp.1,5, 5-8 Sept. 2011
- [3.4] Terzija, V.; Valverde, G.; Deyu Cai; Regulski, P.; Madani, V.; Fitch, J.; Skok, S.; Begovic, M.M.; Phadke, A., "Wide-Area Monitoring, Protection, and Control of Future Electric Power Networks," *Proceedings of the IEEE* , vol.99, no.1, pp.80,93, Jan. 2011
- [3.5] *IEEE Standard for Synchrophasor Measurements for Power Systems*, "IEEE Std C37.118.1-2011 (Revision of IEEE Std C37.118-2005) , vol., no., pp.1,61, Dec. 28 2011
- [3.6] Phadke, A.G.; "Computer relaying: its impact on improved control and operation of power systems," *Computer Applications in Power, IEEE*, vol.1, no.4, pp.5-10, Oct 1988
- [3.7] Song Yunting; Ma Shiyang; Wu Lihua; Wang Quan; He Hailei; , "PMU placement based on power system characteristics," *Sustainable Power Generation and Supply, 2009. SUPERGEN '09. International Conference on* , vol., no., pp.1-6, 6-7 April 2009
- [3.8] Powalko, Michal; Rudion, K.; Komarnicki, P.; Blumschein, J.; , "Observability of the distribution system," *Electricity Distribution - Part 2*,

2009. *CIREN 2009. The 20th International Conference and Exhibition on* , vol., no., pp.1-2, 8-11 June 2009
- [3.9] Salem-Natarajan, D.; Liang Zhao; Wei Shao; Varghese, M.; Ghosh, S.; Subramanian, M.; Lin, G.; Hsiao-Dong Chiang; Hua Li, 2008, *State estimator for CA ISO market and security applications - relevance and readiness*, Power and Energy Society General Meeting - Conversion and Delivery of Electrical Energy in the 21st Century, 2008 IEEE , Pittsburgh, USA.
- [3.10] Mustafa, M.A.; Yusuf, N.S.N.; Terzija, V.V., "Development of wide area monitoring and control applications in Malaysia," in *Power & Energy Society General Meeting, 2009. PES '09. IEEE* , vol., no., pp.1-8, 26-30 July 2009
- [3.11] Tlustý, Josef; Kasembe, Andrew; Müller, Zdeněk; Svec, Jan; Sykora, Tomas; Popelka, Antonín; Mğaya, Erick V.; Diallo, Oumar; , "The monitoring of power system events on transmission and distribution level by the use of phasor measurements units (PMU)," *Electricity Distribution - Part 1, 2009. CIREN 2009. 20th International Conference and Exhibition on* , vol., no., pp.1-4, 8-11 June 2009
- [3.12] Dahlgren, R.W.; , "Dynamic mechanisms of power system instability," *Northcon/94 Conference Record* , vol., no., pp.72-77, 11-13 Oct 1994
- [3.13] Meliopoulos, A.P.S.; Cokkinides, G.J.; Wasynczuk, O.; Coyle, E.; Bell, M.; Hoffmann, C.; Nita-Rotaru, C.; Downar, T.; Tsoukalas, L.; Gao, R.; , "PMU Data Characterization and Application to Stability Monitoring," *Power Systems Conference and Exposition, 2006. PSCE '06. 2006 IEEE PES* , vol., no., pp.151-158, Oct. 29 2006-Nov. 1 2006
- [3.14] Wall, P.; Regulski, P.; Rusidovic, Z.; Terzija, V., "Inertia estimation using PMUs in a laboratory," in *Innovative Smart Grid Technologies Conference Europe (ISGT-Europe), 2014 IEEE PES* , vol., no., pp.1-6, 12-15 Oct. 2014

- [3.15] Deyu Cai; Regulski, P.; Osborne, M.; Terzija, V., "Wide Area Inter-Area Oscillation Monitoring Using Fast Nonlinear Estimation Algorithm," in *Smart Grid, IEEE Transactions on*, vol.4, no.3, pp.1721-1731, Sept. 2013
- [3.16] *IEEE Standard for Synchrophasor Data Transfer for Power Systems*," IEEE Std C37.118.2-2011 (Revision of IEEE Std C37.118-2005), vol., no., pp.1,53, Dec. 28 2011
- [3.17] Roscoe, A.J.; Abdulhadi, I.F.; Burt, G.M., "P-Class Phasor Measurement Unit algorithms using adaptive filtering to enhance accuracy at off-nominal frequencies," *Smart Measurements for Future Grids (SMFG), 2011 IEEE International Conference on*, vol., no., pp.51,58, 14-16 Nov. 2011
- [3.18] Roscoe, A.J.; Abdulhadi, I.F.; Burt, G.M., "P and M Class Phasor Measurement Unit Algorithms Using Adaptive Cascaded Filters," *Power Delivery, IEEE Transactions on*, vol.28, no.3, pp.1447,1459, July 2013
- [3.19] *IEEE Standard for Synchrophasor Measurements for Power Systems -- Amendment 1: Modification of Selected Performance Requirements*," IEEE Std C37.118.1a-2014 (Amendment to IEEE Std C37.118.1-2011), vol., no., pp.1,25, April 30 2014
- [3.20] Phadke, A.G.; Kasztenny, B., "Synchronized Phasor and Frequency Measurement Under Transient Conditions," *Power Delivery, IEEE Transactions on*, vol.24, no.1, pp.89,95, Jan. 2009
- [3.21] Siebert, W., 1985: Fourier Transforms in Discrete-Time Systems. *MIT Press*, pp.558-594
- [3.22] Roscoe, A.J., "Exploring the Relative Performance of Frequency-Tracking and Fixed-Filter Phasor Measurement Unit Algorithms Under C37.118 Test Procedures, the Effects of Interharmonics, and Initial Attempts at Merging P-

Class Response With M-Class Filtering," *Instrumentation and Measurement*,
IEEE Transactions on , vol.62, no.8, pp.2140,2153, Aug. 2013

Chapter 4

Simulation Methodology

4.1 Experimental Setup

4.1.1 Test distribution network

The simulations that underpin the work carried out so far have been performed using the SimPowerSystems elements within MATLAB [4.1]. The network modelled is based on an actual utility network and is illustrated in Figure 36 and the block diagram is shown in Figure 37. This network represents a section of a UK DNO's network that was previously employed in work carried out at the University of Strathclyde which resulted in publication of an Engineering Recommendation relating to the setting of LOM protection in the UK [4.2]. As explained in introduction, converter interfaced DGs are relatively more unstable during islanding. Therefore, synchronous machines are widely acknowledged as representing the most challenging form of generation technology from the perspective of being able to sustain an (unwanted) island and therefore being the most challenging type of generation for loss of mains protection, a synchronous DG with a capacity of 30 MVA is used in these studies. The machine has with either PQ (set to $Q=0$) control

or PV (power and voltage) control (with three types of frequency and voltage droop combinations), and is directly connected to the 33 kV system. The reason for the combination of control setup is to distinguish a proper difference of frequency and voltage behaviour of the synchronous machine during islanding event. It is indicated in [4.2] that a basic ROCOF protection algorithm is sufficient to protect induction, inverter and DFIG-based generation as they are generally much less stable than synchronous machines when experiencing isolation from the main grid. This is due to the complete or partial loss of generation excitation for induction generators [4.3] and the controllers of inverters (which typically need a reference 50 Hz system reference – so in a single-inverter island the system will quickly become unstable) so that it is much easier for ROCOF or other frequency-based techniques to detect and react to islanding events. It is indicated in [4.2] that ROCOF techniques may not even be required for DFIG as under/over frequency protection, which is simpler to implement, is sufficient to detect all islanding events. As already stated, synchronous machines often present the “worst-case” challenges for detecting LOM conditions and that is the reason why they have been used in this study. To characterise the grid connection (indicated as SOURCE in Figure 36), synchronous generators with variable capacities and inertia are used to represent different “strengths” of grid connection to test the capability of the method under a variety of grid system conditions, including the future when power systems may be general “weaker” due to reduced synchronous machines and increasing converter-interfaces sources and HVDC links. All synchronous machine models use IEEE standard controllers [4.4]. The sampling rates of each of the two types of PMU used in the study are set to 4 kHz. A model, validated through previous work, of a commercially available ROCOF-based relay is used with typical settings of 0.14 Hz/s and a time delay of 0 – this is used as a benchmark against which the new method is compared. The second

main technique against which the new method is compared is POR, which is configured to pick up at 0.2 Hz/s and has a 20° phase offset setting. The PAD technique (the final method against which the new method is compared) is set to operate when the phase angle difference exceeds 10°. ROCOF and POR are configured to achieve similar levels of sensitivity.

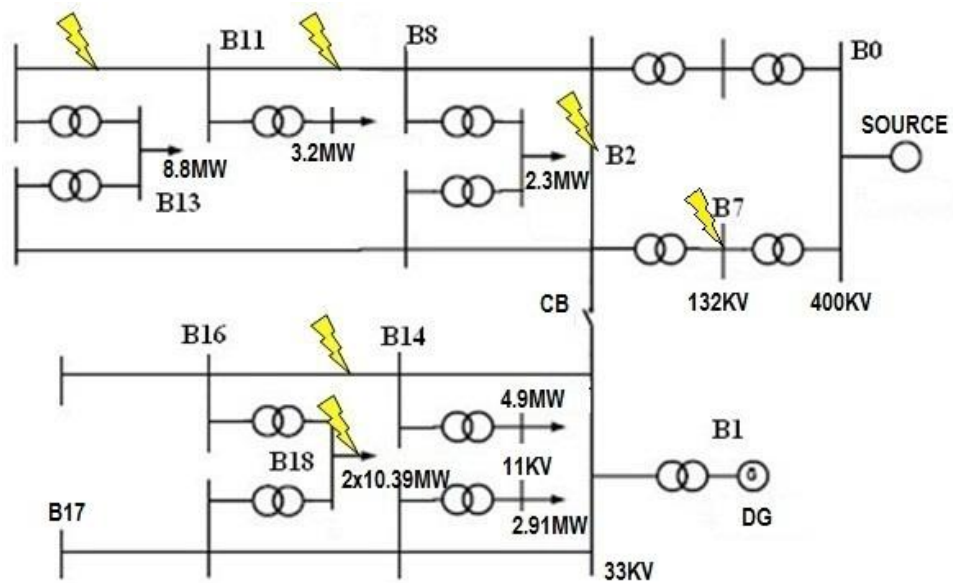


Figure 36: Test network (Buses are indicated as B0, B1, B2 and etc.)

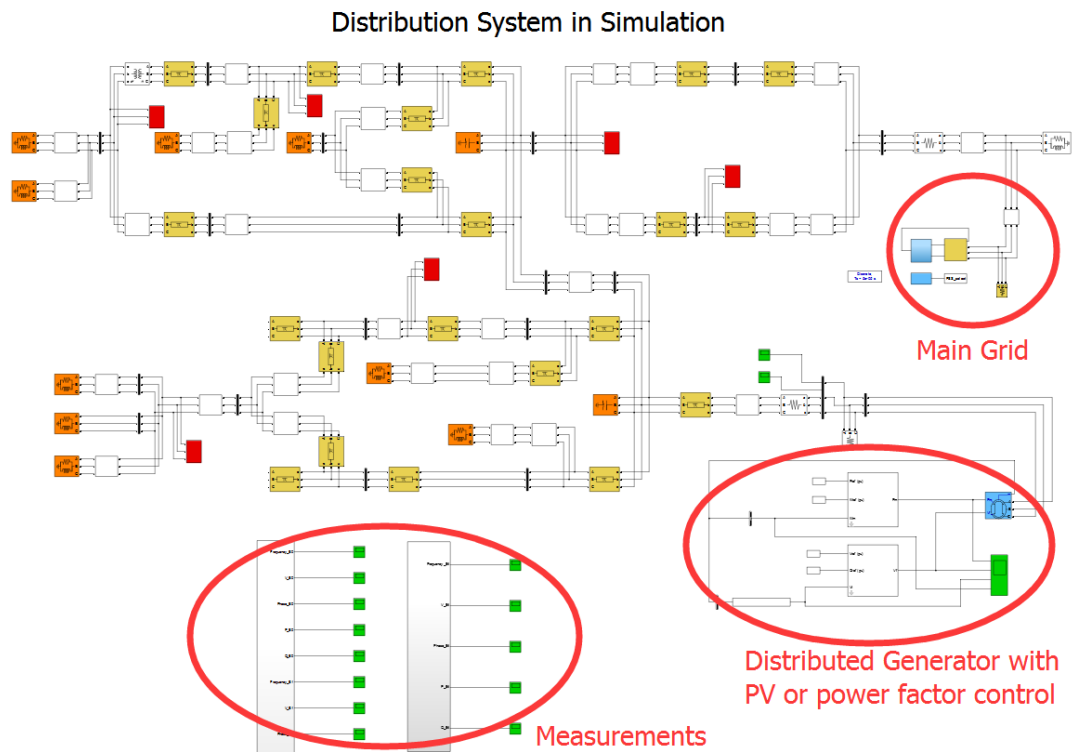


Figure 37: Test network in SimPowerSystems

4.1.2 Test scenarios

Actual islanding events were simulated by opening the circuit breaker CB as illustrated in Figure 36.

A range of scenarios have been simulated to investigate and compare the performance of PRAM against the other three methods:

- Fault level of 5 GVA with inertia of 8s and DG capacity of 30 MVA connected at location B1 in Figure 36 with PQ control (set to $Q=0$).
- Fault level of 5 GVA with inertia of 8s and DG capacity of 30 MVA connected at B1 (Bus location as indicated in Figure 36) with PV control. Three types of

droops are applied within the DG control system during sensitivity tests. Various tests have been conducted with frequency droops of the DG controller set to 20%, 5%, 2% and voltage droops set to 50%, 10%, 1% respectively to represent relatively “passive”, “normal” and “aggressive” types of control. They represent how effectively frequency/voltage are controlled which are explained in Chapter 6.

- Grid capacity of 40 GVA (based on typical summer demand of the UK) with inertia of 8s, 6s, 5s or 4s and DG capacity of 30 MVA connected at B1 with PV control. These types of arrangements are only applied in stability test in terms of very large load (more than 1GW) switching events remote to distribution network.

Several scenarios, representing a wide range of system conditions, have been created using the test network. In all stability tests, the DG is delivering output power of 90% of its capacity (27MW). Additional scenario with DG output of 30% of its capacity is applied in sensitivity tests:

- Tests of sensitivity to islanding events: islanding events with different active power and reactive power imbalances between the DG generation output and local load demand prior to islanding. The imbalance is illustrated as a percentage difference between the power transferred through the interconnecting breaker (CB in Figure 36) prior to islanding and the capacity of DG.
- Tests of stability during local non-LOM faults: three different types of faults (single phase to earth, phase to phase, and three phase) at six different locations between B11&B13, B14&B16, B8&B11 and at B2, B7 and B18 (Bus location

as indicated in Figure 36). It is assumed that faults are cleared 0.25 s after initiation by network protection. As a further test of stability, for single phase faults, reclosing is applied 500ms (although this might be relatively short time for UK practices, it offers a more robust test of the stability of the LOM techniques) after initial clearance, and it is assumed that the fault is transient in nature and no longer on the system when the reclose takes place. It should be also noted that, for phase to phase and three phase fault at location B2, the act of clearing the fault by opening the breakers causes a subsequent islanding condition, which should be detected by the LOM protection.

- Tests of stability during local load switching: loads are switched (in and out) at different sites with magnitudes of 2.91MW, 3.2MW, 4.9MW, 8.8MW, 10.39MW, 20.78MW, and 28.59MW. These values of changes are original settings of the load and they are identical to those used in [4.2] (labelled in Figure 36).
- Tests of stability during large remote system events: this is carried out via remote load switching (at SOURCE in Figure 36) with magnitudes of 1GW, 1.3GW, 1.5GW and 1.8GW (the largest loss of load in the UK which the system should be secure against [1.10]). The grid inertia is also varied during these tests to characterise future systems that may have reduced inertia compared to present systems due to increased use of converter-interfaced renewables and HVDC links.
- Test of stability during capacitor switching events: capacitors are switched out at B2 corresponding to reactive power levels of 8.1 MVar and 11 MVar; these values were chosen based on the prevailing reactive power consumption level of the network.

- Test of stability during transformer inrush: a three-phase fault at B18 was applied and cleared. Subsequently, both transformers connected at B18 were switched in under no load conditions. A further test, using the example “Three-Phase Saturable Transformer” in SimPowerSystems [4.1], has also been carried out using a 450 MVA transformer energised on a 500 kV network.

It is believed that the above set of tests are wide-ranging and provide a comprehensive set of tests of the relative performance of the new LOM method against three other “competing” methods.

Table III: Scenarios of Sensitivity Test

Scenario	Fault Level of Grid	DG Capacity	Generator Control
1	5 GVA	30 MVA	PQ (Q=0)
2	5 GVA	30 MVA	PV (20% F Droop; 50% V Droop)
3	5 GVA	30 MVA	PV (5% F Droop; 10% V Droop)
4	5 GVA	30 MVA	PV (2% F Droop; 1% V Droop)

Table IV: Scenarios of Stability Test

Scenario	Grid Inertia	Locations	Actions
Fault (1ph)	8 s	6 Locations	Initiation Clearing Reclosing
Fault (ph-ph)	8 s	6 Locations	Initiation Clearing
Fault (3ph)	8 s	6 Locations	Initiation Clearing
Small Load Change	4 s	7 Local Locations	Switching In and Out
Large Load Change	8 s, 6 s, 5 s, 4 s	Same Location with Different Load Magnitudes	Switching In and Out
Capacitor Switching	4 s	2 Locations	Switching Out
Transformer Inrush	-	-	Switching In

4.1.3 PRAM relay setup

The PRAM relay is built in SimPowerSystems blockset within Matlab to provide a clear vision of relay performance under tests. A high-level view of the PRAM relay

model is shown in Figure 38. The inputs include ROCOF signal from M class PMU outputs and three settings which are pickup ROCOF (“Minimum ROCOF to cause trip”), PRAM window length (“PRAM Window Setting”) and peak ratio (“Peak ratio to trip”). The system also has a reset function if “Reset Trip” is set to 0. The input “Zero Frequency and ROCOF” is to allow the simulation to “ride through” the initial simulation period (where the system is “settling” but there are relatively high transients) until the system is in steady state. The outputs include the trip signal with reset and a various other signals to assist in monitoring and evaluation of the operation of the systems – these signals include original ROCOF (PMU output), windows triggered, the ROCOF values within triggered windows and peak ratio values.

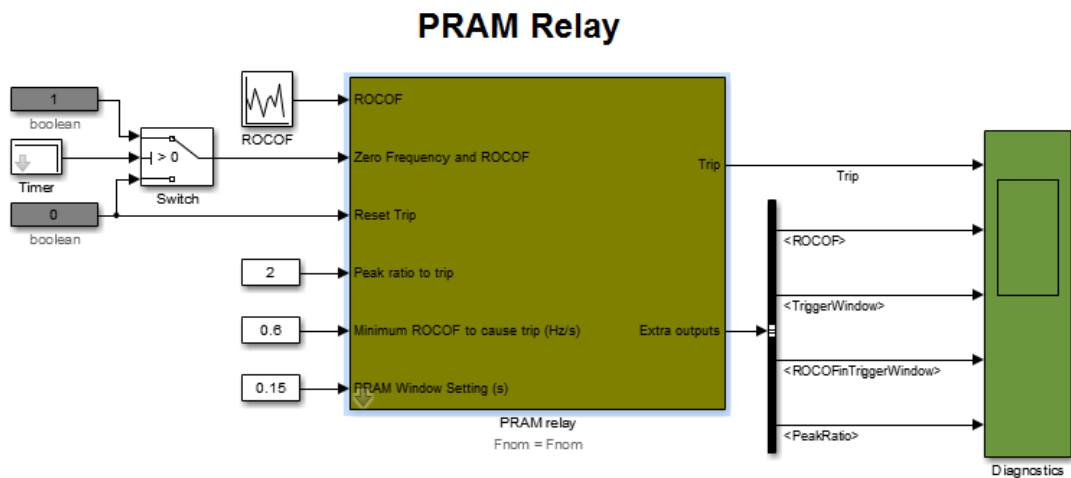


Figure 38: Package view of PRAM relay

The ROCOF trigger algorithm is illustrated in Figure 39. If the absolute value of ROCOF signal is larger than pickup setting, a signal state “ROCOFTrigger” is generated. The data type of “ROCOFTrigger” is Boolean.

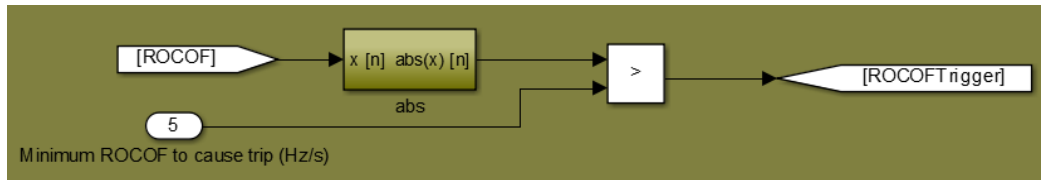


Figure 39: ROCOF trigger algorithm of PRAM relay

The window generator of the PRAM system is shown in Figure 40. Once the ROCOF picks up, a processing window with a preset length is generated for subsequent peak ratio calculation. If “ROCOFTrigger” is still in pickup status following the end of first window, a 2nd window is generated and so on. The data type of “TriggerWindow” is Boolean.

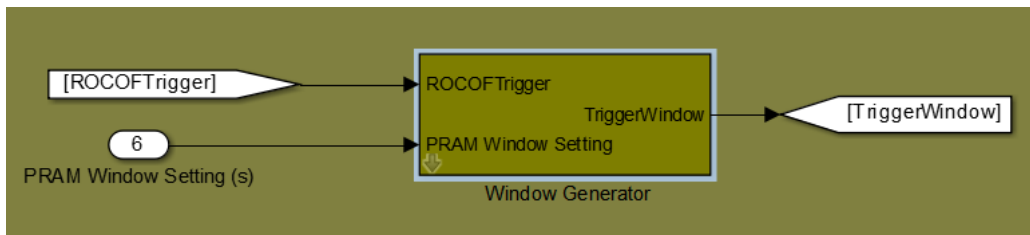


Figure 40: Window generator of PRAM relay

As only the ROCOF values within the triggered windows will be processed, an extraction process is illustrated in Figure 41.

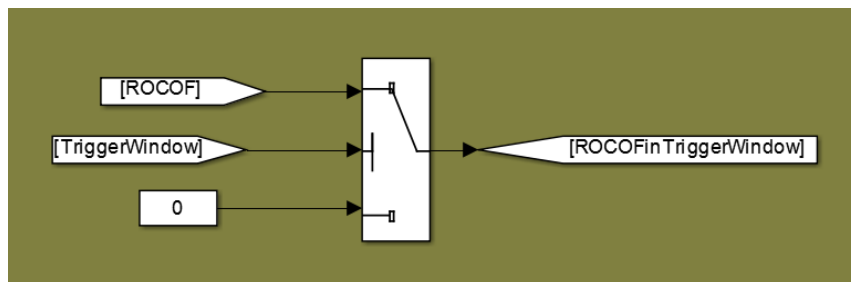


Figure 41: Extraction of ROCOF waveform from windows triggered

The preparation of peak extraction is illustrated in Figure 42. A zero crossing detector is used to identify zero crossings of the ROCOF “waveform” (i.e. the time series of the values of ROCOF calculated over the time period) in triggered windows.

After each zero crossing is detected, the peak extractor searches for a peak value and holds it until the next zero crossing is detected. In this way, the peaks are extracted between adjacent zero-crossings. The “PeaksinTriggerWindow” tag in Figure 42 outputs these peaks.

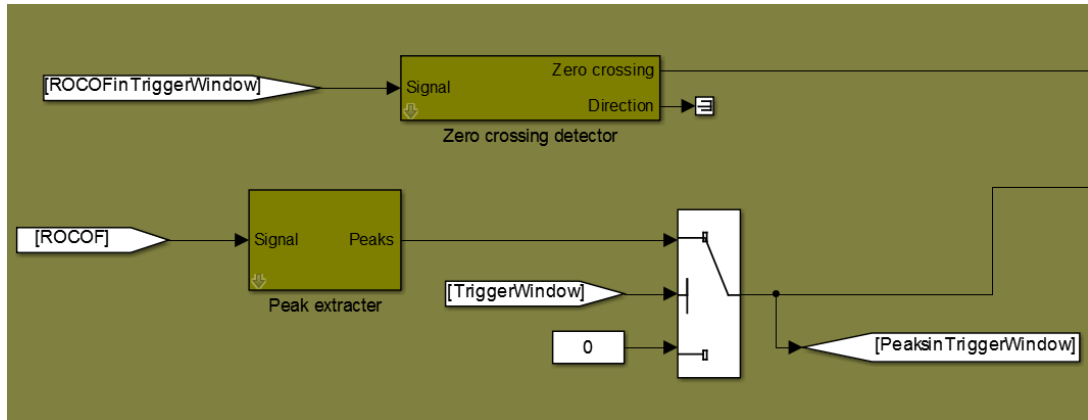


Figure 42: Identification of zero crossings from ROCOF waveform in windows triggered.

The peak separator separates the peaks extracted and outputs them individually as shown in Figure 43.

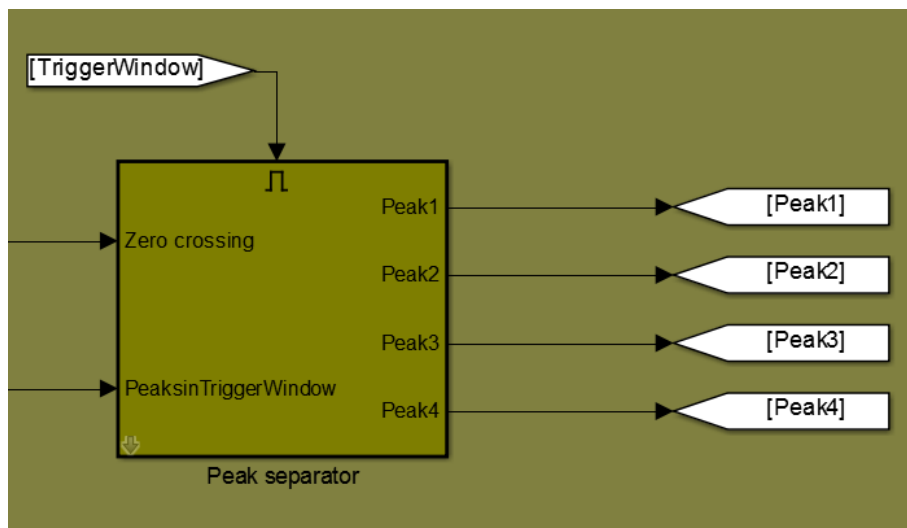


Figure 43: Peak separator

Figure 44 illustrates the process of peak ratio calculation. A peak ratio value is calculated once each triggered window ends. The peaks in the triggered window then enter the peak ratio calculation block to return a value as “PeakRatio”. Please note that only 4 peaks are extracted and further peaks within the same processing window will be ignored.

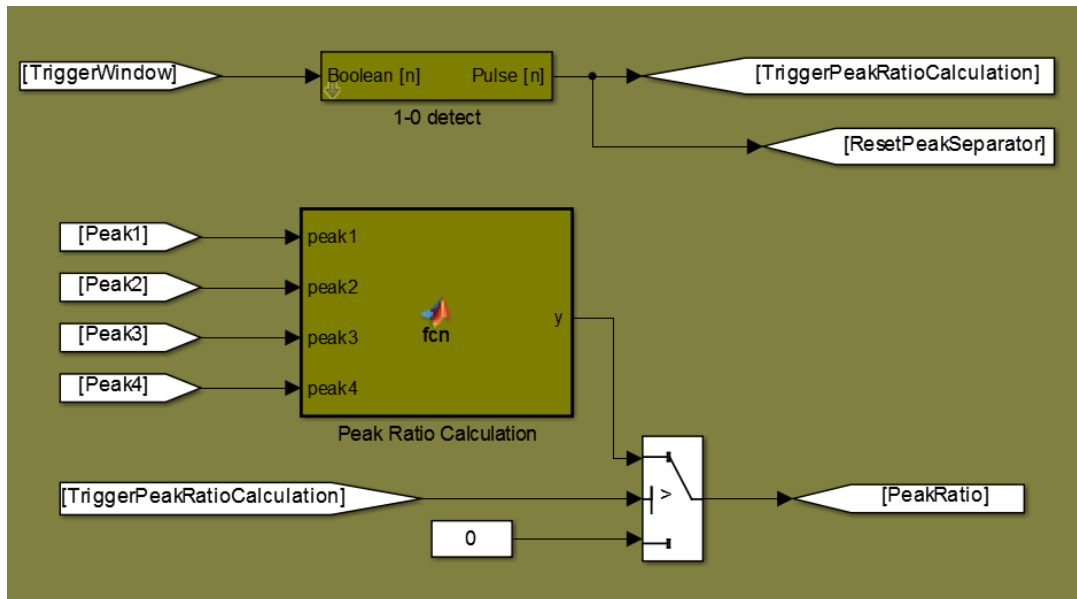


Figure 44: Peak ratio calculation process

Figure 45 illustrates the algorithm is responsible for issuing a trip signal when LOM is detected. The absolute value of peak ratio is compared to a preset threshold and if it is larger, a trip signal is generated.

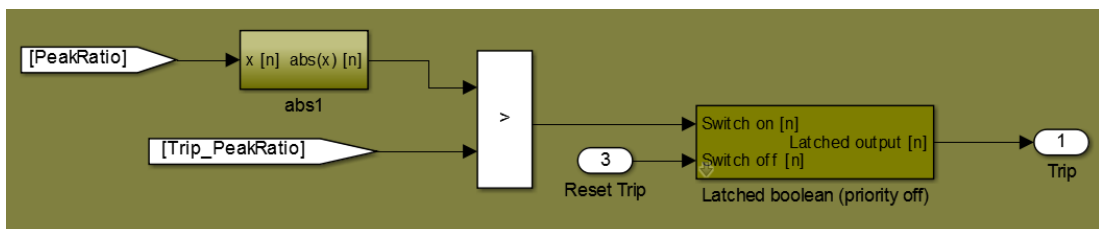


Figure 45: Trip signal generation

4.2 Generator Dynamic Response to LOM Events

[4.6]

Speed and terminal voltage of a synchronous generator are normally controlled by a turbine governor and voltage regulator respectively. Isochronous governors may be used to precisely control generator speeds to constant values by adjusting turbine valves/gates. The target value can be system nominal frequency or a scheduled reference. The scheme of an isochronous governor is shown in Figure 46. Rotor speed ω_r is first measured and compared to a speed reference ω_0 . The error $\Delta\omega_r$ is then amplified and integrated to generate a signal ΔY to control the steam/water input by adjusting the position of valve/gate. When the valve/gate brings the frequency back to the reference value, $\Delta\omega_r$ is zero and ΔY will reach a new steady state.

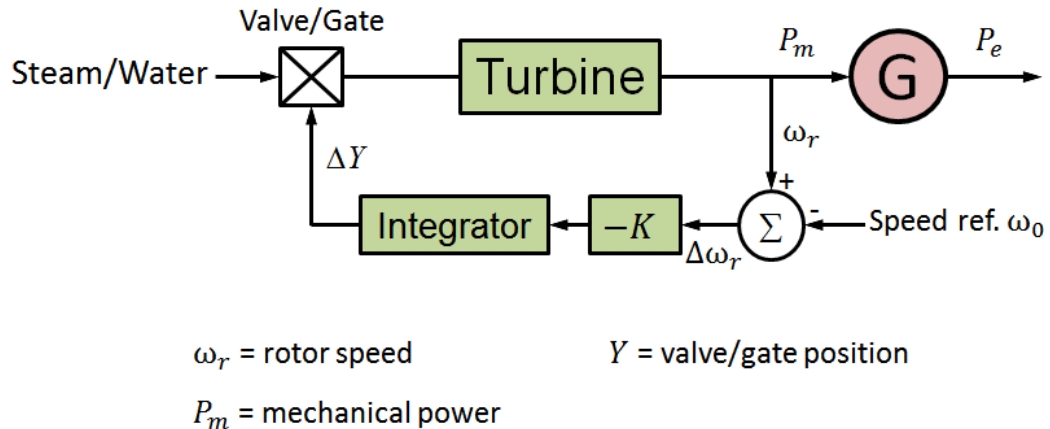


Figure 46: Schematic of an isochronous governor

The major limitation of this control strategy is that there should be at most one generator with isochronous governor connected in the same network unless these generators have exactly the same speed setting since the frequency should be the same at all points of the network. Otherwise, all generators would attempt to control

the frequency to their individual settings and would conflict with each other. In order to ensure stable parallel operation and equitable load sharing across multiple units, speed droop characteristic is introduced. The schematic of a governor with droop control is illustrated in Figure 47. As shown in Figure 47, a feedback loop with a gain value R is added to the isochronous governor.

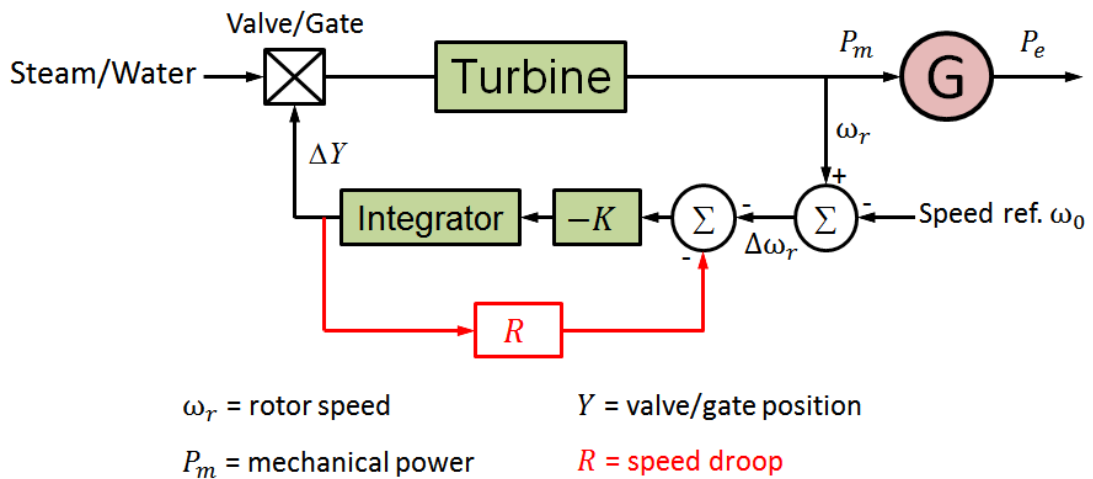


Figure 47: Schematic of a governor with speed droop

Speed droop can be expressed using Equation (5):

$$R_f = \Delta f / \Delta P = (\omega_{NL} - \omega_{FL}) / \omega_0 \quad (5)$$

Where speed droop R_f is normally expressed in percentage. Δf is the frequency variation following the load change. ΔP is the active power output variation. ω_{NL} is the steady-state speed at no load. ω_{FL} is the steady-state speed at full load. ω_0 is the rated speed of the generator.

An example of speed droop of 4% with 50% and 90% load at 100% frequency is shown in Figure 48. As illustrated in Figure 48, frequency rises to 1.02 p.u. at no load and drops to 0.98 p.u. at full load when the speed droop is set to 4% with 50%

load at nominal frequency. It can be deduced that the frequency rises to 1.036 p.u. at no load and drops to 0.996 p.u. at full load when the same droop is set with 90% load at nominal frequency.

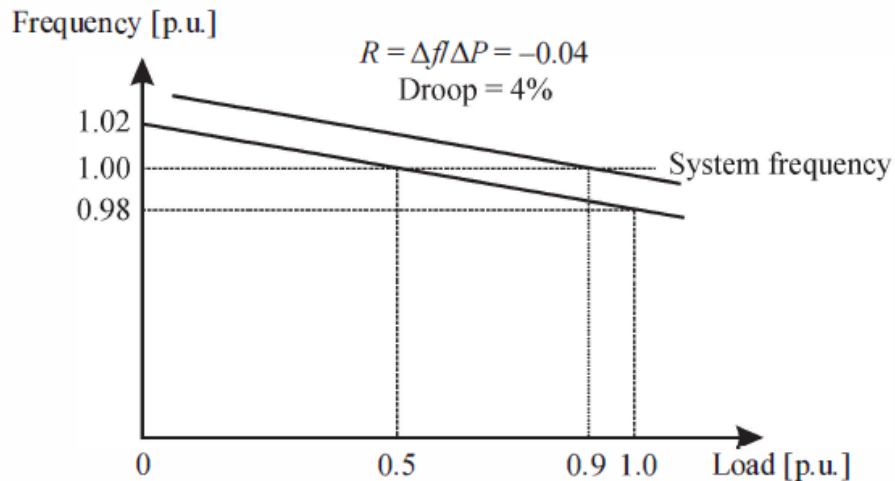


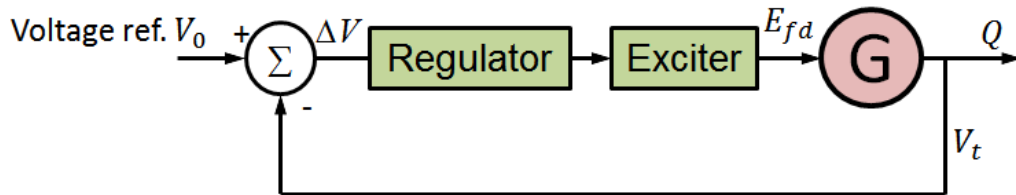
Figure 48: Example of speed droop operation with 50% and 90% load at nominal frequency [4.7]

The terminal voltage and reactive power output (or absorption) of a synchronous generator is controlled by an Automatic Voltage Regulator (AVR). this consists of a voltage regulator and an exciter as shown in Figure 49. The regulator processes and amplifies input control signals to a level and form appropriate for control of the exciter. The exciter generates DC power to provide field voltage to the generator. In contrast to the situation outlined earlier regarding generator speed control and potential conflicts, there is no conflict between generators with different voltage references as clearly the system voltage can vary at individual locations within an interconnected network. This means each generator can choose its own role in terms of contribution to the reactive power and voltage required by the network.

Voltage droop is very similar to speed droop and the principles can be expressed as shown in Equation (6):

$$R_V = \Delta V / \Delta Q = (V_{NL} - V_{FL}) / V_0 \quad (6)$$

Voltage droop R_V is normally expressed in percentage. ΔV is the voltage variation following the load change. ΔQ is the reactive power output variation. V_{NL} is the steady-state voltage at no load. V_{FL} is the steady-state voltage at full load. V_0 is rated voltage of generator.



V_t = terminal voltage Q = reactive power output
 E_{fd} = field voltage

Figure 49: Schematic of generator voltage control loop

Frequency and voltage response with different combinations of droop control following an islanding event are shown in Figure 50 and Figure 51. The selection of droop control values are the same as for those used in sensitivity tests, which are: frequency droops of 20%, 5%, 2% and voltage droops of 50%, 10%, 1% respectively. It is shown that with smaller droop settings, the DG provides more active/reactive power support to the islanded network so that frequency/voltage does not deviate much to reach a new operating point. As DG provides constant power (without extra power support to the network following islanding event) under per-unit power factor control, the islanded network will not be balanced in terms of the balance between

generation and load. Frequency and voltage will deviate rapidly from nominal values and the islanded network will blackout eventually as the local generation trips due to under/over voltage or frequency.

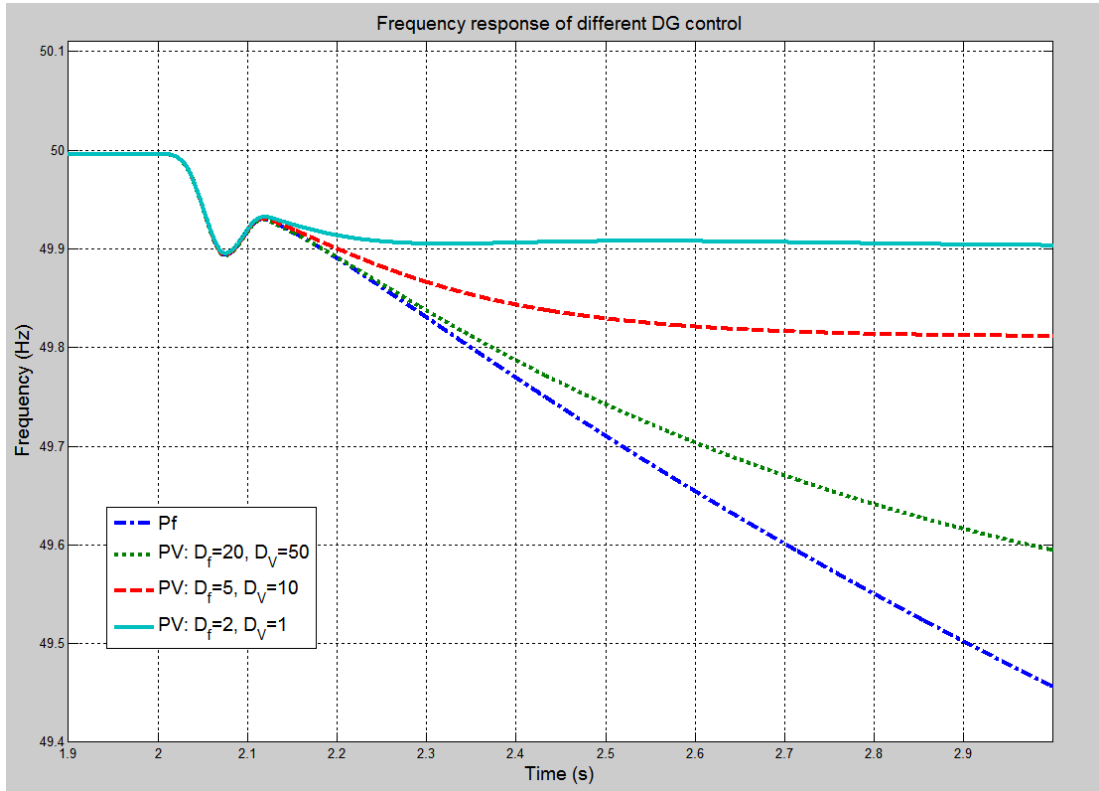


Figure 50: Frequency response for a range of different DG control options following an islanding event

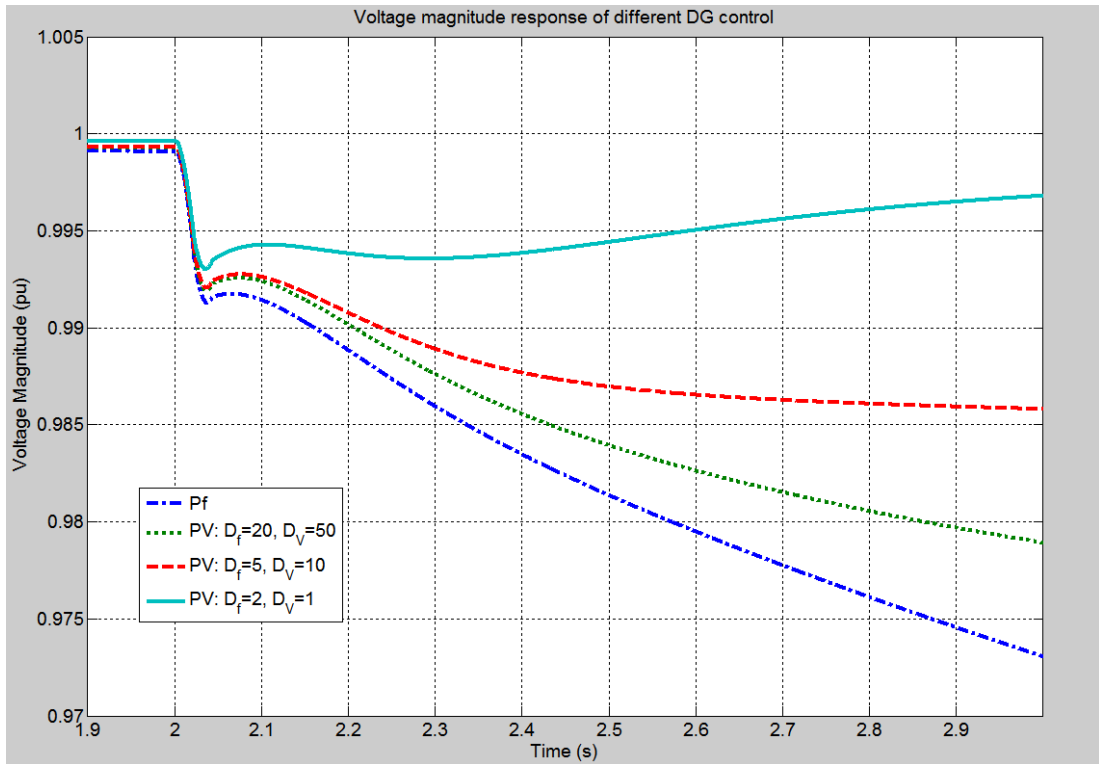


Figure 51: Voltage magnitude response for a range of different DG control options following an islanding event

References

- [4.1] Matlab/Simulink Manual: The Math Works,2009
- [4.2] "Engineering Technical Report NO. 139: Recommendations for settings of loss of mains protection relays", *Energy Networks Association*, 2009.
- [4.3] Edvardsen, H. M.; Winkler, D., "Modelling the system dynamics of islanding asynchronous generators", *Proceedings of the 10th International ModelicaConference*, March 2014.
- [4.4] IEEE Sub-synchronous resonance working group, "Second benchmark model for computer simulation of sub-synchronous resonance," *IEEE Transactions on Power Apparatus and Systems*, vol. PAS-104, no. 5, 1985, pp. 1057-1066.
- [4.5] "Operating the Electricity Transmission Network in 2020", *National Grid*, 2011.
- [4.6] P. Kundur, *Power System Stability and Control*. New York: McGrawHill, 1994.
- [4.7] Eremia, M. ; Shahidehpour, M., *Electrical Power System Dynamics: Modeling, Stability, and Control*. Wiley-IEEE Press, 2013, pp. 291-339.

Chapter 5

PRAM - Sensitivity Tests

5.1 Testing Procedure

In order to test the sensitivity of the PRAM system, actual islanding events were simulated by opening the circuit breaker CB at the 33 kV substation as illustrated in Figure 36. The scenario with a fault causing CB to open, which is also an islanding event, will be compared and analysed with other fault scenarios to generate a better understanding of the benefits of the PRAM algorithm.

In order to provide a comprehensive understanding of the effect of DG output on sensitivity test results, output of 90% and 30% are selected to represent relatively large and small pre-disturbance power contributions to the network respectively.

In addition to considering various levels of pre-islanding active power imbalances, which has been widely investigated and reported by other researchers for various other techniques, reactive power imbalances with balanced active power are also taken into account to provide a full understanding of PRAM system performance over a wide range of scenarios. Active power imbalance and reactive

power imbalance prior to islanding are tested and analysed independently to clarify the effects of both scenarios.

The PRAM system is initially configured to detect 2.5% active power imbalance with the DG outputting 90% of its rated power. The thresholds are selected at 0.6 Hz/s (pick up) and 2 (peak ratio threshold) for fixed-filter PMU through experiment. The instantaneous thresholds are selected as 0.6 Hz/s (pick up) and 2.1 (peak ratio threshold) for the adaptive filter PMU. The method using a fixed-filter PMU is termed PRAM I and the method using the adaptive filter PMU is termed PRAM II. The different peak ratio thresholds between PMUs are for exploration of their effect on PRAM relay performance. The pick up threshold of 0.6 Hz/s also insures the stability of PRAM relay when a 1.8 GW generation loss occurs at the smallest demand of 20 GVA in the UK, assuming grid inertia reduced to 4 s in future [5.1]. The peak ratio setting of 2 and 2.1 also insures the stability when a large constant 0.5625 Hz/s contributes to $Peak_3$ and $Peak_1$ (same polarity with $Peak_3$) which is found to be the largest peak when 1.8 GW generation loss occurs at the smallest demand of 20 GVA in the UK, assuming a reduced grid inertia of 4 s in the future. The peak recording time window must be set to be large enough so that ROCOF curve corresponding to “fake” phasors is recorded – in this case 150 ms (6.5+1 cycles) is defined according to PMU design. These settings were unchanged during the entire sensitivity and stability tests.

As mentioned in Chapter 5, ROCOF relay is used with typical settings of 0.14 Hz/s and time delay of 0. POR is configured to pick up at 0.2 Hz/s and has a 20° phase offset setting. The PAD relay is set to operate when the phase angle difference exceeds 10°. The complete setting for all relays are summarised in Table V.

Table V: Settings for all relays at all tests

	Pick Up	Time Window	Other Settings
PRAM I	0.60 Hz/s	150 ms	Peak Ratio: 2.0
PRAM II	0.60 Hz/s	150 ms	Peak Ratio: 2.1
POR	0.20 Hz/s	-	Phase Offset: 20°
ROCOF	0.14 Hz/s	-	-
PAD	-	-	Phase Difference: 10°

5.2 Discussion of Sensitivity Test Results

5.2.1 Active power imbalance with 90% DG output

Table VI: Test results for islanding with active power imbalances (90% DG output;

X: fail to react; Times: tripping time; F: frequency; V: voltage)

Control	Imbalance	PRAM I	PRAM II	POR	ROCOF	PAD
PQ (Q=0)	2.5%	191ms	211ms	799ms	X	553ms
	5%	180ms	191ms	560ms	140ms	384ms
	7.5%	176ms	191ms	458ms	140ms	309ms
	10%	174ms	191ms	396ms	140ms	264ms
20% F Droop; 50% V Droop	2.5%	191ms	211ms	872ms	X	586ms
	5%	180ms	191ms	592ms	140ms	397ms
	7.5%	176ms	191ms	474ms	140ms	315ms
	10%	174ms	191ms	406ms	136ms	266ms
5% F Droop; 10% V Droop	2.5%	191ms	211ms	X	X	728ms
	5%	180ms	191ms	752ms	145ms	454ms
	7.5%	176ms	191ms	563ms	145ms	345ms
	10%	174ms	191ms	464ms	136ms	285ms
2% F Droop; 1% V Droop	2.5%	191ms	191ms	X	X	1.204s
	5%	180ms	191ms	X	X	634ms
	7.5%	176ms	191ms	X	X	430ms
	10%	174ms	191ms	X	136ms	333ms

It is shown in Table VI that PRAM I can detect islanding with 2.5% active power imbalance in a time of 191 ms for all droop control scenarios. The detection time is further reduced with increasing imbalance as the pick up (at 0.6 Hz/s) happens earlier. However, this reduction in operating time is not so significant when a larger imbalance is experienced as shown in Figure 52. It is also indicated that 2.5% is the edge of NDZ that PRAM can only just pick up. It is also illustrated in Table VI that the detection times for the same levels of power imbalance are exactly the same regardless of DG control scenarios.

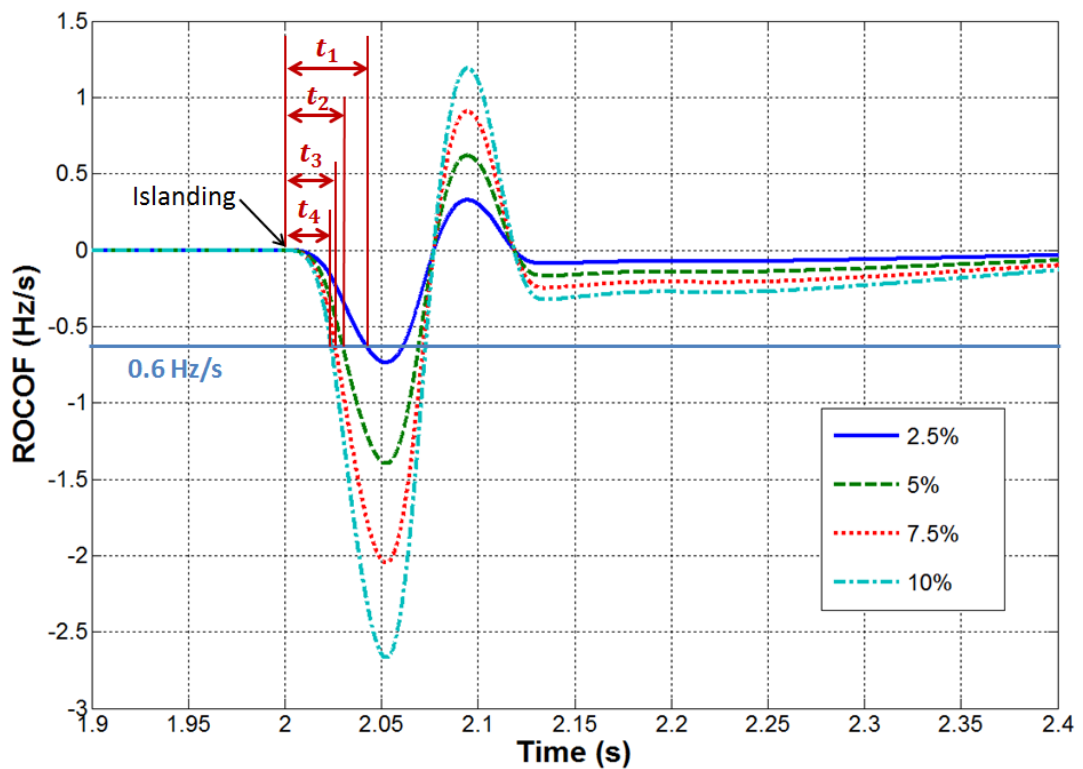


Figure 52: Illustration of pick up time after islanding initiation

PRAM II can detect islanding with 2.5% active power imbalance in 211 ms for all droop control scenarios. It is clear that the detection time for control scenario 4 (2% frequency droop; 1% voltage droop) at 2.5% imbalance is 191 ms, which is less than for the other three scenarios (211ms). This is due to the 50 Hz reporting rate of the PMU with adaptive filter and also caused by slight differences inherent in the simulation environment (e.g. imbalance is not exactly 2.5%) as shown in Figure 53. PRAM II picks up 1 cycle (0.02 ms) earlier for control scenario 4 than for scenario 3 (5% frequency droop; 10% voltage droop). It is illustrated in Table VI that the detection time for the same level of power imbalance is almost the same regardless of the assumed DG control modes.

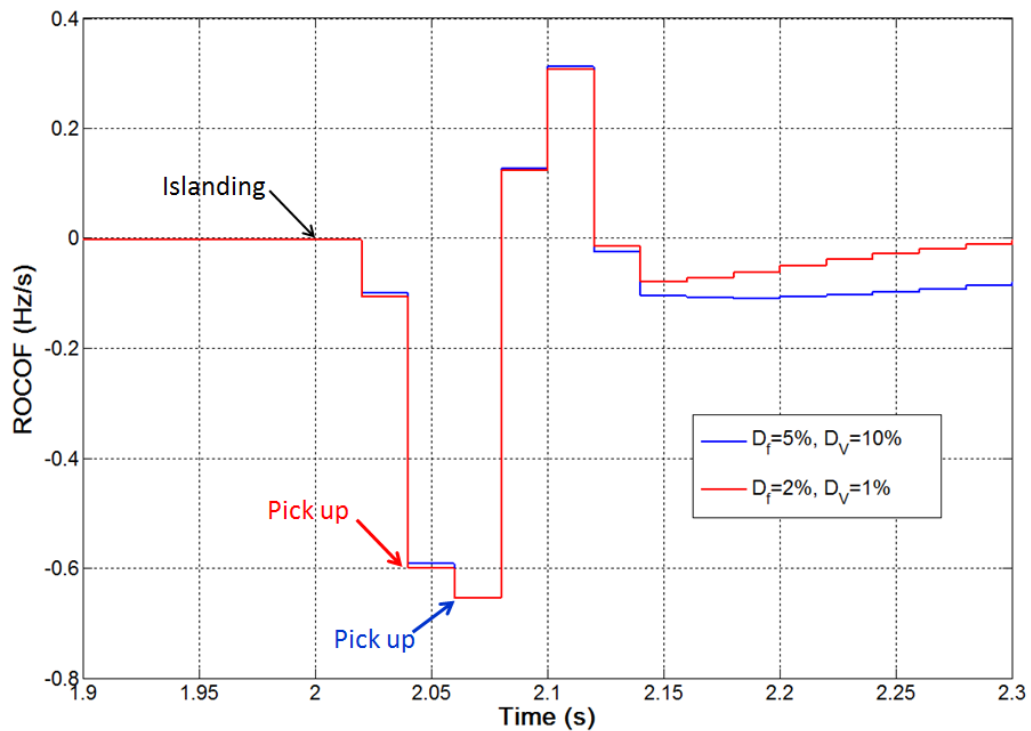


Figure 53: Comparison of simulation results between two droop control scenarios

POR can detect LOM down to a level of 2.5% imbalance prior to islanding in 799 ms for control scenario 1 (per-unit power factor control) and in 872 ms for scenario 2 (20% frequency droop; 50% voltage droop). It fails to detect islanding for this level of imbalance for control scenario 3. The sensitivity of POR is further reduced for control scenario 4 as it failed to detect islanding for scenarios with of up to 10% imbalance prior to islanding. The exact sensitivity of POR is unknown for scenario 4 and it is not important. It is also illustrated in Table VI that the detection time for same power imbalance is longer for more aggressive (smaller droop) DG control scenarios and it is smaller for larger imbalance under same scenario. The reason is that for more aggressive control, it takes less time to bring frequency to a new steady state (less frequency deviation) and it corresponds to a slower angle accumulation (slower to reach threshold). Larger imbalance for the same control scenario leads to more significant frequency deviation at initial period to reach threshold easier.

ROCOF failed to detect 2.5% imbalance prior to islanding under the least aggressive control scenario (scenario 1), but successfully detected 5% imbalance for scenarios 1, 2 and 3. ROCOF can detect 10% imbalance under the most aggressive control scenario. The detection time for ROCOF is relatively stable and independent to imbalances which are around 140 ms. The reason that PRAM with higher pick up of 0.6 Hz/s (compared to 0.14 Hz/s for ROCOF method) can detect lower imbalance (2.5%) which also use ROCOF as estimated signal, is that ROCOF relay is normally implemented a short window (50ms in ROCOF relay in this study).

PAD can detect the smallest imbalances for all control scenarios. The detection time for similar levels power imbalance is longer (1.024 s for 2.5% imbalance under

the most aggressive control scenario) for more aggressive DG control scenarios and smaller for larger imbalances under same scenario.

In this test scenario, it is shown that PRAM has clear advantage of sensitive to detect the smallest imbalance (2.5%) and fast reaction regardless of control strategy. Only ROCOF can achieve faster reaction but it is less sensitive even with its best performance to detect 5% imbalance. Furthermore, ROCOF is less sensitive to the most aggressive control strategy (fail to detect 7.5% imbalance). PAD can achieve the same sensitivity as PRAM but the detection time is longer and it is further delayed with more aggressive control strategy. POR provides both longer detection time and less sensitivity (especially with more aggressive control strategy) compared to PRAM.

5.2.2 Active power imbalance with 30% DG output

It is shown in Table VII that PRAM I can detect islanding with 2.5% active power imbalance prior to islanding in 188 ms for all droop control scenarios. The detection time is further reduced with increasing imbalance as the pick up (at 0.6 Hz/s) happens earlier. This reduction in operating time is smaller for larger pre-islanding imbalance levels for the same reason as explained earlier and as shown in Figure 52. It is also illustrated that the detection time for same power imbalance is almost the same regardless of DG control scenarios.

Table VII: Test results for islanding with active power imbalances (30% DG output)

Control	Imbalance	PRAM I	PRAM II	POR	ROCOF	PAD
PQ (Q=0)	0%	X	X	X	X	X
	2.5%	188ms	191ms	741ms	530ms	508ms
	5%	178ms	191ms	508ms	190ms	339ms
	7.5%	174ms	191ms	402ms	140ms	259ms
	10%	172ms	191ms	336ms	140ms	209ms
20% F Droop; 50% V Droop	0%	X	X	X	X	X
	2.5%	187ms	191ms	798ms	X	528ms
	5%	178ms	191ms	531ms	220ms	346ms
	7.5%	174ms	191ms	414ms	140ms	262ms
	10%	172ms	191ms	344ms	140ms	211ms
5% F Droop; 10% V Droop	0%	X	X	X	X	X
	2.5%	188ms	191ms	1.110s	X	633ms
	5%	177ms	191ms	628ms	X	372ms
	7.5%	174ms	191ms	464ms	195ms	273ms
	10%	172ms	191ms	374ms	140ms	216ms
2% F Droop; 1% V Droop	0%	X	X	X	X	X
	2.5%	187ms	191ms	X	X	959ms
	5%	178ms	191ms	X	X	486ms
	7.5%	174ms	191ms	X	X	318ms
	10%	172ms	191ms	382ms	140ms	222ms

PRAM II can detect islanding with 2.5% active power imbalance in 191 ms for all droop control scenarios. It is also illustrated that the detection time for same power imbalance is the same regardless of the DG control scenarios.

POR can detect 2.5% imbalance prior to islanding in 741 ms for control scenario 1, in 798 ms for scenario 2 and in 1.11 s in scenario 3. The sensitivity of POR is further reduced for control scenario 4 as it failed to detect islanding for values as large as 7.5% imbalance prior to islanding. It is also illustrated that the detection time for same power imbalance is longer for more aggressive DG control scenarios and smaller for larger imbalance under same scenario.

ROCOF can detect 2.5% imbalance prior to islanding in 530 ms for control scenario 1. It failed to detect 2.5% imbalance but successfully detected 5% imbalance for scenario 2. ROCOF can detect 7.5% imbalance for scenario 3 and 10% imbalance under the most aggressive control scenario. ROCOF detection time for same power imbalance is longer for more aggressive DG control scenarios and it is smaller for larger imbalance under same scenario.

PAD can detect the smallest imbalances for all control scenarios. The detection time for similar levels of power imbalance is longer (959 ms for 2.5% imbalance under the most aggressive control scenario) for more aggressive DG control scenarios and smaller for larger imbalances under same scenario.

In this test scenario, all methods perform similar to 90% DG output. PRAM has clear advantage in terms of both sensitivity and detection time regardless of control strategy.

5.2.3 Reactive power imbalance with 90% DG output

Table VIII: Test results for islanding with reactive power imbalances (90% DG output)

Control	Imbalance	PRAM I	PRAM II	POR	ROCOF	PAD
PQ (Q=0)	0%	X	X	X	X	X
	2.5%	X	X	X	580ms	702ms
	5%	195ms	211ms	573ms	155ms	403ms
	7.5%	187ms	191ms	491ms	155ms	343ms
	10%	182ms	191ms	428ms	150ms	296ms
20% F Droop; 50% V Droop	0%	X	X	X	X	X
	2.5%	X	X	X	X	596ms
	5%	195ms	211ms	624ms	175ms	430ms
	7.5%	190ms	191ms	506ms	155ms	346ms
	10%	182ms	191ms	446ms	155ms	303ms
5% F Droop; 10% V Droop	0%	X	X	X	X	X
	2.5%	X	X	X	X	702ms
	5%	195ms	211ms	762ms	X	471ms
	7.5%	190ms	191ms	681ms	155ms	426ms
	10%	182ms	191ms	500ms	155ms	318ms
2% F Droop; 1% V Droop	0%	X	X	X	X	X
	2.5%	X	X	X	X	X
	5%	197ms	211ms	X	X	995ms
	7.5%	190ms	191ms	X	X	518ms
	10%	182ms	191ms	X	X	385ms

It is shown in Table VIII that PRAM I can detect islanding with 5% reactive power imbalance in 197 ms for all droop control scenarios. The detection time is further reduced with the imbalance increases as the pick up is earlier. It is also illustrated that the detection time for same power imbalance is almost the same regardless of DG control scenarios. The slightly different detection time at 7.5% imbalance in scenario 1 (187 ms) and at 5% imbalance in scenario 4 (197ms) is due to the imperfection of practical simulation environment (e.g. reactive power imbalance is not perfectly precise and active power imbalance is not perfectly 0).

PRAM II can detect islanding with 5% reactive power imbalance in 211 ms for all droop control scenarios. It is also illustrated that the detection time for same power imbalance is the same regardless of DG control scenarios.

POR can detect 5% imbalance prior to islanding in 573 ms for control scenario 1, in 624 ms for scenario 2 and in 762 ms in scenario 3. The sensitivity of POR is further reduced for control scenario 4 as it failed to detect at least 10% imbalance prior to islanding. It is also illustrated that the detection time for same power imbalance is longer for more aggressive DG control scenarios and it is smaller for larger imbalance under same scenario.

ROCOF can detect 2.5% imbalance prior to islanding in 580 ms for control scenario 1. It failed to detect 2.5% imbalance but successfully detected 5% imbalance for scenario 2. ROCOF can detect 7.5% imbalance for scenario 3 but failed to detect 10% imbalance under the most aggressive control scenario. ROCOF detection time for same power imbalance is longer for more aggressive DG control scenarios and it is smaller for larger imbalance under same scenario.

PAD only failed to detect 2.5% imbalance under the most aggressive control scenario but successfully detected all other imbalances under all scenarios. The detection time for same power imbalance is longer (995 ms for 5% imbalance under the most aggressive control scenario) for more aggressive DG control scenarios and smaller for larger imbalance under same scenario.

In the most passive control mode (PQ control), ROCOF can detect the smallest imbalance and presents the shortest detection time. However, as control mode being more aggressive, a larger non detection zone is presented compared to other method (as high as 10% imbalance for most aggressive mode). In this test scenario PAD seems to be the most reliable method as it only failed to detect 2.5% imbalance at the most aggressive mode. PRAM presents a steady performance of capable to detect 5% imbalance regardless of control mode. It also shows advantage of short detection time against PAD.

5.2.4 Reactive power imbalance with 30% DG output

It is shown in Table IX that PRAM I can detect islanding with 10% reactive power imbalance in 202 ms for all droop control scenarios. It is also illustrated that the detection time is almost the same regardless of DG control scenarios. The slight difference is due to the imperfection of practical simulation environment. The reason PRAM failed to detect 2.5% imbalance for all control modes is that the largest peak is too small to trigger a 0.6 Hz/s pick up.

Table IX: Test results for islanding with reactive power imbalances (30% DG output)

Control	Imbalance	PRAM I	PRAM II	POR	ROCOF	PAD
PQ (Q=0)	0%	X	X	X	X	X
	2.5%	X	X	X	X	1.069s
	5%	X	X	X	X	829ms
	7.5%	X	X	X	X	636ms
	10%	199ms	211ms	737ms	425ms	509ms
20% F Droop; 50% V Droop	0%	X	X	X	X	X
	2.5%	X	X	X	X	1.161s
	5%	X	X	X	X	829ms
	7.5%	X	X	X	X	666ms
	10%	200ms	211ms	802ms	X	536ms
5% F Droop; 10% V Droop	0%	X	X	X	X	X
	2.5%	X	X	X	X	1.463s
	5%	X	X	X	X	1.055s
	7.5%	X	X	X	X	798ms
	10%	202ms	221ms	X	X	630ms
2% F Droop; 1% V Droop	0%	X	X	X	X	X
	2.5%	X	X	X	X	X
	5%	X	X	X	X	X
	7.5%	X	X	X	X	X
	10%	202ms	221ms	X	X	1.751s

PRAM II can detect islanding with 10% reactive power imbalance in 211 ms for all droop control scenarios. It is also illustrated that the detection time for same power imbalance is the same regardless of DG control scenarios.

POR can detect 10% imbalance prior to islanding in 737 ms for control scenario 1 and in 802 ms for scenario 2. The sensitivity of POR is further reduced for control scenario 3 and 4 as it failed to detect at least 10% imbalance prior to islanding. It is also illustrated that the detection time for same power imbalance is longer for more aggressive DG control scenarios.

ROCOF can only detect 10% imbalance prior to islanding in 425 ms for control scenario 1. It failed to detect all other imbalances under every scenario.

PAD only failed to detect 7.5% imbalance under the most aggressive control scenario but successfully detected all other imbalances under all scenarios. The detection time for same power imbalance is longer (1.751 s for 10% imbalance under the most aggressive control scenario) for more aggressive DG control scenarios and smaller for larger imbalance under same scenario.

It is shown in the results that reduction of DG output from 90% to 30% makes islanding detection more difficult under reactive power imbalance conditions for all algorithms (takes longer for PAD). It means a reduction of DG output makes frequency more stable when active power is balanced. This may be due to slightly different transient stresses on the DG rotors during the islanding events. This factor only marginally affected the results of active power imbalance. The reason is that active power imbalance is the main factor to cause deviation of frequency and ROCOF signal. When active power is balanced, any small factors (reactive power imbalance, DG output and etc.) may affect testing results.

References

- [5.1] (July 2015) National Grid, “System Operability Framework” [Online].
Available: <http://www2.nationalgrid.com/UK/Industry-information/Future-of-Energy/System-Operability-Framework/>

Chapter 6

Stability Tests

6.1 Testing Procedure

In order to test the stability of the PRAM relay, fault events, load switching, capacitor switching and transformer inrush were simulated using the test network. The installed capacity of the synchronous machine-powered grid is 40 GVA. The DG is modelled as having 90% power output prior to system events in all stability tests. It should not affect much on stability tests as they are carried out in grid connected mode. It is selected to reflect a typical condition of power contribution from DG. All settings remain the same as in sensitivity tests.

Three different types of faults (single phase to earth, phase to phase, and three phase) were simulated at six different locations as shown in Figure 36. Faults are set to be cleared 250 ms after initiation by network protection. For single phase to earth faults, reclosing is applied 500 ms after initial clearance, and all faults simulated in this test are transient and no longer exist after initial clearance by circuit breakers, so all reclose operations are successful. For phase to phase and three phase faults at

location 2, islanding of the DG is caused when the CBs open to clear the fault, and this should of course be detected by the LOM protection.

For load switching events, local load switching at 33 kV network and remote large load changes at the 400 kV level were simulated. Both modes of switching out and in loads were simulated. Load switching at 33 kV at different sites with magnitudes of 3.2 MW, 4.9 MW, 8.8 MW, 10.39 MW, 20.78 MW, and 28.59 MW was used. Load switching at 400 kV with magnitudes of 1 GW, 1.3 GW, 1.5 GW and 1.8 GW was carried out. 1.8 GW is the largest credible loss of load in the UK according to [6.1]. 1.5 GW and 1.3 GW were selected as the interval values between 1.8 GW and 1 GW. The inertia of the external power grid was varied to include values of 8 s, 6 s, 5 s, 4 s to represent present to future system strengths according to [6.1]. For local load switching events, results with system inertia of 4 s is presented as only the POR relay tripped under the largest load change of 28.59 MW. It is proposed that all relays will be generally more stable with larger system inertia as any frequency perturbation arising from a short circuit will be less pronounced for higher levels of inertia. For large remote load changes, tests with a variety of system inertias and magnitudes of load changes were carried out with the inertia and load changes applied in descending orders of magnitude. Once all relays successfully rode through the events, further load switching tests with lower magnitudes were deemed unnecessary and tests were continued with only reducing values of grid inertia at the fixed value of “minimum” load change (for which all protection types remained stable).

Capacitor switching out at the previously-mentioned fault location 2 with the magnitudes of 8.1 MVar and 11 MVar was carried out. These values were chosen based on the prevailing reactive power consumption level of the network.

Transformer inrush test contains two separate stages:

1. A three-phase fault at location 6 was applied and cleared. Subsequently, both transformers connected at this location were switched in under no load conditions.

2. The example of “Three-Phase Saturable Transformer” in SimPowerSystem is used as shown in Figure 54. It models a 450 MVA transformer energised on a 400 kV network.

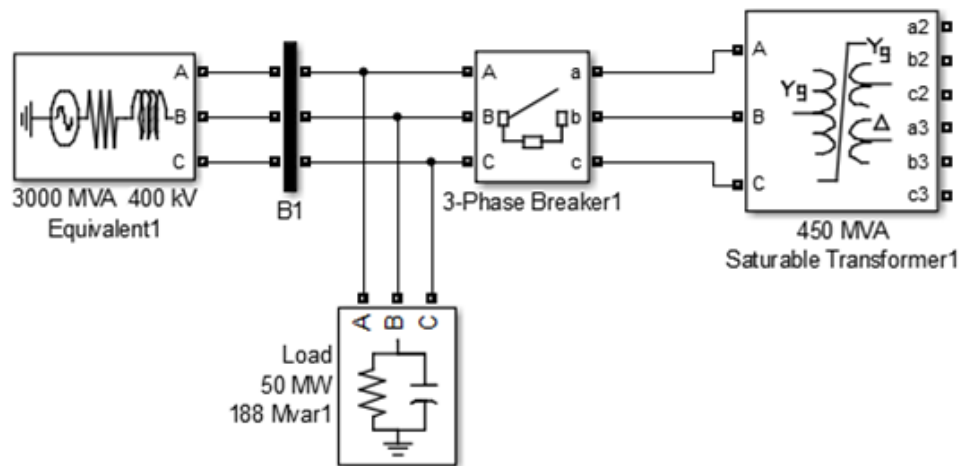


Figure 54: Single source network for transformer inrush test

6.2 Discussion of Stability Test Results

6.2.1 Single phase to earth fault

It is shown in Table X that PRAM I was stable for both single phase fault initiation and subsequent reclosing at all simulated fault locations. It tripped for fault clearing at location 3 but remained stable at all other locations in this scenario. ROCOF behaviour of PRAM I is shown in Figure 55 and Figure 56 (scaled to provide detailed waveform), and the peak ratios are shown in Figure 57.

It is shown in Figure 57 that PRAM I picked up at all 6 locations but the largest peak ratio just exceeds 1.4 at location 2. It indicates that peak ratios are not close to the setting value of 2 and PRAM I is very stable for single phase fault initiation at all locations. PRAM I did not pick up fault clearing at location 6 but picked up at all other locations. Peak ratios at all locations remained stable at the first pick up after fault clearing with the largest value of 1.56 and the second largest value of 1.42. It indicates that PRAM I is also stable immediately after single phase fault clearing. However, PRAM I picked up again twice at location 3 with the peak ratio magnitude of 1.98 and infinite. It should be noticed that although the tripping signal was sent after reclosing (2.75s), almost the entire processing window was before reclosing and the mal-operation of PRAM I was contributed to by the action of fault clearing as shown in Figure 58. Therefore, this tripping is not included in the effect of CB reclosing. It can be seen in Figure 36 that location 3 is on the 132 kV transmission line and relatively closer to the main grid (which is modelled as a synchronous machine and not as an ideal source). It involves a very large fault current contribution from the grid, and therefore disturbs the grid more so than other faults.

Table X: Test results for single phase faults at various locations (√: Successfully rode through; X: Failed to remain stable)

	PRAM I	PRAM II	POR	ROCOF	PAD
Fault Initiation					
Location 1	√	√	√	X	√
Location 2	√	√	√	√	√
Location 3	√	√	√	√	√
Location 4	√	√	√	X	√
Location 5	√	√	√	√	√
Location 6	√	√	√	√	√
Fault Clearing					
Location 1	√	√	√	√	√
Location 2	√	√	√	√	√
Location 3	X	X	X	X	X
Location 4	√	√	√	√	√
Location 5	√	√	X	X	√
Location 6	√	√	√	√	√
Reclosing					
Location 1	√	√	√	√	√
Location 2	√	√	√	√	√
Location 3	√	√	X	X	X
Location 4	√	√	√	√	√
Location 5	√	√	√	√	√
Location 6	√	√	√	√	√

Reclosing at all locations except for location 1 and 5 were picked up with the largest peak ratio magnitude of 1.23 at location 4. It illustrates that PRAM I is very stable for single phase fault reclosing.

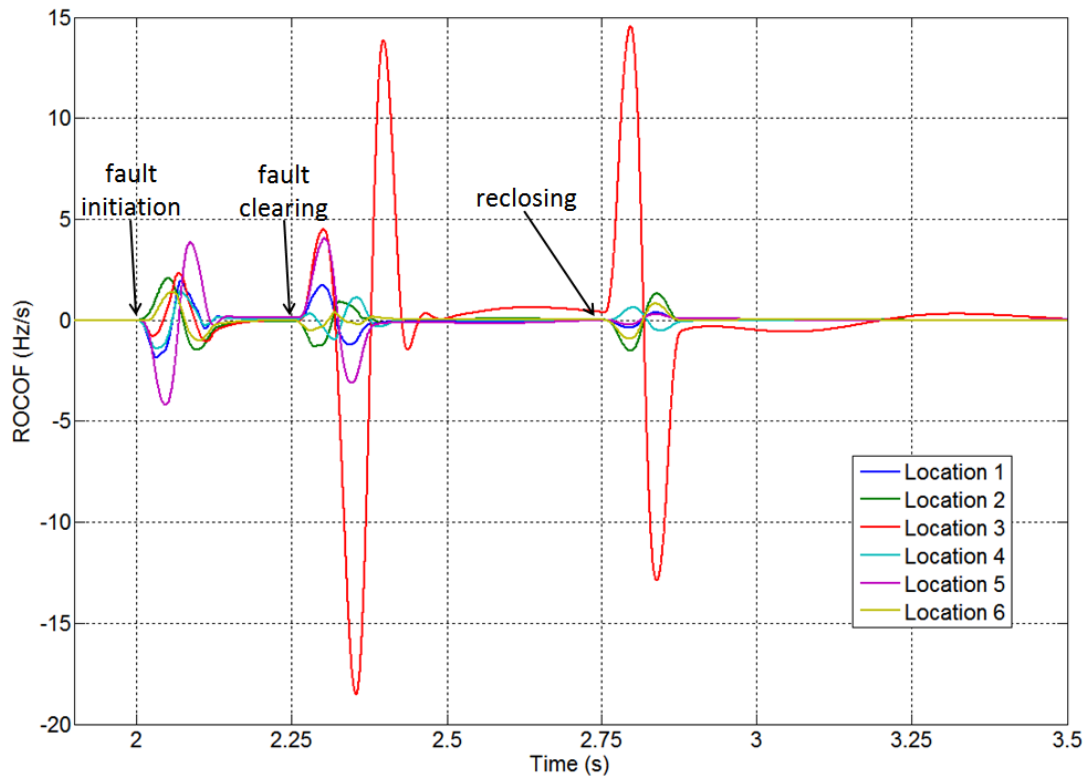


Figure 55: ROCOF output of PRAM I during single phase fault initiation, clearing and reclosing

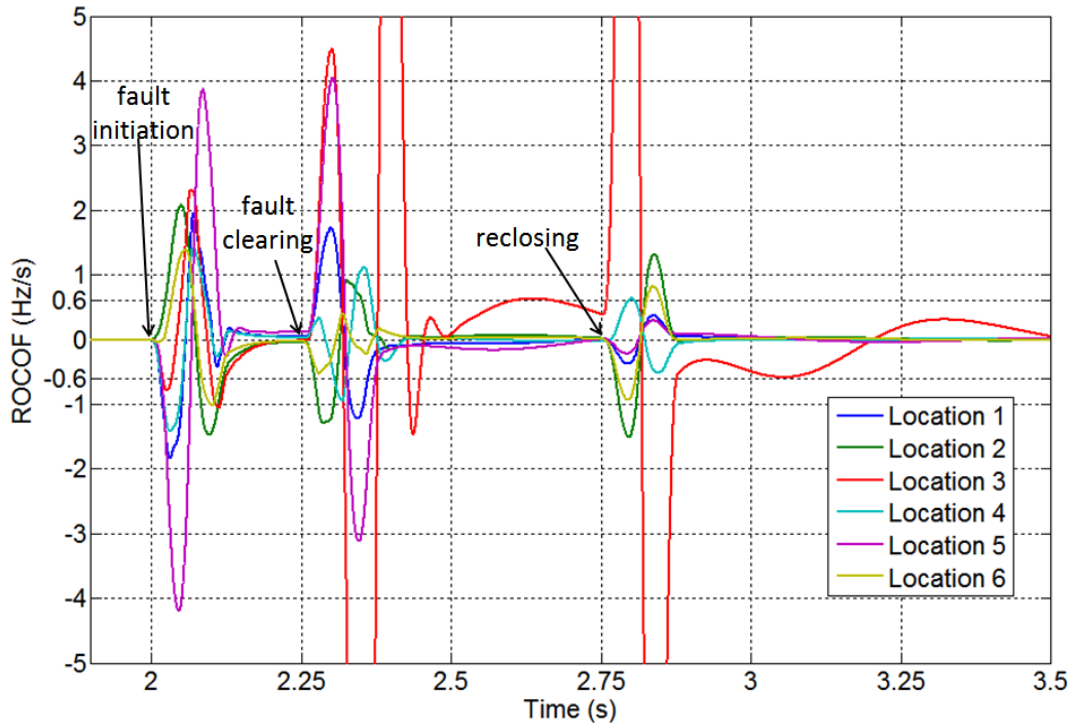


Figure 56: Scaled ROCOF output of PRAM I during single phase fault initiation, clearing and reclosing

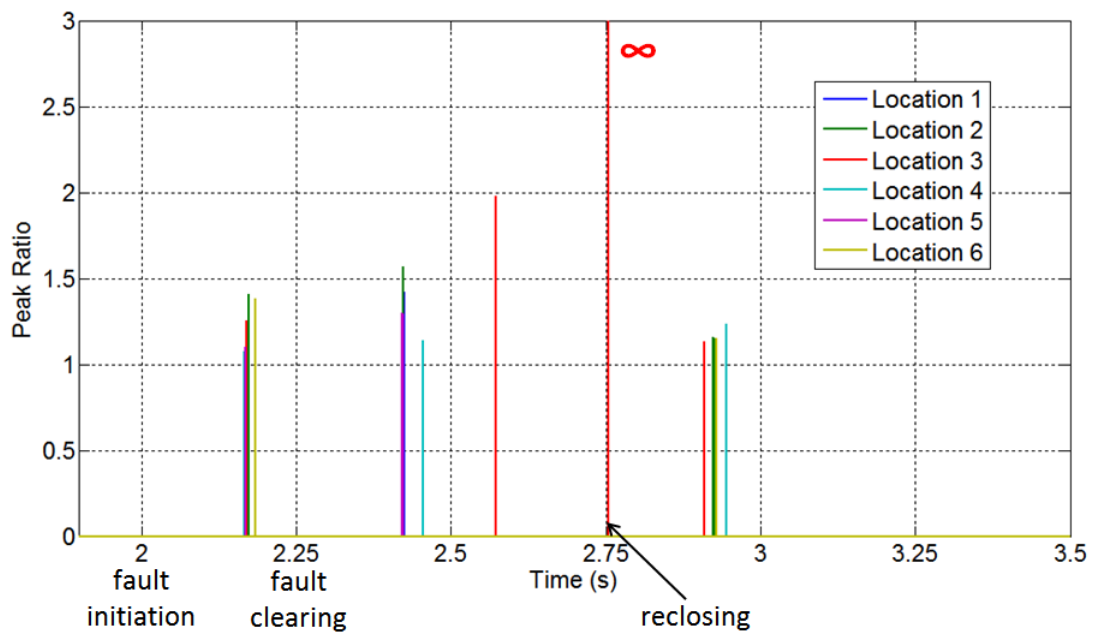


Figure 57: Peak ratio output of PRAM I during single phase fault initiation, clearing and reclosing

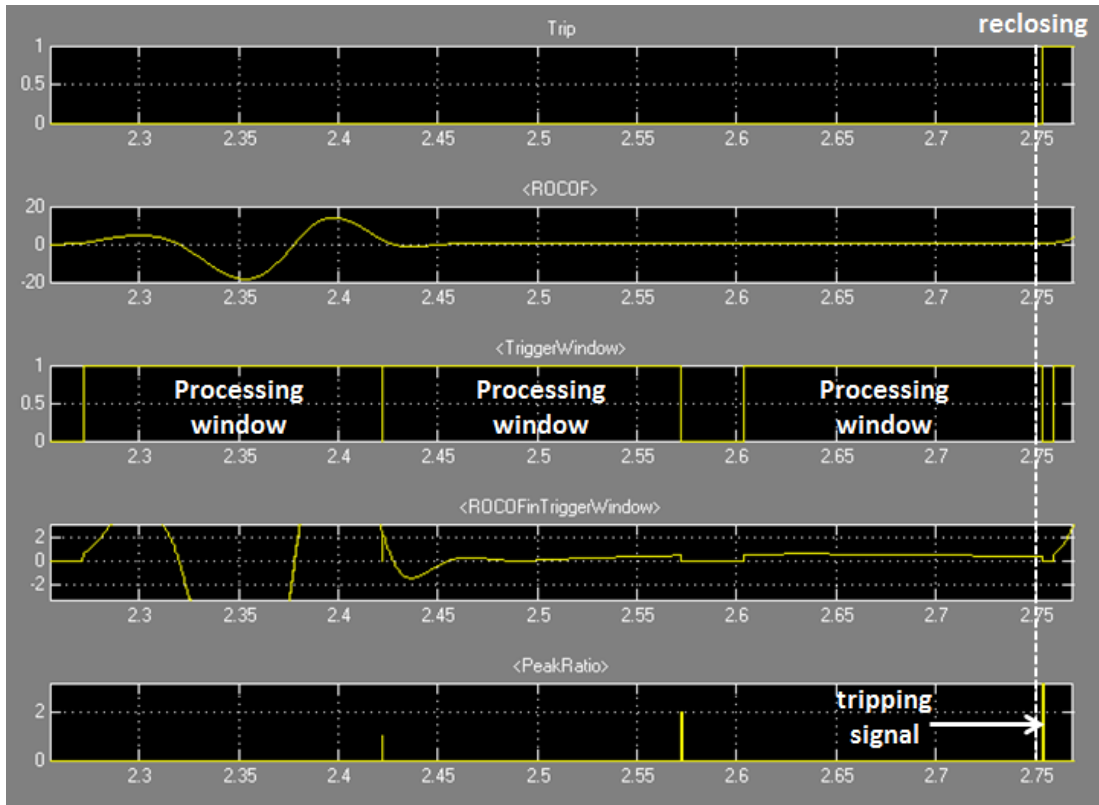


Figure 58: Output of PRAM I during single phase fault clearing at location 3

It is shown in Table X that PRAM II was stable for single phase fault initiations and reclosing at all locations. It tripped for fault clearing at location 3 but remained stable at all other locations in this scenario. ROCOF behaviour of PRAM II is shown in Figure 59 and Figure 60, and the peak ratios are shown in Figure 61.

It is shown in Figure 61 that PRAM II picked up at all 6 locations but the largest peak ratio just exceeds 1.62 at location 1 and the second largest peak magnitude is 1.36 at location 6. It indicates that peak ratios are not close to the setting value of 2.1 and PRAM II is very stable for single phase fault initiation at all locations.

PRAM I did not pick up fault clearing at location 6 but picked up at all other locations. Peak ratios at all locations remained stable at the first pick up after fault clearing with the largest value of 1.77 at location 2. This value is relatively larger than the corresponding value of PRAM I (1.56) but yet close to the peak ratio

threshold which is 2.1. The second largest value is 0.94 which indicates that PRAM II is stable at all locations immediately after single phase fault clearing. However, PRAM II picked up again twice at location 3 with a peak ratio magnitude of 3.09 and infinite (i.e. there was no second peak). Refer to the same explanation in PRAM I, although the second tripping signal was sent after reclosing (2.75s), almost the entire processing window was before reclosing and the mal-operation of PRAM II was caused by fault clearing as shown in Figure 62. Therefore, this tripping is not included in the effect of CB reclosing.

Reclosing at all locations except for location 1 and 5 were picked up, with the largest peak ratio magnitude of 1.3 at location 4. It illustrates that PRAM I is very stable for single phase fault reclosing.

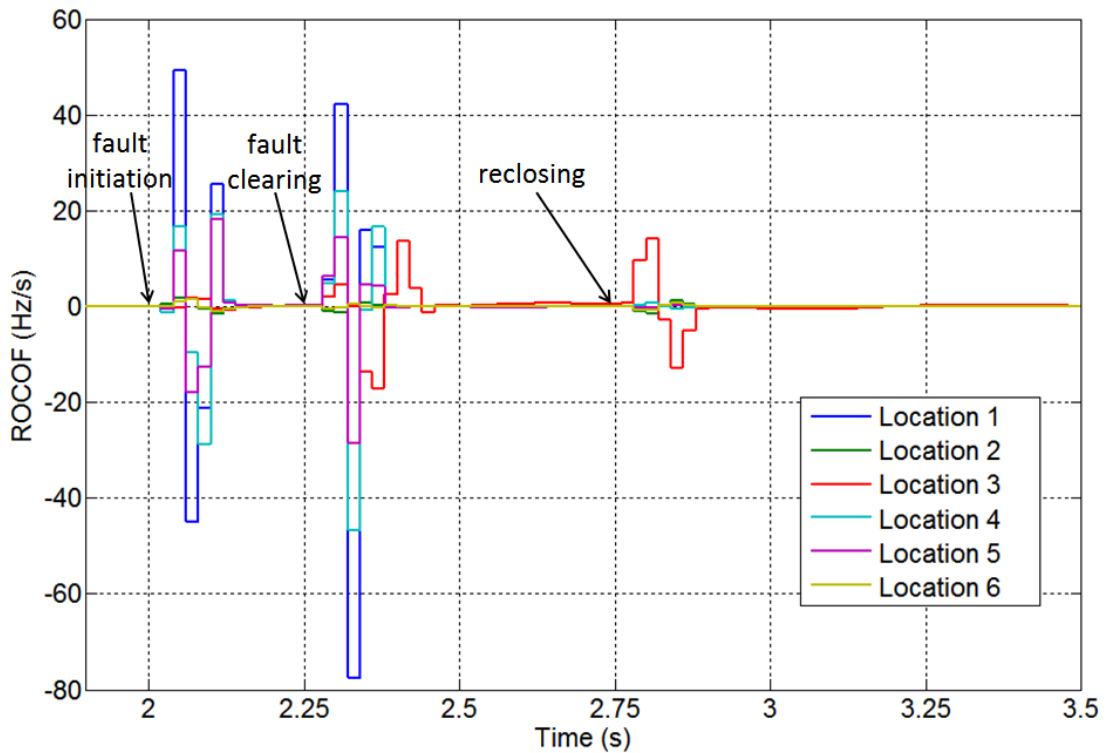


Figure 59: ROCOF output of PRAM II during single phase fault initiation, clearing and reclosing

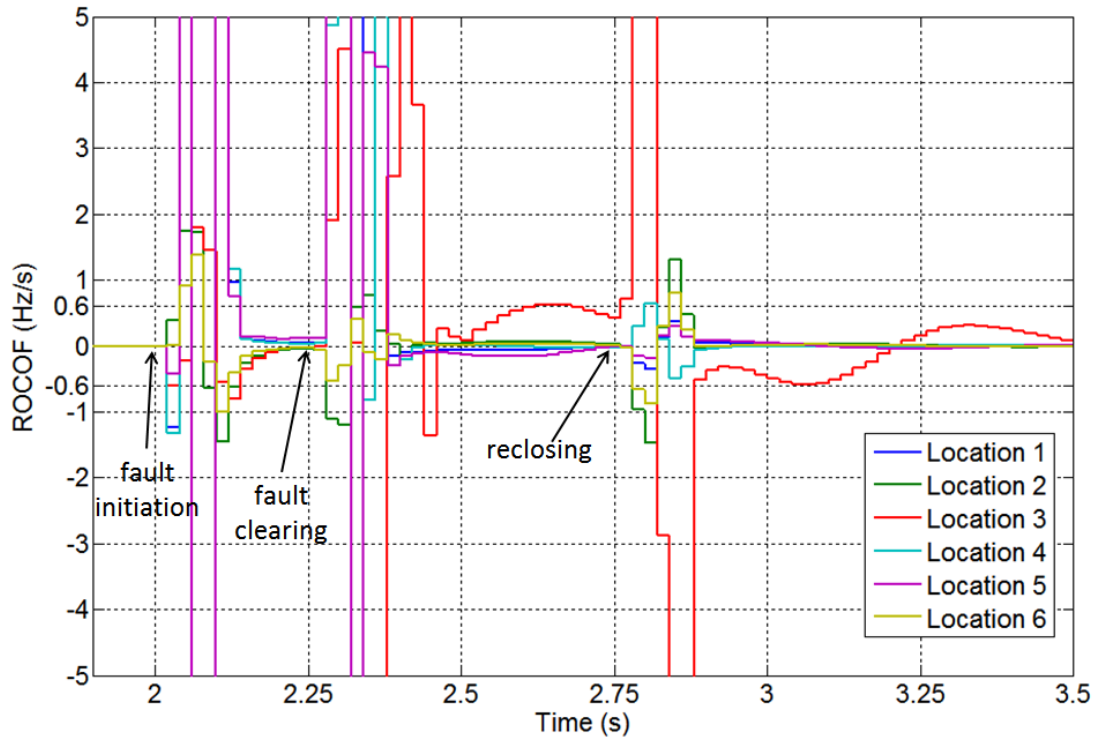


Figure 60: Scaled ROCOF output of PRAM II during single phase fault initiation, clearing and reclosing

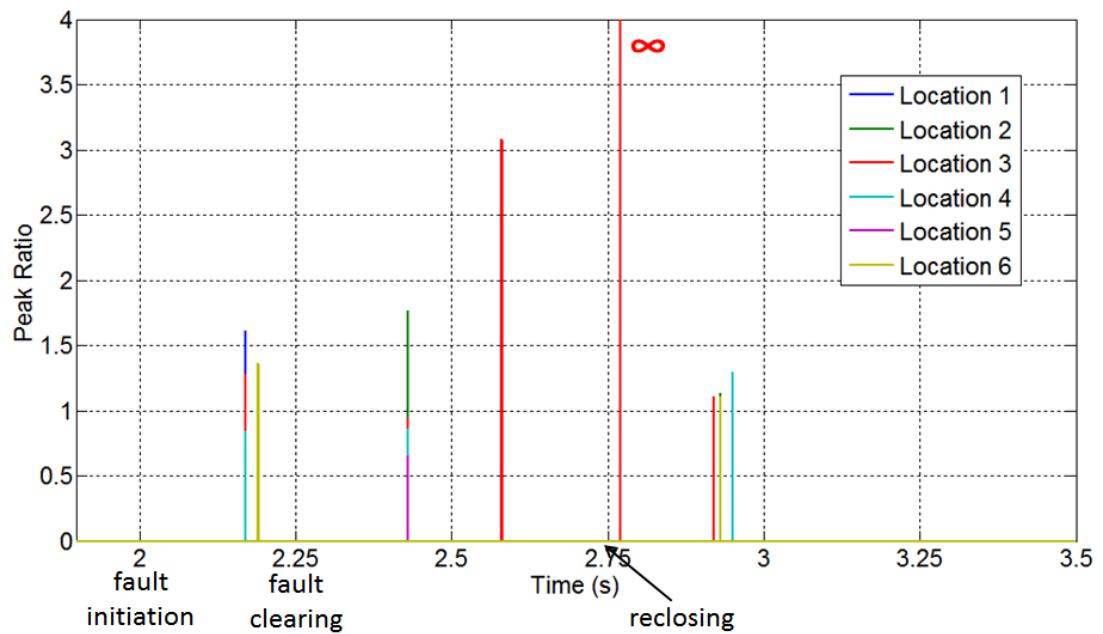


Figure 61: Peak ratio output of PRAM II during single phase fault initiation, clearing and reclosing

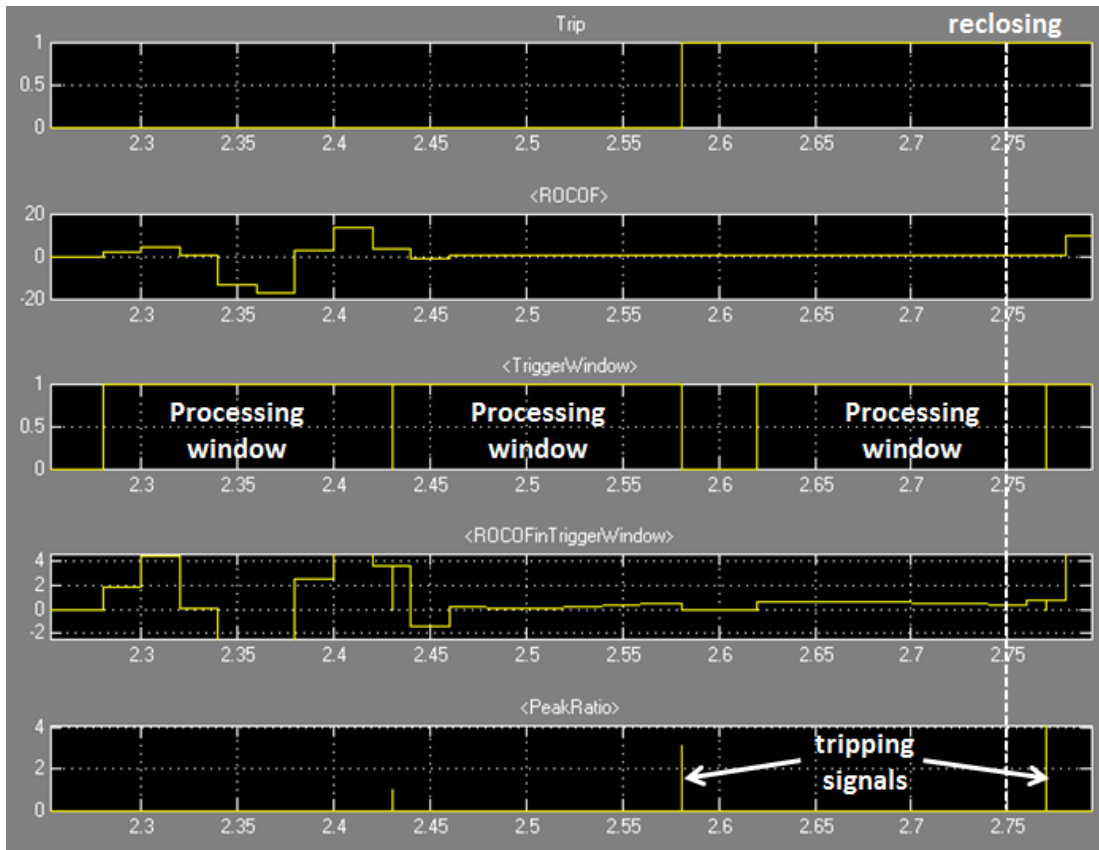


Figure 62: Output of PRAM II during single phase fault clearing at location 3

POR is stable for single phase fault initiation at all locations and stable for reclosing at all locations except for location 3. POR trips incorrectly for fault clearing at location 3 and 5. It has been established through testing that, in order to avoid tripping for fault clearing, the minimum phase offset setting should be 31° , but this is at the expense of sensitivity with respect to detection of islanding. It was also established that the phase offset reached -136° after reclosing; it is unreasonable to set the threshold at this level. A phase offset setting of 23° will only trip for fault clearing at location 5 and reclosing at location 3.

ROCOF is unstable for fault initiation at location 1 and 4. It failed to ride through fault clearing and reclosing at location 3 and fault clearing at location 5. In order to remain stable for fault initiation at location 1, it was established that the ROCOF setting should be as large as 6.5 Hz/s, which is a totally infeasible setting to use in

practice. To ride through fault initiation at location 4, ROCOF threshold should be set to 0.5 Hz/s, which may sacrifice a degree of sensitivity. For fault clearing, even a threshold of 10 Hz/s is not high enough for ROCOF relay at location 5. Finally, a setting of 2.6 Hz/s is required to ensure stability for faults at location 3. Threshold of 0.5 Hz/s will ensure ROCOF to ride through reclosing at location 3.

PAD is very stable for all scenarios at all locations except for fault clearing and reclosing at location 3. PAD will be stable with a threshold of 16.3° for these two scenarios.

6.2.2 Phase to phase fault

It is shown in Table XI that PRAM I is stable for phase to phase fault initiations at all locations. It tripped for fault clearing at location 3 but remained stable at all other locations in this scenario. ROCOF behaviour of PRAM I is shown in Figure 63 and Figure 64 (scaled), and the peak ratios are shown in Figure 65. It is clear in Figure 65 that PRAM I picked up at all 6 locations for fault initiation. The largest peak ratio exceeds 1.93 at location 3 which presents a high risk of false tripping if the peak ratio threshold is set to be lower than this. The second largest peak ratio is 1.53 at location 6 and it indicates that peak ratios are not close to the setting value of 2 and PRAM I is stable for phase to phase fault initiation at all locations except for location 3. Again this may be due to the large fault contribution from grid which is modelled as a synchronous machine.

Table XI: Test results for phase to phase faults (fault clearing at Location 4 led to islanding)

	PRAM I	PRAM II	POR	ROCOF	PAD
Fault Initiation					
Location 1	√	√	√	√	√
Location 2	√	√	√	√	√
Location 3	√	√	√	√	√
Location 4	√	√	√	X	√
Location 5	√	√	√	√	√
Location 6	√	√	√	√	√
Fault Clearing					
Location 1	√	√	√	X	√
Location 2	√	√	√	√	√
Location 3	X	√	√	X	√
Location 4	√	√	√	√	√
Location 5	√	√	√	√	√
Location 6	√	√	√	√	√

PRAM I also picked up for fault clearing at all locations and tripped at location 3 (same reason as above) with peak ratio value of 2.11. The second largest peak ratio is 1.38 at location 1 and this indicates that peak ratios are not close to the setting value of 2 and that PRAM I will remain stable for phase to phase fault clearing at all locations except for location 3. It should be noted that fault clearing at location 4 also led subsequently to an islanding event as showing in Figure 63 and Figure 64. It is

illustrated in Figure 65 and Figure 66 that PRAM I successfully tripped 308 ms after islanding with the value of peak ratio being infinite.

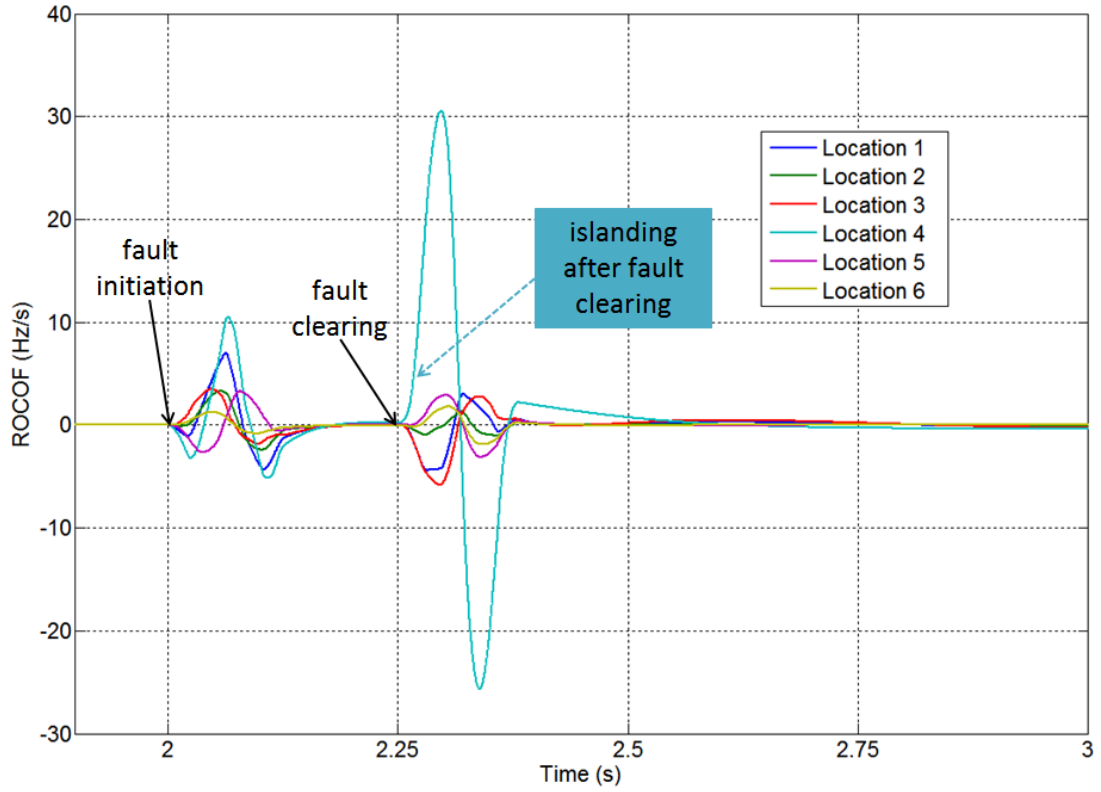


Figure 63: ROCOF output of PRAM I during phase to phase fault initiation and clearing

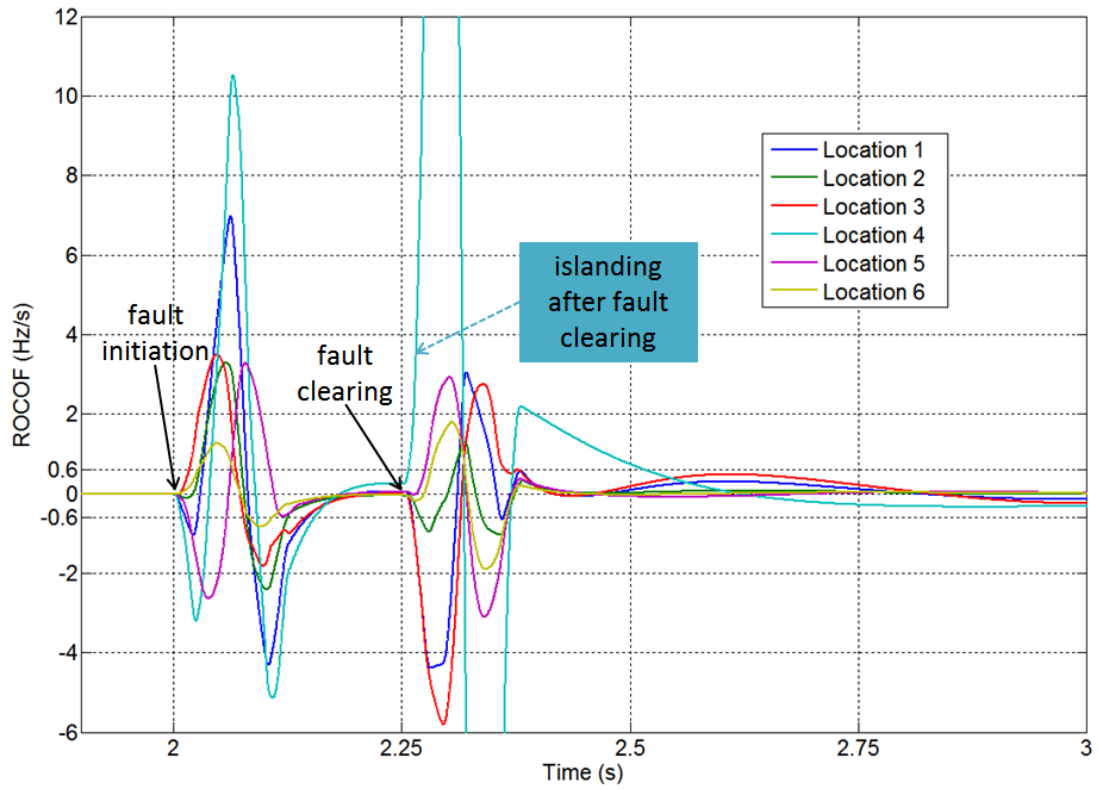


Figure 64: Scaled ROCOF output of PRAM I during phase to phase fault initiation and clearing

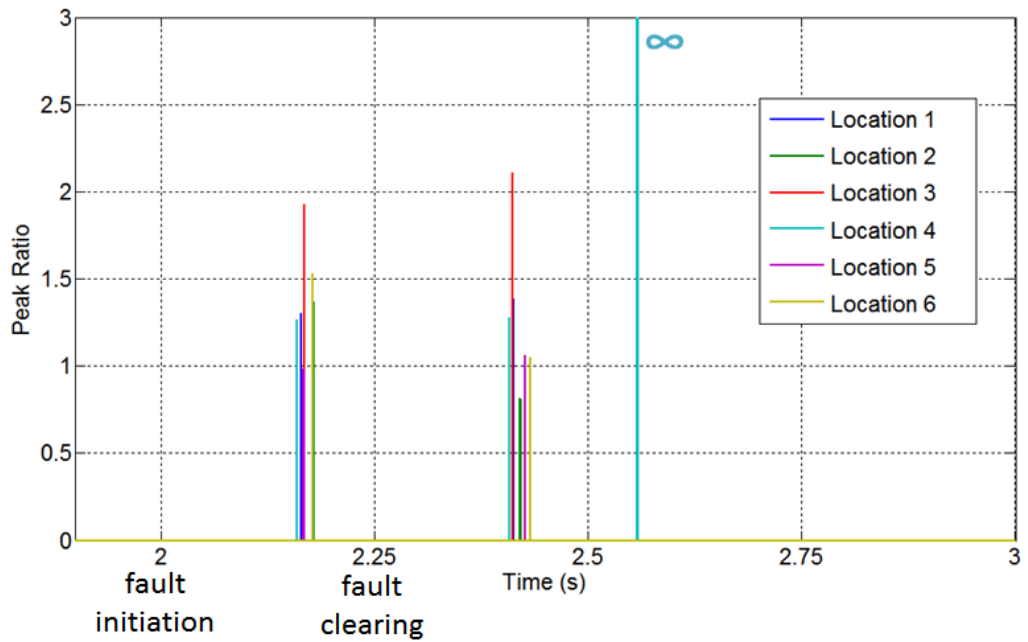


Figure 65: Peak ratio output of PRAM I during phase to phase fault initiation and clearing

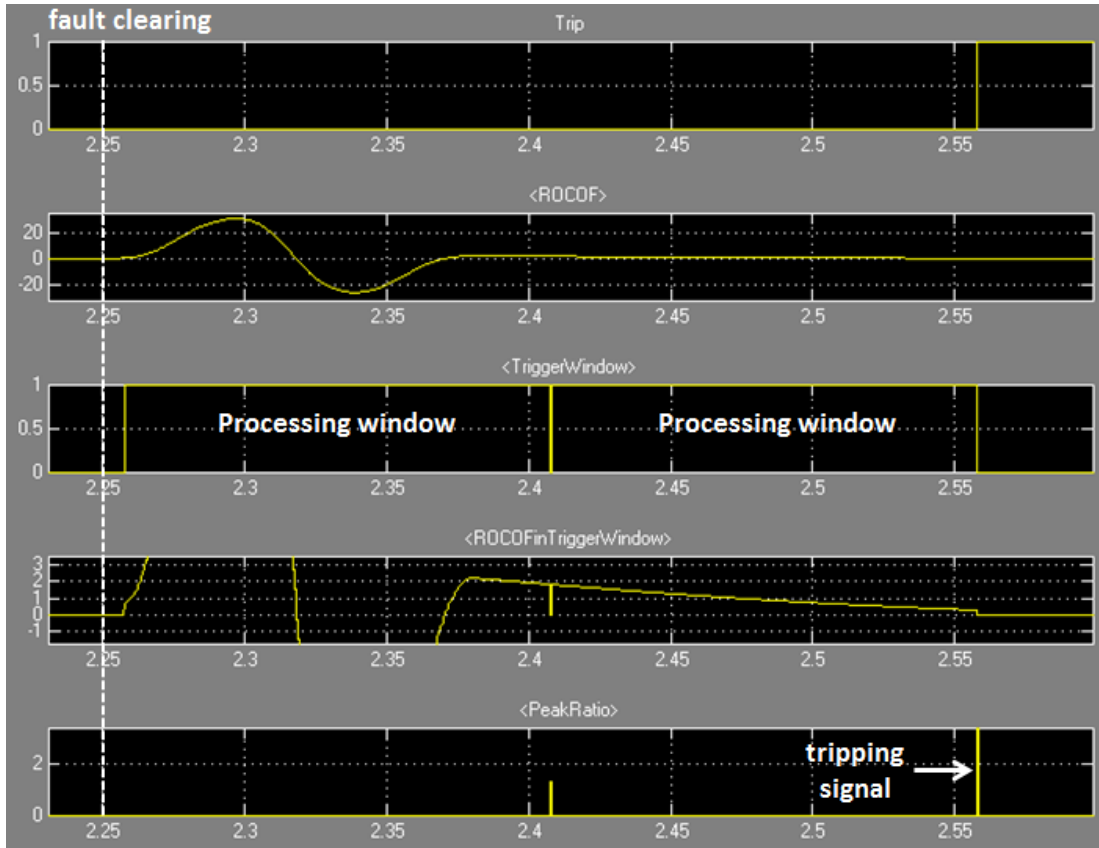


Figure 66: Output of PRAM I during phase to phase fault clearing

It is shown in Table XI that PRAM II remains stable for phase to phase fault initiations and clearing at all locations. The ROCOF behaviour of PRAM II is shown in Figure 67 and Figure 68 (scaled) and the peak ratios are shown in Figure 69.

It is shown in Figure 69 that PRAM II picked up at all 6 locations for fault initiation. The largest peak ratio exceeds 1.96 at location 3 which leads to a high risk of false tripping if the peak ratio threshold is lower than 2. The second largest peak ratio is 1.38 at location 2 and this indicates that peak ratios are not close to the setting value of 2.1 and PRAM II is very stable for phase to phase fault initiation at all locations except for location 3. Again this may due to the large fault contribution from grid which is modelled as a synchronous machine.

PRAM II also picked up at all locations for fault clearing. The largest peak ratio is 1.92 at location 3 which is again close to the threshold and could be risky. The second largest peak ratio is 1.37 at location 1, which indicates that peak ratios are not close to the setting value of 2.1 and PRAM II is very stable for phase to phase fault clearing at all locations except for location 3 (same reason as above). It should be noticed that again fault clearing at location 4 led to islanding event as showing in Figure 67 and Figure 68. Figure 69 and Figure 70 show that PRAM II successfully tripped 311 ms after islanding with a peak ratio of infinite.

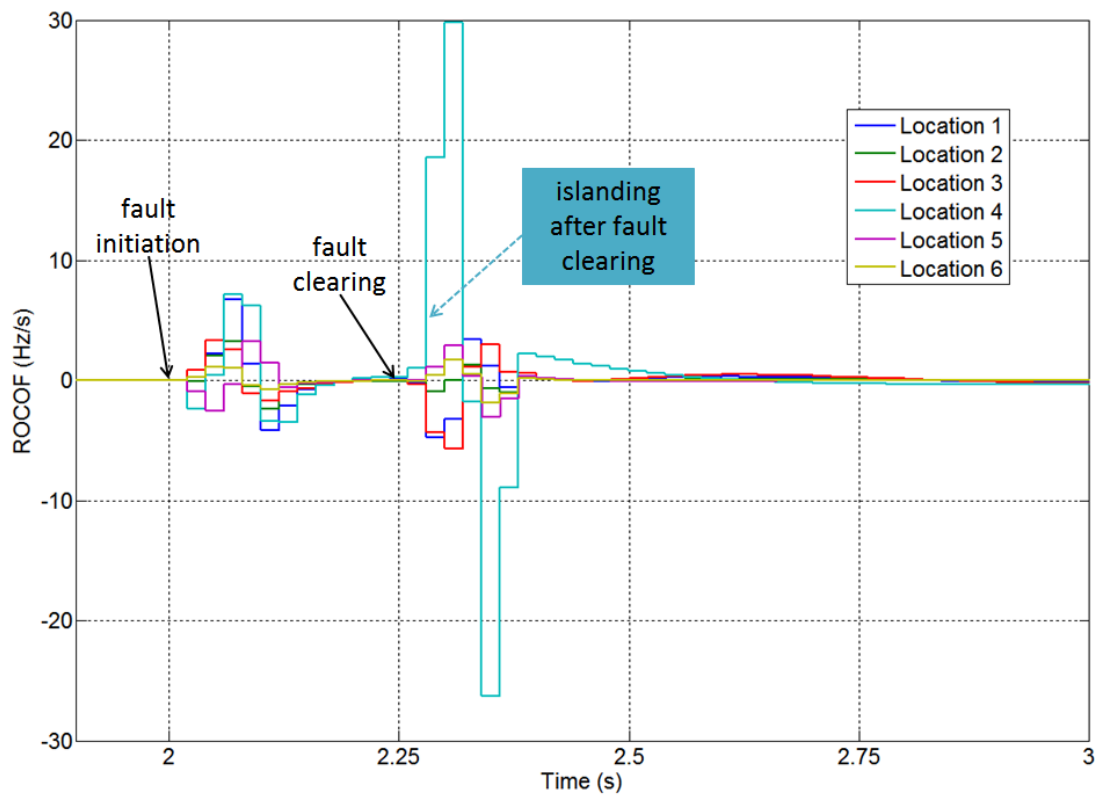


Figure 67: ROCOF output of PRAM II during phase to phase fault initiation and clearing

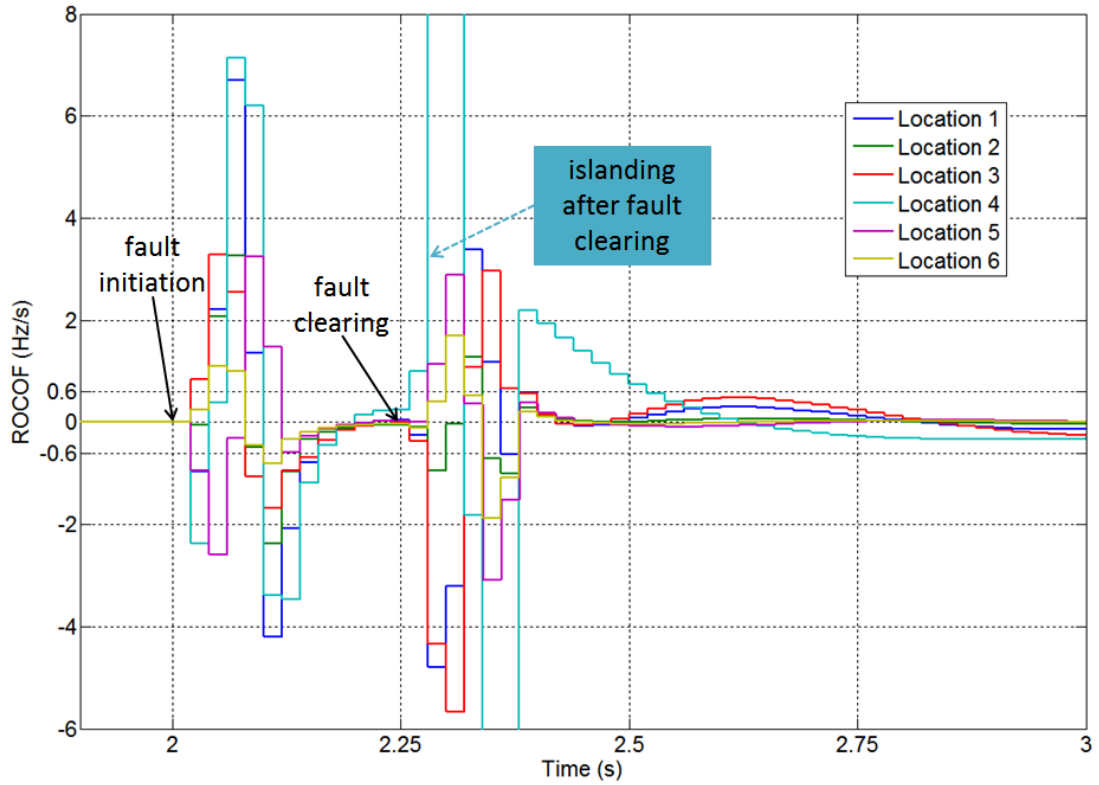


Figure 68: Scaled ROCOF output of PRAM II during phase to phase fault initiation and clearing

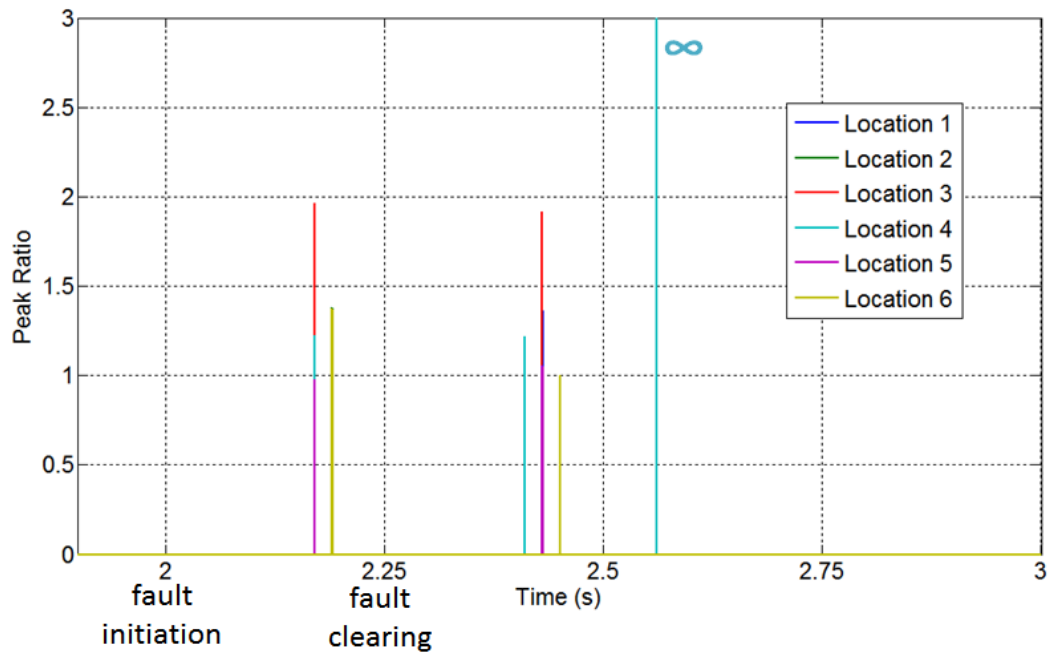


Figure 69: Peak ratio output of PRAM II during phase to phase fault initiation and clearing

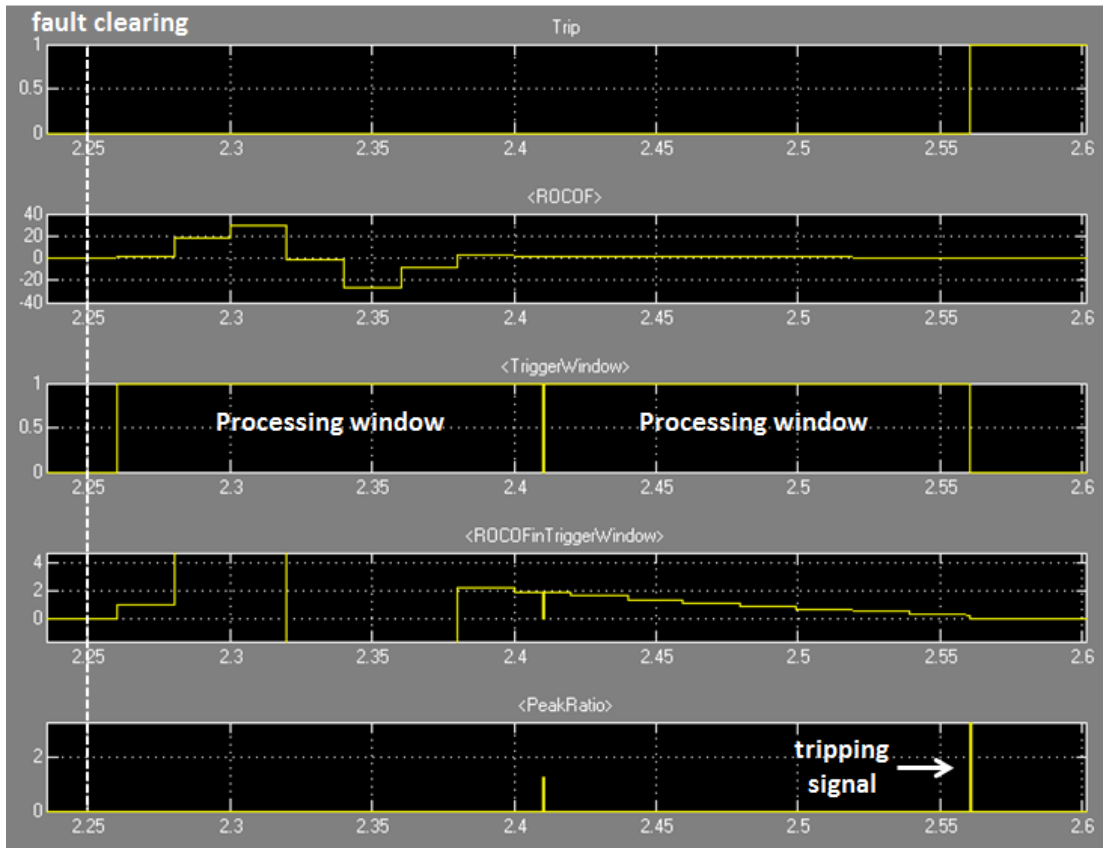


Figure 70: Output of PRAM II during phase to phase fault clearing

POR is stable for phase to phase fault initiation and clearing at all locations according to Table XI. POR also accurately detected islanding event after fault clearing at location 4. It has been established through testing that the maximum phase offset for fault initiation is 14° and 15.3° for fault clearing, both for faults at location 3. These values are not very close to the phase offset setting of 20° and this is a further indication of the fact that POR is very stable for phase to phase faults. It was also established that the POR successfully tripped at 68 ms and reached 26.6° quickly (128 ms) after the islanding event (at fault clearing when the circuit breaker is opened to clear the fault – and cause an island) at location 4. This indicates that POR is reliable under phase to phase fault scenario.

ROCOF is unstable for fault initiation at location 4, and failed to ride through fault clearing at location 1 and 3. ROCOF accurately detected the islanding event

140 ms after fault clearing at location 4. In order to remain stable for fault initiation at location 4, ROCOF setting should be 0.25 Hz/s. For fault clearing, threshold of 0.25 Hz/s is enough for ROCOF relay to ride through at location 1 and it can remain stable for 0.45 Hz/s setting at location 3.

PAD is stable for phase to phase fault initiation and clearing at all locations. However, it is tested that PAD reached 9.2° for fault clearing at location 3 which is very close to the threshold (10°) and dangerous of mal-operation. PAD also accurately and quickly (23 ms) detected islanding event at location 4.

6.2.3 Three phase to earth fault

It is shown in Table XII that PRAM I was stable for three phase to earth fault initiation at all locations except for location 4. It tripped for fault clearing at location 1 and 3 but remained stable at all other locations in this scenario. ROCOF behaviour of PRAM I is shown in Figure 71 and Figure 72 (scaled), and the peak ratios are shown in Figure 73. It is shown in Figure 73 that PRAM I picked up at all 6 locations and the largest peak ratio reaches 2.34 at location 4. And it is seen from Figure 71 that transient ROCOF after fault initiation hits 31.4 Hz/s which is very large. As location 4 is the substation from 132 kV to 33 kV, two parallel paths of large symmetrical fault current are contributed from the grid. The second largest peak ratio is 1.71 which is at location 3 and all other peak ratios are below 1.6. It indicates that PRAM I is very stable for three phase fault initiation at all locations except for location 4. PRAM I also picked up fault clearing at all locations. For all non-islanding scenarios, the largest peak ratio immediately after fault clearing is 1.7 which contributed from location 3. All other first peak ratios of non-islanding scenarios are below 1.5. They indicate that the nature of ROCOF curve immediately

after three phase fault tend to be stable under PRAM I algorithm. However, symmetrical three phase fault obviously caused ROCOF curve swing at locations (location 1, 3 and 4) closer to grid source. Fault clearing at location 4 caused further islanding whose largest peak ratio is infinite which will always be successfully detected. But the other two non-islanding scenarios at location 1 and 3 whose peak ratios are also infinite led to mal-operation of PRAM I. It is also shown in Figure 73 that islanding caused by fault clearing at location 4 are detected 74 ms after the incident which is very fast.

Table XII: Test results for three phase fault (fault clearing at Location 4 led to islanding)

	PRAM I	PRAM II	POR	ROCOF	PAD
Fault Initiation					
Location 1	√	√	√	X	X
Location 2	√	√	√	X	√
Location 3	√	√	√	X	X
Location 4	X	X	X	X	X
Location 5	√	√	X	√	√
Location 6	√	√	√	X	√
Fault Clearing					
Location 1	X	X	X	X	X
Location 2	√	√	X	X	√
Location 3	X	X	X	X	X
Location 4	√	√	√	√	√
Location 5	√	√	X	X	√
Location 6	√	√	√	√	√

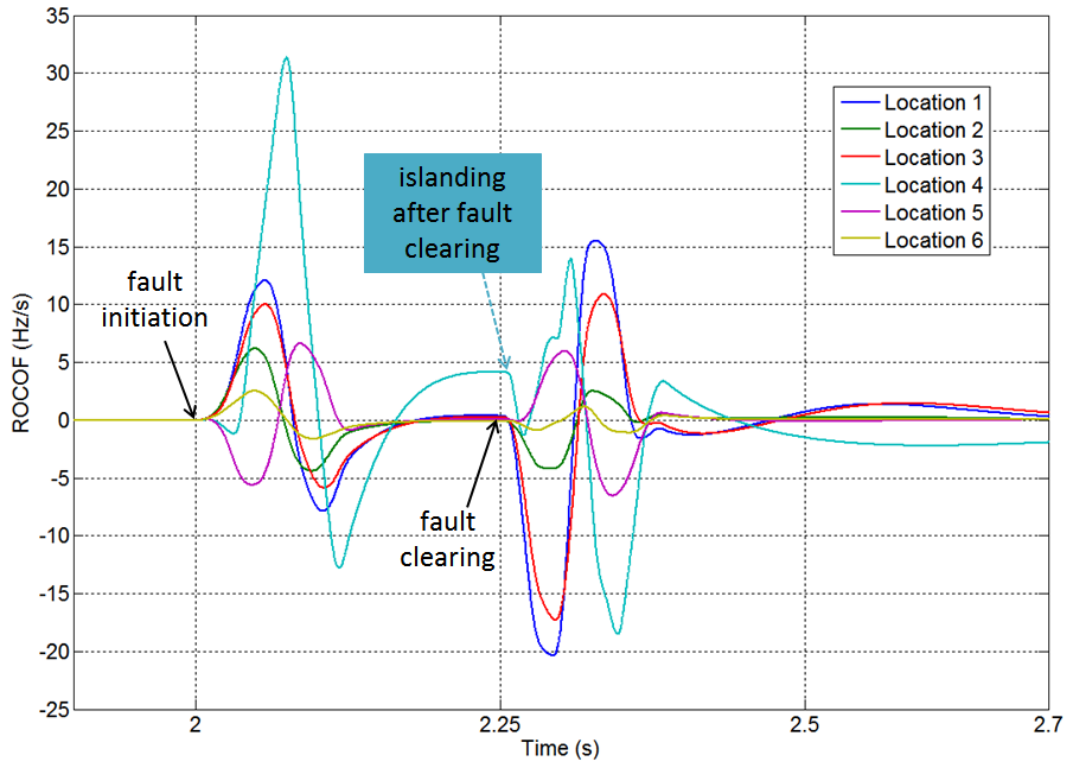


Figure 71: ROCOF output of PRAM I during three phase fault initiation and clearing

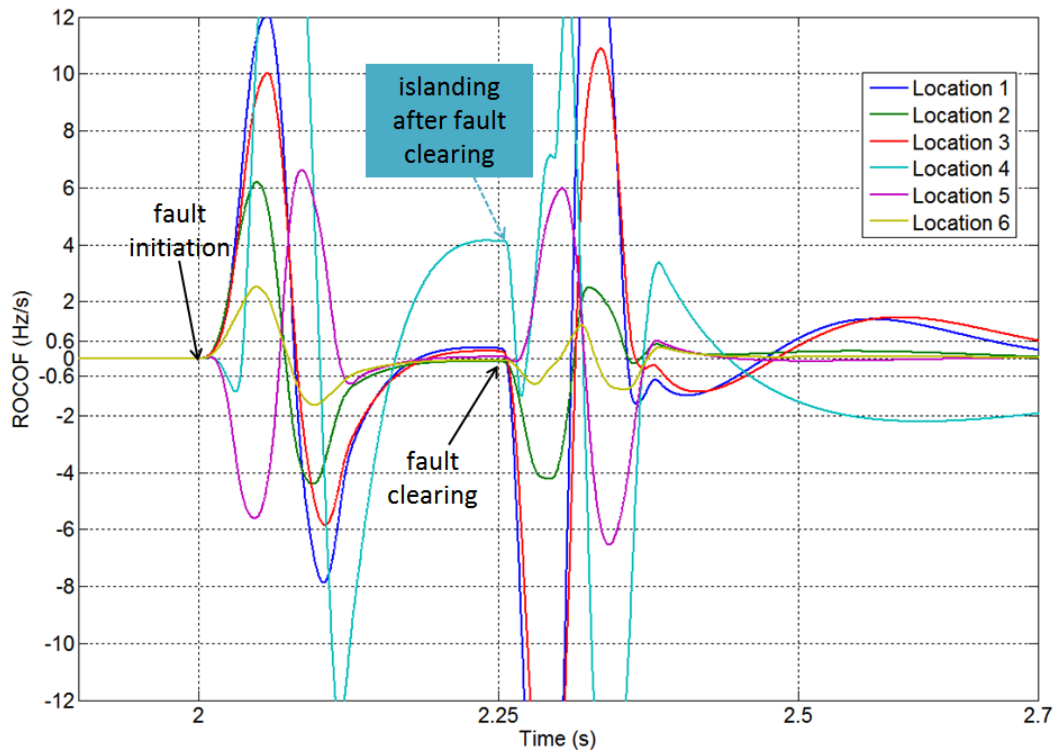


Figure 72: Scaled ROCOF output of PRAM I during three phase fault initiation and clearing

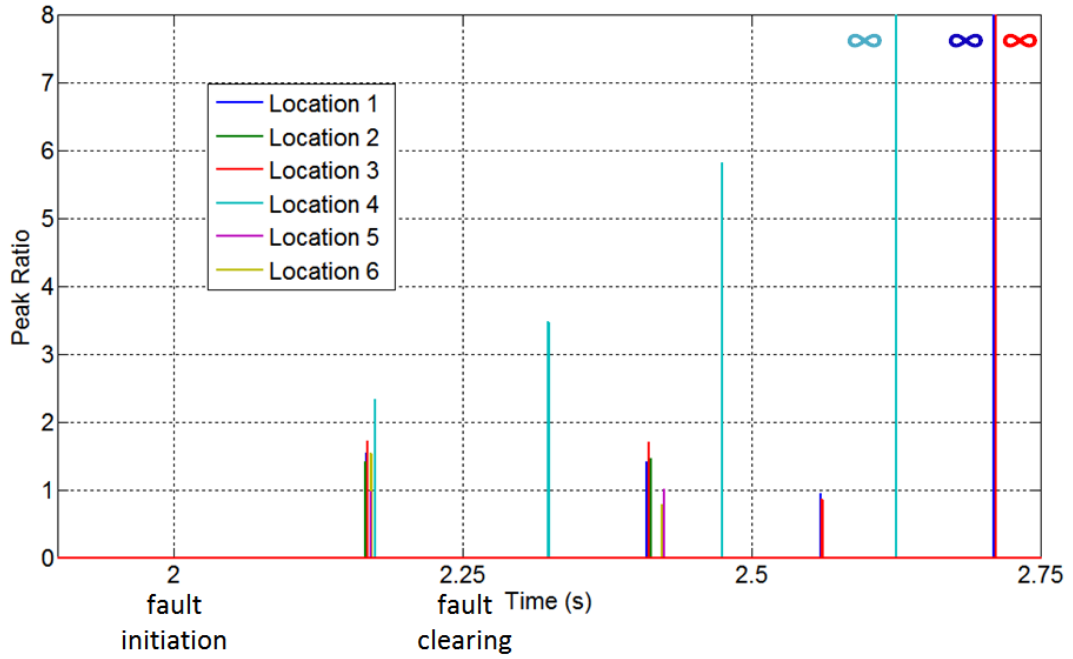


Figure 73: Peak ratio output of PRAM I during three phase fault initiation and clearing

It is shown in Table XII that PRAM II was stable for three phase to earth fault initiation at all locations except for location 4. It tripped for fault clearing at location 1 and 3 but remained stable at all other locations in this scenario. ROCOF behaviour of PRAM I is shown in Figure 74 and Figure 75 (scaled), and the peak ratios are shown in Figure 76. It is shown in Figure 76 that PRAM I picked up at all 6 locations and the largest peak ratio reaches 2.42 at location 4. And it is seen from Figure 74 that transient ROCOF after fault initiation hits 28.5 Hz/s which is very large. As the same argument in test scenarios of PRAM I, location 4 is the substation from 132 kV to 33 kV and two parallel paths of large symmetrical fault current are contributed from the grid. The second largest peak ratio is 1.81 which is at location 3 and all other peak ratios are below 1.6. It indicates that PRAM II is very stable for three phase fault initiation at all locations except for location 4. PRAM II also picked up

fault clearing at all locations and symmetrical three phase fault obviously caused ROCOF curve swing at locations (location 1, 3 and 4) closer to grid source. Fault clearing at location 4 caused further islanding whose largest peak ratio is infinite which will always be successfully detected. But the other two non-islanding scenarios at location 1 and 3 whose largest peak ratios are also infinite led to mal-operation of PRAM II. It is also shown in Figure 76 that islanding caused by fault clearing at location 4 are detected 241 ms after the incident which is very fast.

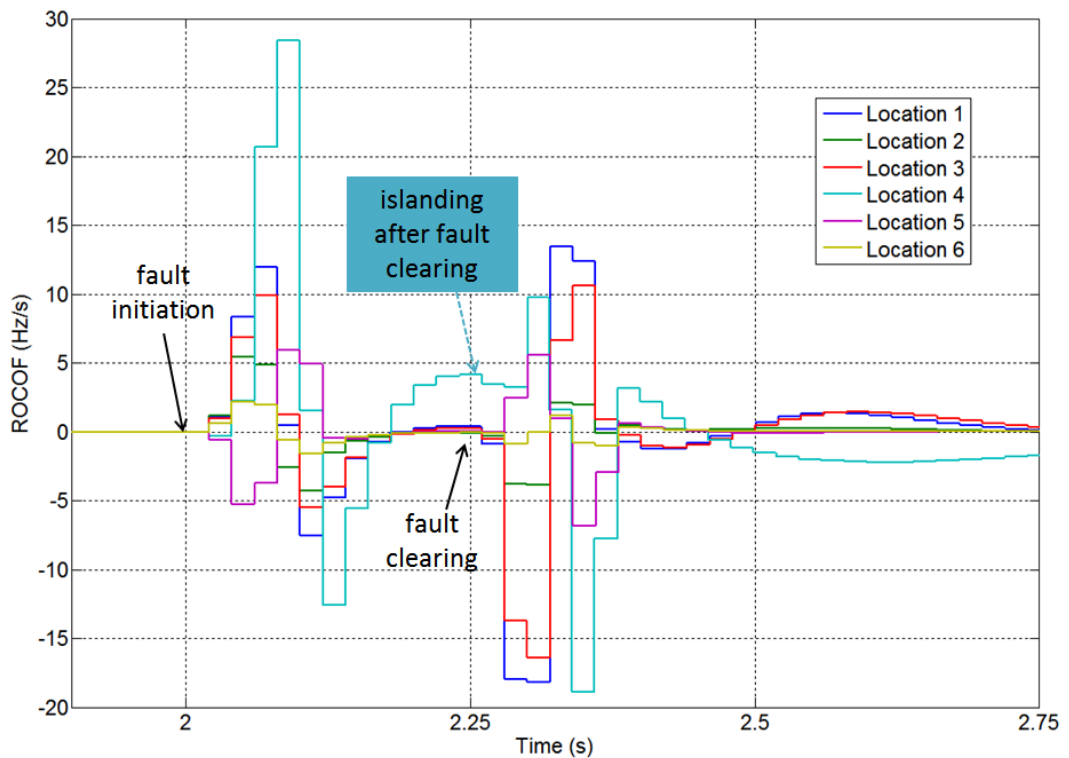


Figure 74: ROCOF output of PRAM II during three phase fault initiation and clearing

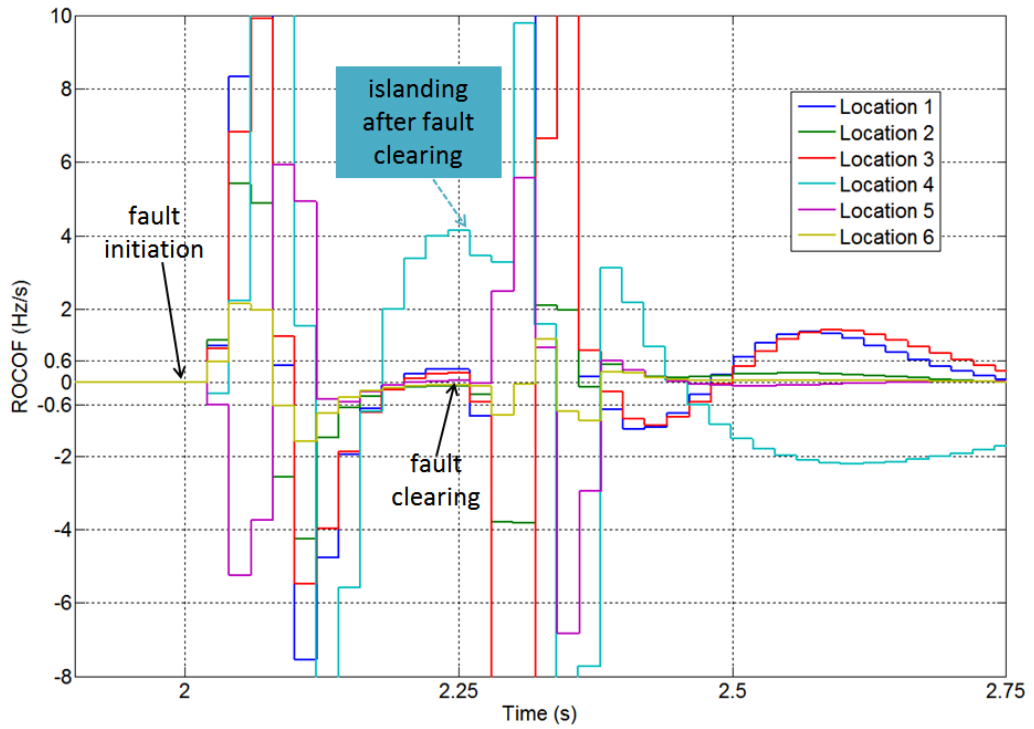


Figure 75: Scaled ROCOF output of PRAM II during three phase fault initiation and clearing

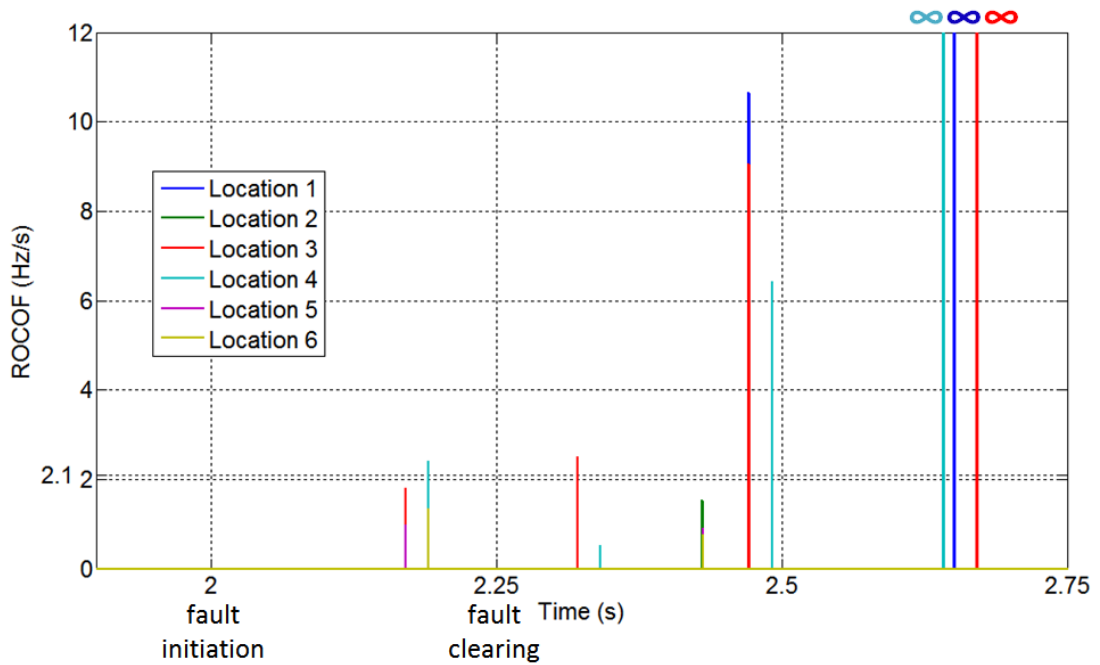


Figure 76: Peak ratio output of PRAM II during three phase fault initiation and clearing

POR is stable for three phase fault initiation at all locations except for location 4 and 5 according to Table XII. POR also accurately detected islanding event after fault clearing at location 4. It is tested that the maximum phase offset for fault initiation is 55° at location 4 and sensitivity will be significantly sacrificed if the threshold is increased to this level. Maximum phase offset at location 5 is 20.3° and a slight increase of threshold can remain POR stable. The largest phase offset value for stable scenarios is 13.7° at location 1 and it is not close to phase offset setting of 20° . It is tested that phase offset is very unstable for three phase fault clearing according to Table XII. The largest phase offset values are 42.9° for location 1, 25.7° for location 2, 32.3° for location 3 and 21.2° for location 5. POR successfully tripped 187 ms after islanding event (fault clearing) at location 4.

ROCOF is very unstable for three phase fault initiation as it only remained stable at location 5. And it is also unstable for fault clearing as it only remained stable at location 6. ROCOF accurately detected islanding event 140 ms after fault clearing at location 4. In order to remain stable for fault initiation at location 1, ROCOF setting should be 0.25 Hz/s. And this setting could be widening to 0.55 Hz/s at location 2, 0.7 Hz/s at location 3 and 0.35 Hz/s at location 6 so that ROCOF can ride through three phase fault initiation with sacrifice of sensitivity. And even a “ridiculous” setting of 2 Hz/s is not enough for ROCOF to remain stable to fault initiation at location 4. For fault clearing, ROCOF threshold is required to be set as large as 1.3 Hz/s at location 1 and 1.35 at location 3. Sensitivity will be significantly sacrificed for these two settings. And this setting should be widening to 0.25 Hz/s at location 2 and 0.9 Hz/s at location 5 so that ROCOF can ride through three fault clearing.

PAD is unstable for three phase fault initiation at location 1, 3 and 4 according to Table XII. It is tested that the threshold of PAD could be set to 16.2° at location 1

and 18.4° at location 3 to remain stable for fault initiation with sacrifice of sensitivity. However, a 70° threshold is not enough for PAD to ride through fault initiation at location 2. The largest phase difference experienced at other three locations is 6.7° and they are very stable for the original setting (10°). PAD is relatively stable for three phase fault clearing but still suffers from mal-operation at location 1 and 3. It is tested that PAD could widen its setting to 22.2° at location 1 and 20.2° at location 3 to ride through three phase fault clearing with sacrifice of sensitivity. Non-islanding fault clearing at other locations caused the phase differences below 5° which are very stable. PAD accurately and quickly (28 ms) detected islanding event at location 4.

It can be seen from Table X, Table XI and Table XII that three phase to earth fault is the most challenging fault scenario for all LOM methods. ROCOF is the least stable method under fault scenarios while PRAM II offers the best performance. PRAM I provided equally best performance in single phase and three phase to earth fault scenario as PRAM II except that it tripped during phase to phase fault clearing at one location.

6.2.4 Local small load change

As shown in Table XIII, PRAM I is stable under all load changing scenarios. ROCOF behaviour from PRAM I during load switching out and in is shown in Figure 77. It is illustrated that all load changes were picked up by PRAM I except 3.2 MW. And it is tested that peak ratios of local load switching are very stable (between 1.11 and 1.14 for switching out, between 1.13 and 1.16). PRAM II is stable under all load changing scenarios as shown in Table XIII. ROCOF behaviour from PRAM II during load switching out and in is shown in Figure 78. It is illustrated that all load changes were picked up by PRAM I except 3.2 MW. And it is tested that peak ratios

of local load switching are very stable (between 1.01 and 1.07 for switching out, between 1.22 and 1.29).

POR is stable for all load changes except for the largest load switching out and in according to Table XIII. It is tested that the phase offset magnitude is larger when a larger load change is experienced. To be stable under these scenarios, phase offset setting should be widen to 28° with sacrifice of POR relay sensitivity. ROCOF and PAD are also stable under all load change scenarios. The largest load change of 28.59 MW only caused 3.4° of phase angle difference.

Table XIII: Test results for local load switching

	PRAM I	PRAM II	POR	ROCOF	PAD
Load Out					
8.8 MW	√	√	√	√	√
10.39 MW	√	√	√	√	√
3.2 MW	√	√	√	√	√
4.9 MW	√	√	√	√	√
20.78 MW	√	√	√	√	√
28.59 MW	√	√	X	√	√
Load In					
8.8 MW	√	√	√	√	√
10.39 MW	√	√	√	√	√
3.2 MW	√	√	√	√	√
4.9 MW	√	√	√	√	√
20.78 MW	√	√	√	√	√
28.59 MW	√	√	X	√	√

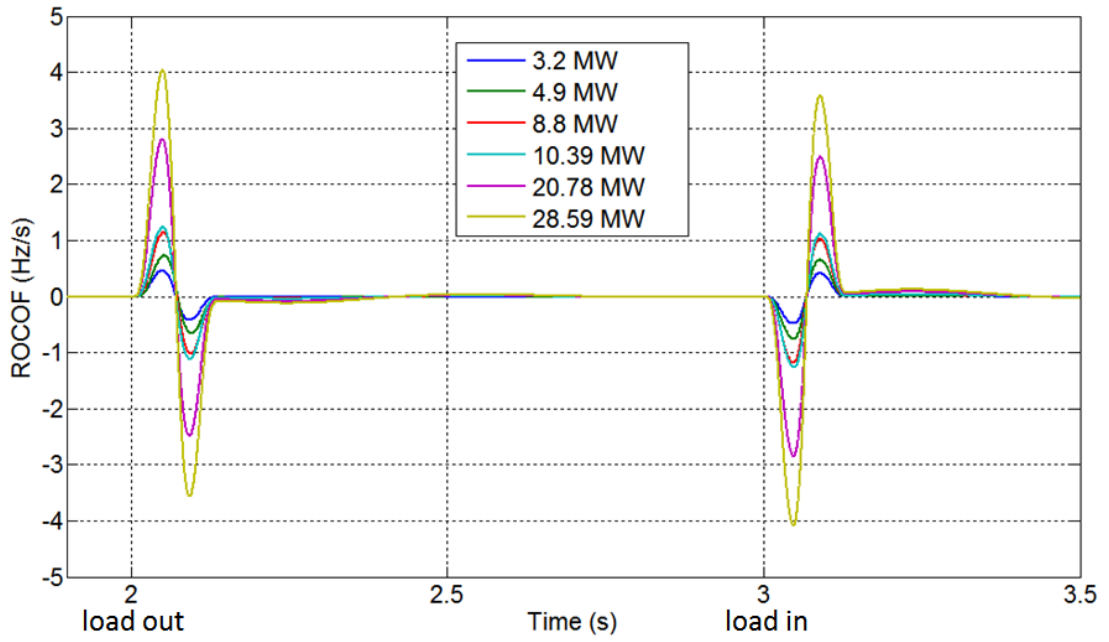


Figure 77: ROCOF output of PRAM I during local load switching out and in

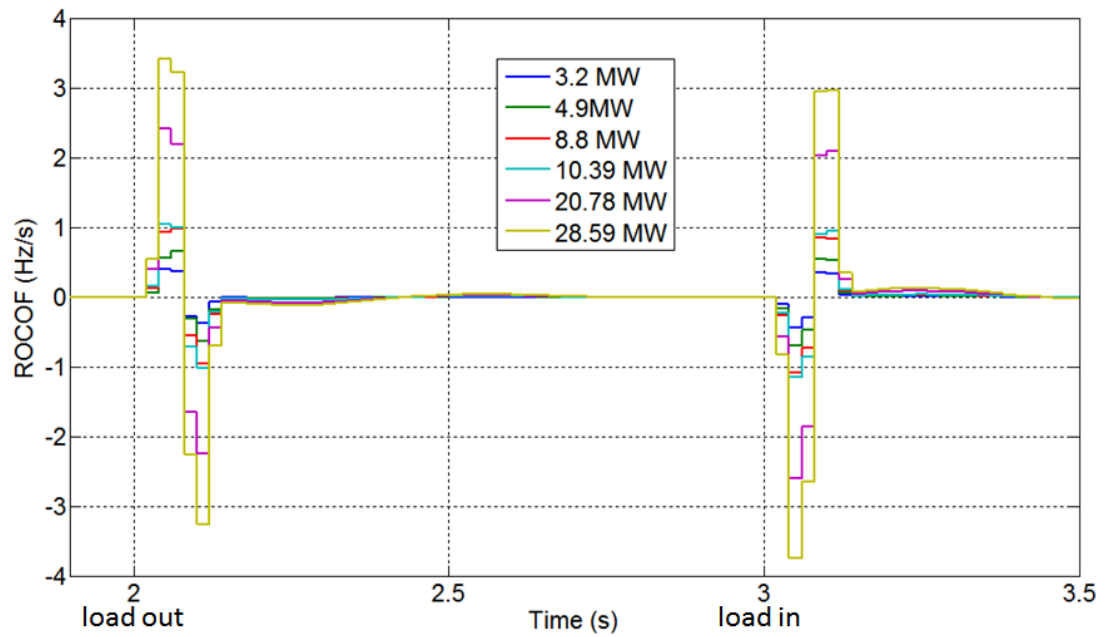


Figure 78: ROCOF output of PRAM II during local load switching out and in

6.2.5 Remote large load change

Table XIV: Test results for remote large load switching

		PRAM I	PRAM II	POR	ROCOF	PAD
Grid Inertia	Load Switching Out					
8 s	1.8 GW	√	√	√	√	√
6 s	1.8 GW	√	√	√	√	√
5 s	1.8 GW	√	√	X	X	√
	1.5 GW	√	√	√	√	√
4 s	1.8 GW	√	√	X	X	√
	1.5 GW	√	√	X	X	√
	1.3 GW	√	√	√	X	√
	1 GW	√	√	√	√	√
Grid Inertia	Load switching In					
8 s	1.8 GW	√	√	√	√	√
6 s	1.8 GW	√	√	√	X	√
	1.5 GW	√	√	√	√	√
5 s	1.8 GW	√	√	X	X	√
	1.5 GW	√	√	X	X	√
	1.3 GW	√	√	√	√	√
4 s	1.8 GW	√	√	X	X	√
	1.3 GW	√	√	X	X	√
	1 GW	√	√	√	√	√

As shown in Table XIV, all relays successfully rode through both load of 1.8 GW switching out and in with system inertia of 8 s.

With system inertia of 6 s, all relays except for ROCOF remained stable during both load switching out and in of 1.8 GW. ROCOF tripped during load of 1.8 GW switching in but remained stable when load magnitude was reduced to 1.5 GW.

When system inertia was reduced to 5 s, PRAM I, PRAM II and PAD were stable for both load of 1.8 GW switching out and in. However, PAD and ROCOF maloperated during both events. Both relays remained stable when load magnitude was reduced to 1.5 GW during switching out and 1.3 GW during switching in.

With system inertia of 4 s, PRAM I, PRAM II and PAD were still stable for the worst case during both load switching out and in. POR could remain stable only when load magnitude was reduced to 1.3 GW for switching out and 1 GW for switching in. ROCOF could remain stable only when load magnitude was reduced to 1 GW for both switching out and in.

The largest challenge for relays to ride through large load switching is the “constant” ROCOF after the initial two peaks as shown in Figure 79. Figure 79 shows an example of ROCOF output of PRAM I during remote large load switching in with magnitude of 1.8 GW, 1.5 GW and 1.3 GW with grid inertia of 4s and 5s. Load switching out events are reversely similar to switching in and PRAM II behaviour is similar to PRAM I in the period of “constant” ROCOF. And according to Equation (1) in Chapter 3, with nominal system frequency of 50 Hz and fixed grid capacity of 40 GVA in this test scenario, only load/generation switching magnitude and system inertia can have an effect on the level of “constant” ROCOF. For all reasons above, the examples in Figure 79 are able to illustrate and compare the effect

of the two factors. It shows that with the combination of lower system inertia and larger load switching magnitude, the “constant” ROCOF level is larger. It is difficult for single point ROCOF, frequency (integration from ROCOF) and phase angle (integration from frequency) based techniques to ride through, even they have a time delay setting. PRAM I and PRAM II are stable as they have a large pick up threshold (0.6 Hz/s). Once they pick up during “constant” ROCOF, the peak ratio magnitude will be infinite and will eventually maloperate. POR and ROCOF suffer from the scenarios with larger ROCOF level and they can increase the stability using the same method. However, sensitivity of both relays will be sacrificed. PAD is stable as it takes the angle difference from two sites and the aggregate effect is small.

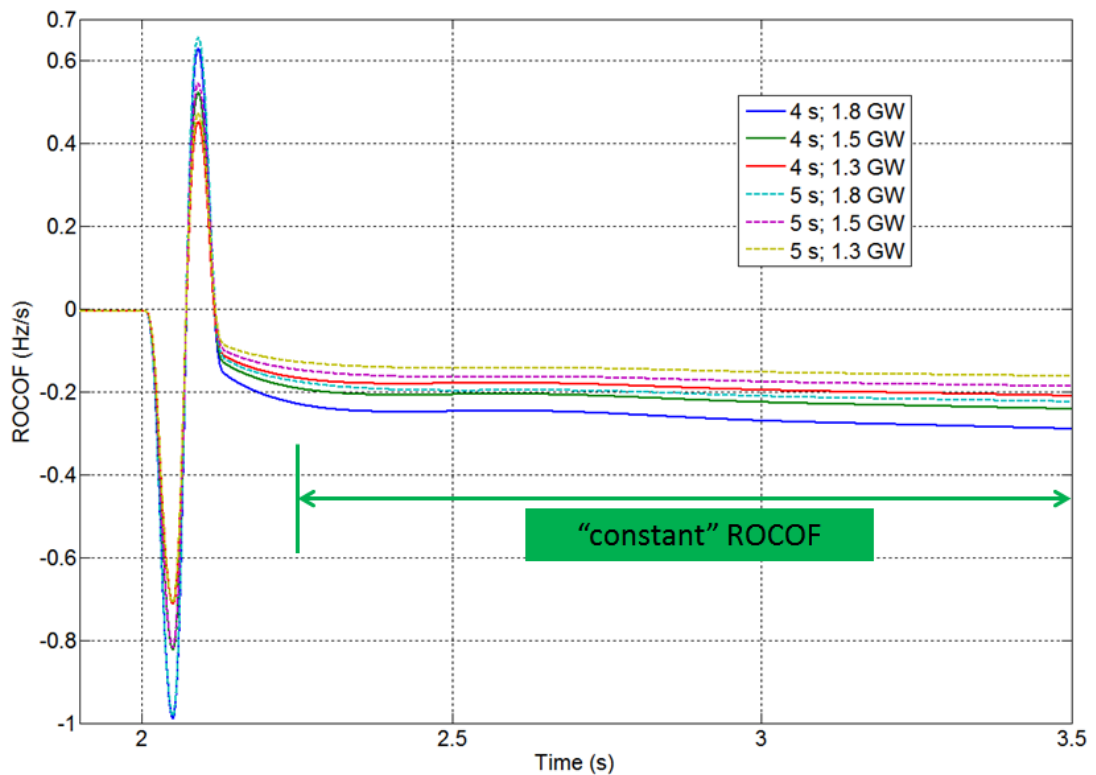


Figure 79: ROCOF output of PRAM I during remote large load switching in with magnitude of 1.8 GW, 1.5 GW and 1.3 GW with grid inertia of 4s and 5s

Table XV: Test results for capacitor switching out and transformer inrush

	PRAM I	PRAM II	POR	ROCOF	PAD
Capacitor Switching Out					
8.1 MVar	√	√	√	√	√
11 MVar	√	√	√	√	√
Transformer Inrush					
Scenario 1	√	√	√	√	√
Scenario 2	√	√	√	√	√

6.2.6 Capacitor switching

It is shown in Table XV that all relays remained stable under capacitor switching out for both magnitude of 8.1 MVar and 11 MVar. Figure 80 presents the ROCOF behaviours of both PRAM I and PRAM II for both scenarios. It is shown that no PRAM relay picked up during both tests. Peak ratios of PRAM I are 1.55 and 1.61 for switching magnitude of 8.1 MVar and 11 MVar respectively. And peak ratios for PRAM II are 1.58 and 1.53. All peak ratios are not close to tripping thresholds for both scenarios. It is predicted that with a large enough capacitor switching magnitude which leads to PRAM pick up, the peak ratio will still be too small to trip PRAM relay. However, in terms of achieving voltage management of the distribution network in this test, a capacitor with magnitude larger than 11 MVar is unnecessary. Therefore, PRAM algorithms are very stable during capacitor switching events.

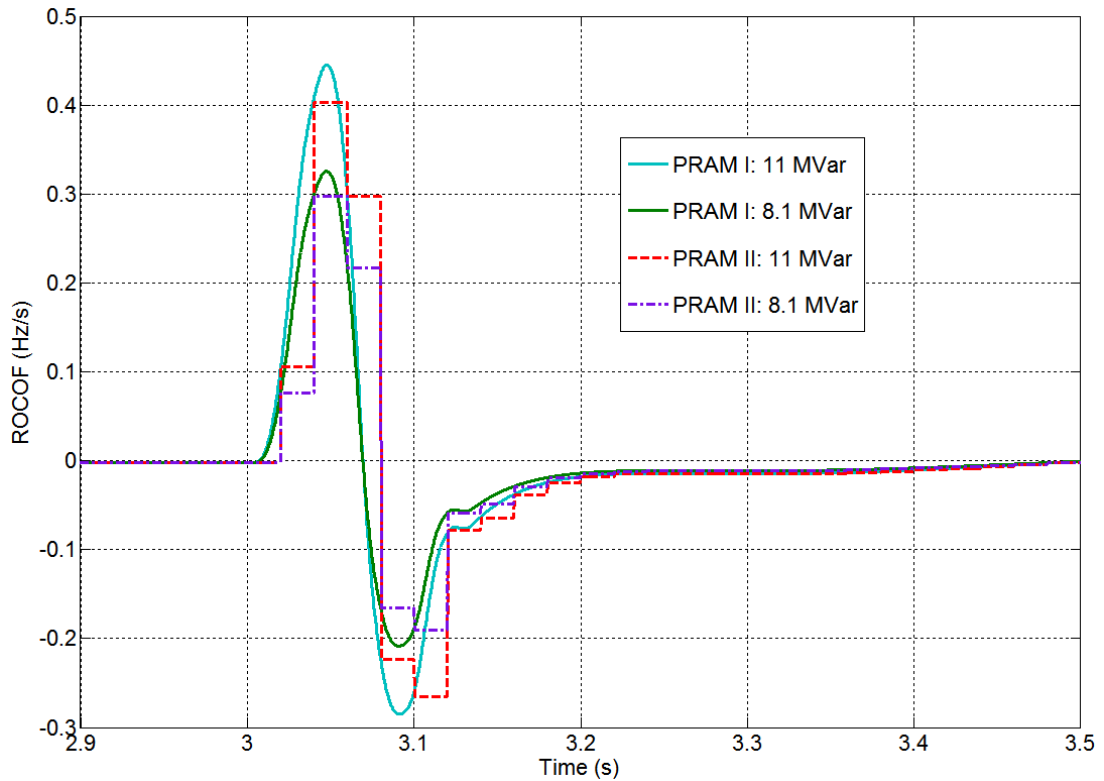


Figure 80: ROCOF output of PRAM I and PRAM II during capacitor switching out with magnitude of 11 MVar and 8.17 MVar

6.2.7 Transformer inrush

It is shown in Table XV that all relays remained stable under transformer inrush for both scenarios. In scenario 1, it is tested that inrush of a single transformer in grid connected distribution system has no effect on ROCOF waveform, as the capacity of the transformer is negligible comparing to which of the grid. In scenario 2, a large transformer (450 MVA) is directly connected to grid source (3 GVA) as shown in Figure 54. Figure 81 presents the ROCOF behaviours of both PRAM I and PRAM II for this scenario. It is shown that both relays picked up for the event. However, the

peak ratios calculated are 0.90 and 1.02 and they are not close to the thresholds. Therefore, PRAM is very stable during transformer inrush events.

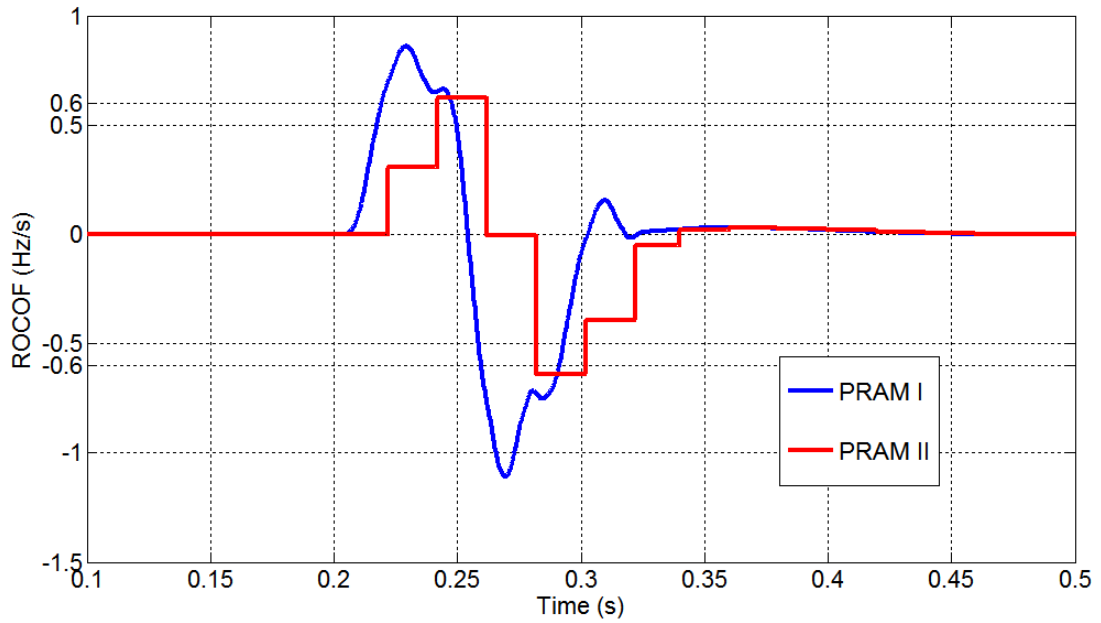


Figure 81: ROCOF output of PRAM I and PRAM II for scenario 2 of transformer inrush

References

- [6.1] (July 2015) National Grid, “System Operability Framework” [Online].
Available: <http://www2.nationalgrid.com/UK/Industry-information/Future-of-Energy/System-Operability-Framework/>

Chapter 7

Conclusions and Future Work

This thesis has presented a description of a new anti-islanding technique which analyses the dynamic behaviour of the ROCOF measurement produced by PMUs during and following system transients. It exhibits high sensitivity to genuine islanding events and good levels of stability during fault, load change, capacitor switching and transformer inrush including events where the grid system inertia is reduced, as may be the case in the future as the penetration of renewables increases. The operation of PRAM has been tested against three alternative techniques: ROCOF, POR and PAD. PRAM only requires local voltage measurements, so there is no need for communications.

It is clear that PAD seems to be an “ideal” method as it has a very small NDZ, and is relatively stable to load changes and fault events, except for three phase faults at certain locations. This is to be expected, as it directly monitors the phase angle difference between that measured at the DG and that measured at a grid location. However, this comes at the expense of communications being required, and cost, availability and reliability are all concerns. POR uses a local ROCOF measurement and requires no communications. It exhibits a relatively larger NDZ when the droops

of the DG controller are set to be more aggressive (lower) and trips falsely during large load changes when compared to PRAM. As expected, ROCOF is sensitive and fast to trip during genuine islanding events, but suffers from stability problems during faults and load changes – particularly when system inertia is reduced. In the UK, ROCOF settings of 1 Hz/s with a 500 ms time delay have been proposed for future application [2.24]. However, applying such settings will mean that the LOM protection will obviously be much less sensitive to real islanding events, and while this could solve the stability problem, it will greatly decrease sensitivity and lead to much larger NDZs for detection of islanding conditions, which could be a potentially dangerous situation.

PRAM possesses a very small NDZ for both active and reactive power imbalances regardless of DG controller configuration. For reactive power imbalances, it is relatively more difficult to detect islanding. The peak ratios are always infinite, but a relatively smaller magnitude (when compared to purely active power) of ROCOF is experienced for reactive power-only imbalances, so sensitivity is reduced; however, this also applies to ROCOF. A large reduction in DG active power output from 90% to 30% makes islanding detection marginally easier for all algorithms under active power imbalance conditions. Theoretically, the ROCOF level remains the same as all the parameters remain unchanged according to Equation (1). The marginal change in behaviour of the algorithms may be due to slightly different transient stresses on the DG rotors during the islanding events. The reduction of DG output also makes islanding detection more difficult under reactive power imbalance conditions. The peak ratios remain infinite but an even smaller magnitude of ROCOF is experienced and this affects all algorithms.

The major benefit of PRAM is that it is more stable during large grid disturbances, even when system inertia is reduced. This could be a major benefit in the future.

Furthermore, the use of M class PMUs for PRAM has benefits in terms of significantly reducing the risk of errors during off-nominal frequency conditions and when signals with harmonic content are being measured. To further increase the performance of PRAM, a greater number of averaging cycles may be added to the measurement window of the PMU – this will increase the magnitudes of the peak ratios and make it easier to detect islanding, particularly when reactive power is flowing prior to islanding, but perhaps at the expense of increased times of operation. Future work should concentrate on analysing performance under different application scenarios (varying DG capacity and varying grid “strength” further) and on establishing rules for deriving setting thresholds (i.e. peak ratios) under different application scenarios. Increasing the sensitivity and reducing the NDZ, particularly where reactive power imbalances are encountered prior to islanding, is also an area of on-going and future activity.

References

- [7.1] “Frequency Changes during Large Disturbances and their Impact on the Total System [Online]. Available: <http://www.nationalgrid.com/NR/rdonlyres/D3F18F81-BFE8-4BA1-8B82-CCD6CD0A0A4F/62018/GC0035IndustryConsultationv10.pdf>